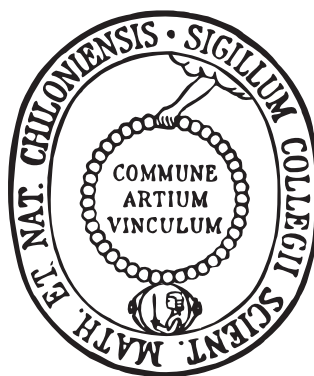


PHOTOSWITCHABLE SPIN-CROSSOVER
COMPOUNDS FOR SURFACE
MODIFICATION



DISSERTATION

ZUR ERLANGUNG DES DOKTORGRADES

DER MATHEMATISCH-NATURWISSENSCHAFTLICHEN FAKULTÄT

DER CHRISTIAN-ALBRECHTS-UNIVERSITÄT ZU KIEL

vorgelegt von

DIPL.-CHEM. ALEXANDER BANNWARTH

GEBOREN 20. OKTOBER 1980 IN BAD SÄCKINGEN

PHOTOSWITCHABLE SPIN-CROSSOVER
COMPOUNDS FOR SURFACE
MODIFICATION

DISSERTATION

ZUR ERLANGUNG DES DOKTORGRADES

DER MATHEMATISCH-NATURWISSENSCHAFTLICHEN FAKULTÄT

DER CHRISTIAN-ALBRECHTS-UNIVERSITÄT ZU KIEL

vorgelegt von

DIPL.-CHEM. ALEXANDER BANNWARTH

GEBOREN 20. OKTOBER 1980 IN BAD SÄCKINGEN

Referent: Prof. Dr. Felix Tuczek
Koreferent: Prof. Dr. Christian Näther
Datum der mündl. Prüfung: 14. April 2011
Zum Druck genehmigt: 14. April 2011

Prof. Dr. Lutz Kipp, Dekan

Für Paul und Monika

Abstract

The scope of this thesis is the synthesis and characterisation of new spin-crossover coordination compounds with photoswitchable ligands and the evaluation of their potential for the development of molecular switching units. The first part of the thesis is concerned with the synthesis of iron(II)- and iron(III) coordination compounds with a photoisomerisable azo-function directly coordinated to the metal center and the characterisation of the resulting compounds with Mößbauer- and UV/Vis spectroscopy.

Basing on the results of these experiments, photoswitchable azopyridines were reacted with an otherwise coordinatively saturated iron(III)-system that was supposed to be able to undergo a thermal spin-transition as well as a photoisomerisation of the coordinated azoligands. These new spin-crossover compounds were characterised with UV/Vis, vibrational-, NMR- and Mößbauer-spectroscopy as well as quantum-chemical methods to gain insights into the influence of the *cis-trans*-isomerisation of coordinated pyridine-donors on the spin-state of the coordination center.

To further enhance the switching properties of coordination compounds, as well as to gain access to a stable switchable spin-crossover compound suited for the modification of various surfaces, new chelating azo-ligands were successfully synthesized and characterised. These new ligands were used to equip an iron(II)-spin-crossover complex with a photoswitchable unit. This complex as well as the not switchable parent compounds were characterised extensively with UV/Vis- vibrational-, NMR- and Mößbauer-spectroscopy.

This class of iron(II) spin-crossover complexes showed to be able to form thin layers on various substrates by sublimation. The effects on the spin-transition were studied with optical spectroscopy.

Kurzzusammenfassung

Das Ziel der vorliegenden Arbeit war die Synthese und spektroskopische Charakterisierung neuer Eisen-basierter Spin-Crossover Koordinationsverbindungen mit photoschaltbaren Liganden und deren Untersuchung im Hinblick auf ihr jeweiliges Potential für die Entwicklung von molekularen Schaltern. Der erste Abschnitt der Arbeit befasst sich mit der Synthese neuer Eisen(II)- und Eisen(III)-Komplexe mit einer direkt koordinierten Azo-Einheit und der Charakterisierung der Verbindungen mit Mößbauer- und UV/Vis-Spektroskopie.

Aufbauend auf diesen Ergebnissen wurden photoisomerisierbare Phenylazopyridine mit einer anderweitig koordinativ gesättigten Eisen(III) Stammverbindung umgesetzt, welche sowohl zu einem thermisch induzierten Spinübergang befähigt sein sollte als auch zur Photoisomerisierung des koordinierten Azopyridins. Die neu synthetisierten Spin-Crossover Komplexe wurden mittels UV/Vis- Schwingungs-, NMR- und Mößbauerspektroskopie und mit Hilfe der Dichtefunktionaltheorie untersucht, um Erkenntnisse über den Einfluß der *cis-trans*-Isomerisierung des koordinierten Pyridinderivats auf den Spinzustand des Metallzentrums zu gewinnen.

Um die Schalteigenschaften der Spin-Crossover Verbindungen weiter zu optimieren, wurden neue schaltbare Chelatliganden synthetisiert. Diese wurden dazu verwendet einen neuen, mit einer photoschaltbaren Azogruppe ausgestatteten, Spin-Crossover Komplex zu synthetisieren, welcher mit Hilfe von UV/Vis-, Schwingungs-, NMR- und Mößbauerspektroskopie charakterisiert wurde, wie auch die nicht photoschaltbaren Stammverbindungen.

Diese Gruppe von Komplexen ist gut dazu geeignet dünne Filme durch Vakuumsublimation auf Oberflächen abzuschneiden. Der Einfluß der Filmbildung auf den Spinübergang wurde mittels optischer Spektroskopie untersucht.

Contents

1	Motivation	1
2	Introduction	3
2.1	Spin-Crossover Systems	3
2.1.1	Spin-Crossover in Nature	3
2.1.2	Artificial spin-crossover Systems	4
2.1.3	Ligand-Field-Theoretical Considerations	6
2.1.4	Mechanism of the Spintransition	8
2.1.5	Classification of Spin Transitions	10
2.1.6	External Influences	12
2.1.7	Mößbauer-Spectroscopy	12
2.1.8	Density Functional Theory	15
2.1.9	DFT on Spin Crossover Compounds	16
2.2	Photoswitchable Systems	17
2.2.1	Natural Photoswitches	17
2.2.2	LIESST Effect	17
2.2.3	LD-LISC Effect	20
2.2.4	Azobenzene-Isomerisation	21
2.2.5	Alternatives to the E/Z-Isomerization of Azobenzene	22
2.2.6	Organic Paramagnetism	23
2.3	Molecular Switches	24
2.3.1	Technical Applications	24
2.3.2	Switches	24

2.3.3	Displays	25
3	Coordinated Azo-functions	27
3.1	Switching Concept	27
3.2	Design	28
3.3	Results	30
3.3.1	Optical Switching	30
3.4	Syntheses	36
3.4.1	Synthesis of 4-methyl-2-(phenyldiazenyl)phenol	36
3.4.2	Synthesis of 4-methyl-2-(phenyldiazenyl)naphtol	37
3.4.3	Synthesis of 2-(phenyldiazenyl)pyridine	38
3.4.4	Synthesis of $[\text{Fe}(\text{CH}_3\text{CN})_6](\text{BF}_4)_2$	39
3.4.5	Synthesis of $[\text{Fe}(2\text{-(phenyldiazenyl)pyridine})_2\text{Cl}_2]$	40
3.4.6	Synthesis of $[\text{Fe}(2\text{-(phenyldiazenyl)pyridine})_3](\text{BF}_4)_2$	41
3.4.7	Synthesis of $[\text{Fe}(4\text{-(pyridin-2-yl)diazenyl})\text{-resorcinol}]_2$	42
3.4.8	Synthesis of $[\text{Fe}(4\text{-methyl-2-(phenyldiazenyl)naphtol})_3]$	43
3.4.9	Synthesis of $[\text{Fe}(4\text{-methyl-2-(phenyldiazenyl)phenol})_3]$	44
4	Azopyridines	45
4.1	Design of a switchable SCO-complex	45
4.1.1	Salten-type complexes	45
4.2	Thermal Spin Crossover	47
4.2.1	Möbbauser-Spectra	47
4.2.2	Magnetic Measurements	51
4.3	Photoinduced Switching	52
4.3.1	Optical Switching	52
4.3.2	Evans Measurements	53
4.4	Quantum-chemical Analysis	61
4.4.1	Calculations	61
4.5	Results and Discussion	65

4.6	Syntheses	66
4.6.1	Synthesis of 4-azaheptamethylene-1,7-bis(salicylideneiminate)	66
4.6.2	Synthesis of 3-(phenyldiazenyl)pyridine	67
4.6.3	Synthesis of 4-(phenyldiazenyl)pyridine	68
4.6.4	Synthesis of [Fe(salten)Cl]	69
4.6.5	Synthesis of [Fe(salten)py]BPh ₄	70
4.6.6	Synthesis of [Fe(salten)3-(phenyldiazenyl)py]BPh ₄	71
4.6.7	Synthesis of [Fe(salten)4-(phenyldiazenyl)py]BPh ₄	72
4.6.8	Synthesis of [Fe(salten)4-methyl-3-(phenyldiazenyl)py]BPh ₄ . .	73
5	Azochelates	75
5.1	The non-coordinating azo-group	75
5.2	Ligand Design and Synthetic Routes	75
5.2.1	Substituted Phenanthrolines and Bipyridines	75
5.2.2	Symmetrically and asymmetrically substituted bipyridines . .	77
5.2.3	Curtius Rearrangement	81
5.2.4	Formation of Nitrosopyridine	83
5.2.5	Asymmetrically substituted bipyridine	87
5.2.6	Azocoupling	90
5.3	Switchable Complexes	100
5.3.1	Iron-chloride precursors	100
5.3.2	Bispyrazolylborate	102
5.4	SCO of Azochelates	105
5.4.1	Mössbauer-spectra	105
5.4.2	Magnetic Measurements	109
5.5	Photoinduced Switching	110
5.5.1	Ligand Switching	110
5.5.2	Complex Switching	112
5.6	Syntheses	114
5.6.1	Synthesis of 2,2'-bipyridine-5,5'-dicarboxylate with K ₂ Cr ₂ O ₇ .	114

5.6.2	Synthesis of 2,2'-bipyridine-5,5'-dicarboxylate with KMnO_4	115
5.6.3	Synthesis of diethyl-2,2'-bipyridine-5,5'-dicarboxylate	116
5.6.4	Synthesis of 2,2'-bipyridine-5,5'-dicarboxylic dihydrazide	117
5.6.5	Synthesis of 2,2'-bipyridine-5,5'-dicarboxylic diazide	118
5.6.6	Synthesis of 5,5'-bis(ethoxycarbonylamino)-2,2'-bipyridine	119
5.6.7	Synthesis of 5,5'-diamino-2,2'-bipyridine	120
5.6.8	Synthesis of 5,5'-bis(phenyldiazenyl)-2,2'- bipyridine	121
5.6.9	Synthesis of 1-(2-Pyridylacetyl)pyridinium iodide	122
5.6.10	Synthesis of 5-Methyl-2,2'-bipyridine	123
5.6.11	Synthesis of 2,2'-bipyridinyl-5-carboxylic acid	124
5.6.12	Synthesis of Ethyl-2,2'-bipyridinyl-5-carboxylate	125
5.6.13	Synthesis of 2,2'-bipyridine-5-carboxylic hydrazide	126
5.6.14	Synthesis of 2,2'-bipyridine-5-carboxylic azide	127
5.6.15	Synthesis of 5-ethoxycarbonylamino-2,2'-bipyridine	128
5.6.16	Synthesis of 5-amino-2,2'-bipyridine	129
5.6.17	Synthesis of 5-phenyldiazenyl-2,2'-bipyridine	130
5.6.18	Synthesis of Potassium Dihydrobis(pyrazolyl)borate	131
5.6.19	Synthesis of $[\text{Fe}(\text{H}_2\text{B}(\text{pz})_2)_2\text{phen}]$	132
5.6.20	Synthesis of $[\text{Fe}(\text{H}_2\text{B}(\text{pz})_2)_2\text{bipy}]$	133
5.6.21	Synthesis of $[\text{Fe}(\text{H}_2\text{B}(\text{pz})_2)_2\text{monoazobipy}]$	134
6	Thin Films of SCO Compounds	135
6.1	Assignment	135
6.2	Deposition	135
6.3	Optical Spectroscopy	137
7	Scientific Methods	141
7.1	Synthetic Procedures	141
7.2	Spectroscopic Methods	141
7.3	Quantum-chemical Calculations	143

8 Summary and Outlook	145
Bibliography	147

1 Motivation

Truly bistable coordination compounds having two distinct states between which switching via external stimuli is possible are rather uncommon for the time being. Most known examples exhibit bistability only at very low temperatures (below 100K) and can be switched from one state into the other by, for example, irradiation.

Solid state physics knows several cooperative phenomena which can increase this operating temperature significantly, but those substances can no longer be considered to be molecular switches since there are no single molecules involved. The scope of this thesis is the synthesis and characterization of such bistable coordination compounds on the base of iron coordination compounds bearing photoswitchable pyridine and bipyridine derivatives. These possible molecular switches are synthesized, characterized and their potential for the modification of various surfaces and the characterization of these surfaces are presented.

2 Introduction

2.1 Spin-Crossover Systems

2.1.1 Spin-Crossover in Nature

The most prominent molecule in nature which utilises the spin-crossover phenomenon is hemoglobin.

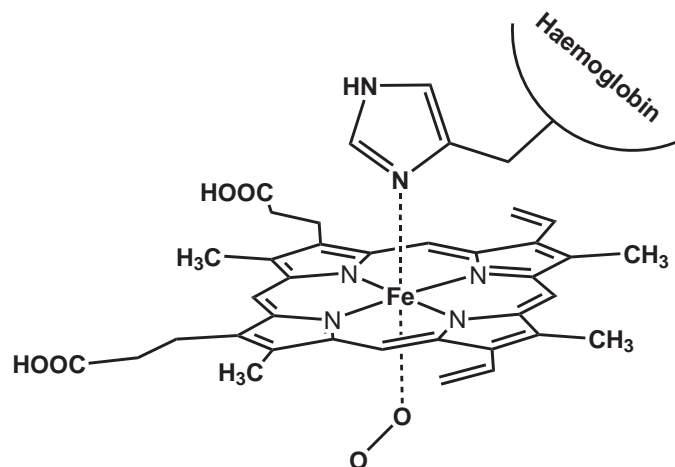


Figure 2.1: Active site of protoporphyrin IX, oxygenated form

The active iron-core inside the hemoglobin protein is responsible for its red colour. The protein itself consists of four monomer subunits, who themselves are very similar to the other known oxygen-transport vessel of virtually all known vertebrates, the myoglobin, which is responsible for oxygen transport inside the muscle filaments. The iron-center of hemoglobin has the oxidation-state +2, which is changed to +3 during the uptake or release of molecular oxygen. If it does nevertheless (e.g. caused by poisoning with oxidation agents such as nitrites or hydrogen peroxide), the hemoglobin

is irreversibly converted to methemoglobin, the deactivated form of hemoglobin. In its initial oxygen-free highspin state, the radius of the iron atom is too large to fit into the porphyrine-plane completely and is thus standing out of it slightly. The iron is further coordinated (aside from the four nitrogen atoms inside the porphyrine-ring) by a proximal histidine (see Figure 2.1). The sixth coordination-site is reserved for the binding of a dioxygen molecule. With the binding of this oxygen, the iron center is converted to the low-spin state, reducing its ionic radius and now fitting completely into the porphyrin-plane. This movement of the iron atom and the tension it performs on the coordinated histidine is responsible for the cooperative binding effects.

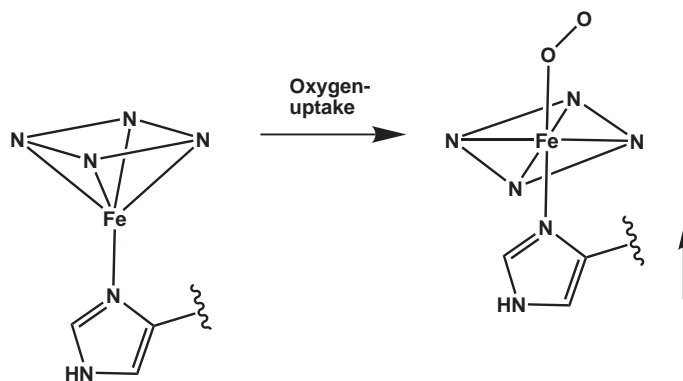


Figure 2.2: Geometry change induced by oxygen binding

It has been shown by EPR-studies on the isolated protein^[1] that the iron-center undergoes spin-transitions from a iron(II) high-spin form to an iron(III) low-spin form during oxygenation.

2.1.2 Artificial spin-crossover Systems

The first observation of the temperature-dependence of the spinstates in a transition-metal compound dates back to Cambi and Szegö in 1931^[2]. Two decades later the research on these so-called spin-crossover systems was vastly extended, at first mainly with regard only to the temperature dependence of the magnetic moments. Only later the influence of e.g. pressure or other external stimuli were studied more in detail. Also the first examples of manganese, cobalt, chromium and nickel compounds exhibiting the spin-crossover behaviour were published^[3].

The most thoroughly studied spin-crossover compound is $[\text{Fe}(\text{phen})_2(\text{NCS})_2]$ (figure 2.3). First synthesized in 1963 by Madeja and König^[4], its unusual magnetic behaviour was discovered shortly afterwards^[5].

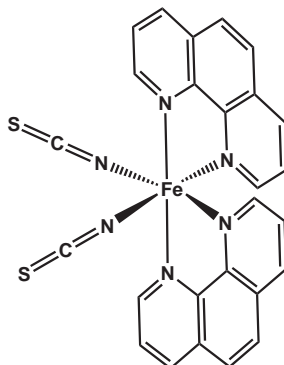
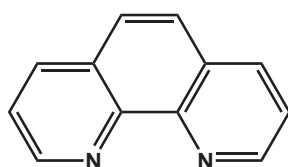
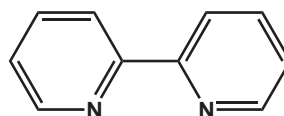


Figure 2.3: $[\text{Fe}(\text{phen})_2(\text{NCS})_2]$

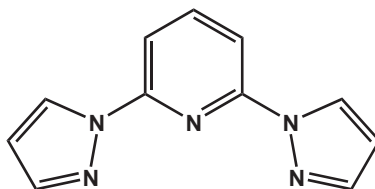
The complex undergoes an abrupt spin transition from high-spin to low-spin configuration at a temperature of 174 K, where half of the magnetic moment has vanished. Although the first published example of a thermal spin transition in a coordination compound was an iron(III)-center with carbamate-ligands, the vast majority of known spin-crossover compounds is based on an iron(II)-center. The typical coordination sphere is composed of six nitrogen donor-atoms.



(a) 1,10-phenanthroline



(b) 2,2'-bipyridine



(c) 2,6-bis(pyrazolyl)pyridine

Figure 2.4: A Selection of typical ligands used in SCO-compounds

These ligands (figure 2.4) now can be further functionalized to tune the ligand-field imposed on the metal center.

2.1.3 Ligand-Field-Theoretical Considerations

In general, spin-crossover can only occur in transition metal compounds with four to seven d-electrons, since only these configurations have two possible spin states: The high-spin state with a maximum number of unpaired electrons and the low-spin state with the maximum amount of paired electrons.

In an octahedral coordination sphere, the five d-orbitals are split into two sets of three and two orbitals by interaction with the six coordinated ligands (figure 2.5).

The two subsets consist of the irreducible representations t_{2g} (d_{xy} , d_{xz} and d_{yz} orbitals) and e_g (d_{z^2} and $d_{x^2-y^2}$). The t_{2g} subset is hereby of non-bonding nature and therefore lower in energy than the anti-bonding e_g set.

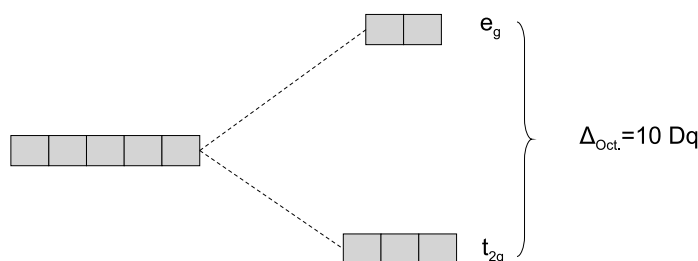
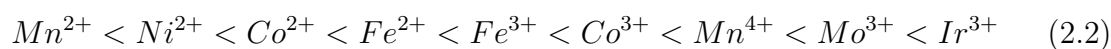


Figure 2.5: Orbital energy splitting in an ideal octahedral field.

The energetic difference of the two orbital subsets is designated $10Dq$, the ligand field parameter, depending on the surrounding ligands and on the metal ion as well. A weak ligand field leads to a small ligand field splitting and vice versa for strong ligands. All ligands can therefore be arranged with respect to the ligand-field strength they generate.



This so-called spectrochemical series can also be established for the metal centers, since the ligand-field splitting also depends on the charge of the metal cation.



In both series, the more to the left the ligand/metal is located, the higher the tendency

to form high-spin complexes.

In systems with one to three d-electrons, Hund's rules force the three t_{2g} -orbitals to be populated first. With four to seven d-electrons there are two possibilities:

- The electron spins are paired and the t_{2g} -orbitals are populated, having the minimal possible spin multiplicity and therefore named low-spin configuration
- The electron spins are not paired and the e_g -orbitals are also populated, having the maximum possible spin multiplicity and so named high-spin configuration.

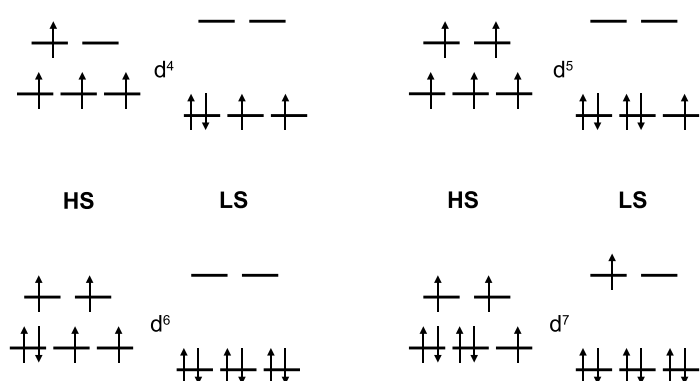


Figure 2.6: All possible configurations from four to seven d-electrons.

The resulting spin state is depending on two parameters, the spin-pairing energy P and the ligand-field splitting $10Dq$. The spinpairing energy has two contributions:

- Coulomb repulsion of two electrons when being put into the same orbital.
- Exchange energy. For paired electron spins it equals zero and contributes a stabilizing portion for unpaired spins. Exchange energy does not have an analogon in classical physics, thus being a pure quantum-mechanical quantity.

Regarding the fact that the d-orbitals in the second and third transition metal row are far more diffuse than in the first row, thus drastically reducing the energetic contribution to the spin pairing, coordination compounds of the second and third transition metal row always have a low-spin configuration.

If the magnitude of the spin pairing energy is greater than that of the ligand field splitting, all five d-orbitals will be populated, resulting in a high-spin configuration.

Vice versa, the system will have a low-spin configuration with all t_{2g} -orbitals doubly occupied first.

The Coulomb-repulsion of the d-electrons leads to a series of states that can be classified by their multiplicity $2S+1$ and their orbital momentum L . The energetic level can be described with two electron-electron interaction parameters, the so-called Racah-parameters B and C .

The influence of ligand fields on the energy-levels of an undisturbed free metal ion is usually plotted in a Tanabe-Sugano diagram (figure 2.7).

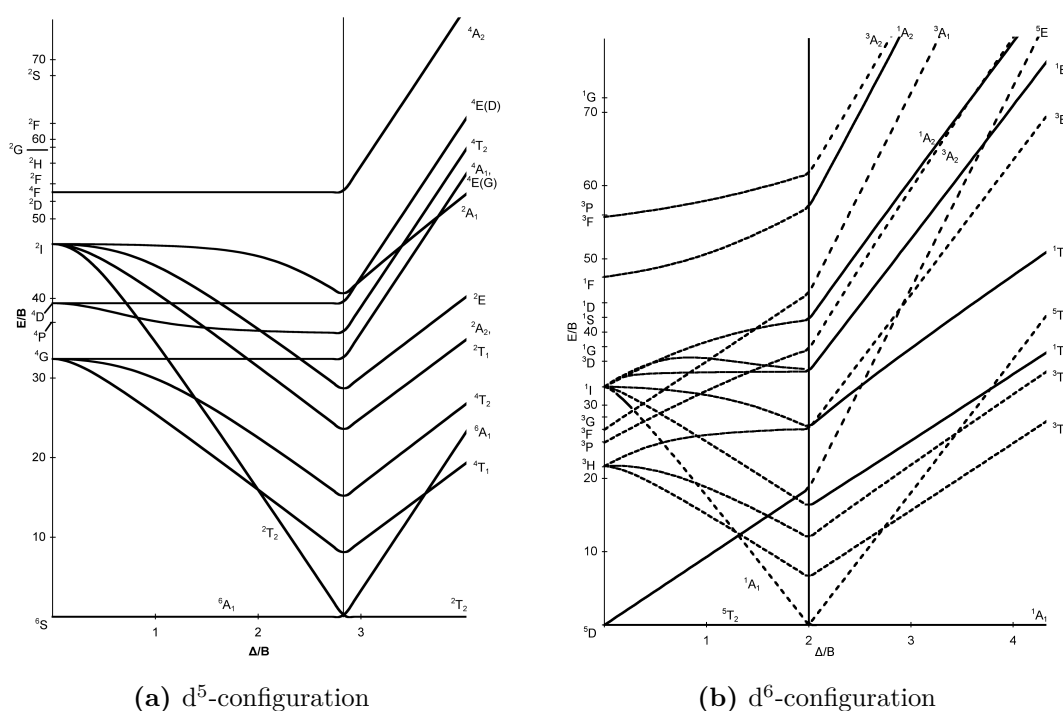


Figure 2.7: Tanabe-Sugano Diagrams

The plot shows the energy of the respective states in orders of the parameter B plotted versus the ligand-field strength, also in units of B .

2.1.4 Mechanism of the Spintransition

On a molecular level, the spin-crossover can be described as an intramolecular electron transfer process. The anti-bonding e_g -orbitals are more populated in the high-spin

state, so the average bond lengths between metal center and donor atom are shortened while undergoing the transition from high-spin to low-spin. The change can be in the magnitude from 100 pm to 200 pm, depending on the metal center.

The groundstate of spin-crossover compounds is always the one with the lowest free energy G , which is composed of the entropy S and the enthalpy H .

$$\Delta G = \Delta H - T\Delta S \quad (2.3)$$

Δ being the difference of the respective contributions in the high-spin and the low-spin state. The change in entropy ΔS has an electronic and a vibronic component. In an ideal octahedral environment, the high-spin state has a 15-fold degeneracy of the electronic states, while the low-spin state is only onefold degenerated. The vibrational entropy is also higher in the highspin state, for the bonds are being longer than in the low-spin state. The minimum of the low-spin potential is located slightly below the high-spin potential. The change in entropy becomes dominant at higher temperatures, thus favoring the high-spin state, while at lower temperatures, the enthalpy contribution favors the low-spin state.

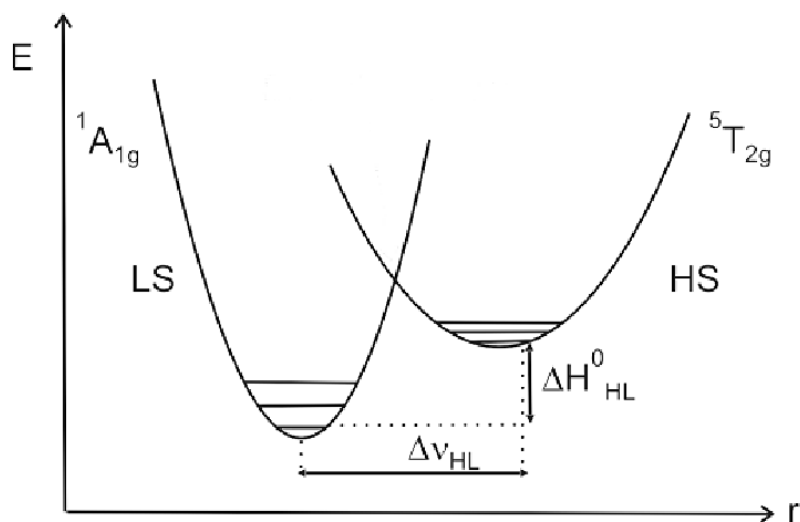


Figure 2.8: Schematic potential well for an iron(II)-spin-crossover system.

For iron(II) spin-crossover-systems, the change in enthalpy ranges from about 10-20 kJ/mol and the entropy-change from 50 to 80 J K⁻¹ mol⁻¹[6]. The change in

entropy can be attributed roughly one third to the electronic portion and two thirds to intramolecular vibrations.

2.1.5 Classification of Spin Transitions

Thermally induced spin transitions are usually plotted as the portion of the molecules in the high-spin state γ as a function of the temperature. The simplest way to measure such plots is to determine the temperature dependence of the molar susceptibility. The product of χT is constant when all molecules are in the same spin state. Therefore, $\gamma_{HS}=f(T)$ -plots can be derived from χT -measurements as followed:

$$\gamma_{HS} = \frac{\chi T - (\chi T)_{LS}}{(\chi T)_{HS} - (\chi T)_{LS}} \quad (2.4)$$

The prerequisite for differentiating between high-spin and low-spin state is the flipping of the spinstates happening on a slower timescale than the measuring method. Otherwise, spinstates can not be distinguished and the resulting measurement shows an averaged spinstate as a result. In solutions, the spin transition from high-spin to low-spin of each individual molecule is always gradual, following a standard Boltzman distribution of the spin states. In the solid state, cooperative interactions between molecules have to be taken into account, so the spin transitions can occur in several different ways. The spin-crossover can be classified by means of the course of the actual transition from high-spin to low-spin^[7].

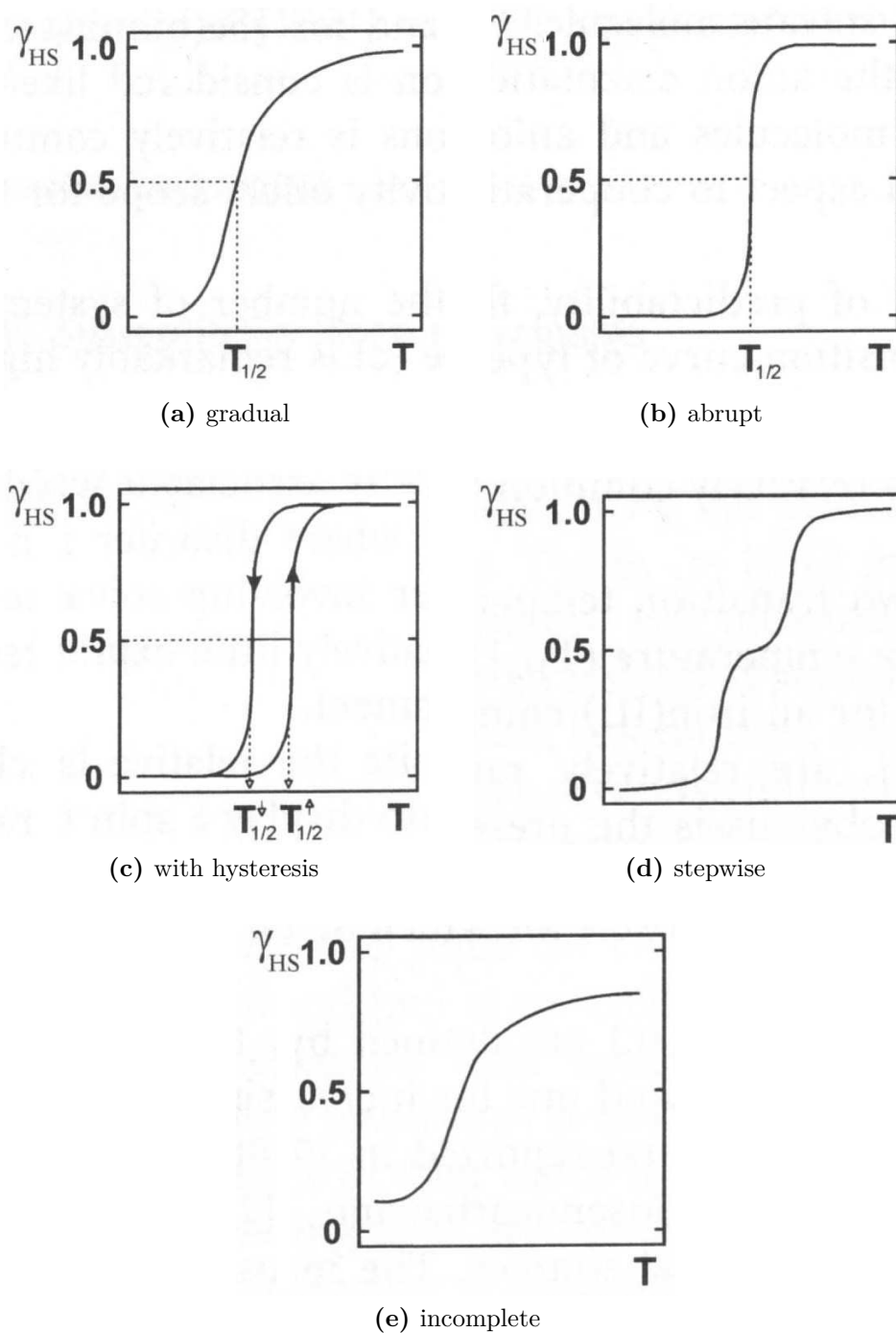


Figure 2.9: Different types of spin-crossover gradients

The remaining high-spin fraction at low temperatures is a common occurrence, with the help of powder-diffraction experiments it could be accounted to crystal defects or disordering of the lattice. The amount of the remaining high-spin fraction could be influenced by sample preparation, e.g. through extensive pestling of the powder.

2.1.6 External Influences

Apart from the change in temperature, there are other external stimuli that have an direct influence on the spin-crossover behaviour:

- While undergoing a spin transition, the metal-ligand bondlengths are changed, so by imposing a strong **pressure** on the crystal increases the temperature of the transition. For several octahedral cobalt(II) and iron(II) complexes that exhibit a thermal spin-crossover, pressures around 1GPa were utilised to induce a complete spin conversion, which was investigated with near-edge X-ray absorption spectroscopy (XANES). Several high-spin compounds that do not switch their spin state thermally required several GPa to influence the spin state^{[8][9][10]}. The reported spin changes were always complete, fully reversible and did not show any hysteresis.
- **External magnetic fields** execute a different influence on the more paramagnetic high-spin state than on the low-spin state. While the effect of static fields is rather limited (e.g. a shift in transition temperature of 2 K needs a field of 5 Tesla^[11]), pulsed fields (up to 32 Tesla) were shown to be more effective^[12].
- **External electric fields** have also been shown to have strong influence on the spin transition^{[13][14][15]} of Prussian Blue-analogons and cobaltocenes.
- **Chemical influences**, like the dilution of the spin-crossover compound in a crystal lattice of chemically similar compounds, which are unable to undergo a thermal spin change, shows very well the cooperative effects in the solid state, since the cooperativity can be effectively tuned by increasing dilution and thus forcing the spin-crossover molecules into an isolated behaviour similar to that in solution.

2.1.7 Mößbauer-Spectroscopy

Probably the most common method for the characterization of iron-containing substances is Mößbauer-spectroscopy. Since the discovery of the Mößbauer-Effect in

1958^[16] it has developed into a very important type of spectroscopy. The effect has been reported in 80 nuclides of 43 different elements, but 9 out of 10 publications deal with iron compounds. Apart from that, the isotopes ^{119}Sn , ^{121}Sb , ^{125}Te and ^{197}Au have been studied further.

The basic principle of Mößbauer-spectroscopy is the recoilless absorption of γ -radiation by the nucleus. Such nucleus in an excited state will relax back to its ground state and thus releasing the excess energy as a γ -photon. This photon can now be absorbed by another nucleus of the same composition which puts this nucleus into the same excited state as the emitting one. This phenomenon is called resonant absorption.

The Mößbauer-effect is only observable in the solid state, since here the energy of the emitted photon is decreased by the recoil which the nucleus experiences while emitting the γ -photon. This energy may be insignificant compared to the total energy of the photon (for iron: about 10^{-3} eV compared to 14.4 keV), but this is already six orders of magnitude bigger than the natural linewidth of the nuclear transition. This energy difference shifts the spectral emission which does now no longer overlap the spectral absorption and thus lacking the essential prerequisite for a resonant absorption. In addition to this, the molecules have high relative speeds in the gasphase and gives the emitted photon an additional energy about the magnitude of the recoil energy. This even further decreases the (already very small) possibility of a resonant process. In the solid state, the nuclei are not free to move but rather embedded in an unflexible grid. The recoil energy has a translational contribution, which can be neglected due to the vanishing mass of on nucleus compared to the whole crystallite. The recoil is transferred to the grid virtually in full as vibrational energy. With a certain probability there is no vibrational excitation during the emission or absorption of the γ -photons (these being the recoilless transitions).

The portion of these recoilless transitions is described by the Debye-Waller factor f , which is characteristic for each individual Mößbauer transition (e.g. $f=0.91$ for the 14.4 keV transition in ^{57}Fe). In Mößbauer measurements, the emission and absorption line have to overlap, which is achieved utilizing the Doppler effect. The emitting and the absorbing substance are in constant movement relative to each other with

a defined velocity, thus adding (or subtracting) a defined energy to the emitted γ -photons. In a standard experiment, the transmitting photons are then detected with respect to their relative velocities.

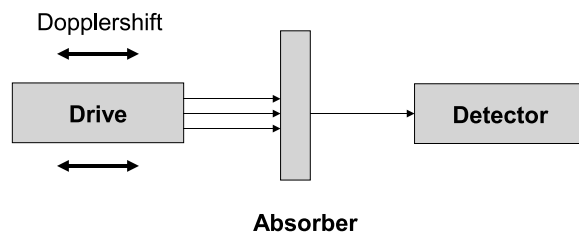


Figure 2.10: Schematic depiction of a standard transmission setup

Standard Mößbauer spectrometers contain a radioactive compound which is transformed via nuclear reactions into the excited state of the target absorber nucleus and relaxes under emission of γ -radiation into the ground state of the target nucleus. For ^{57}Fe the respective isotope would be ^{57}Co , which itself is prepared by deuterium bombardment of ^{56}Fe .

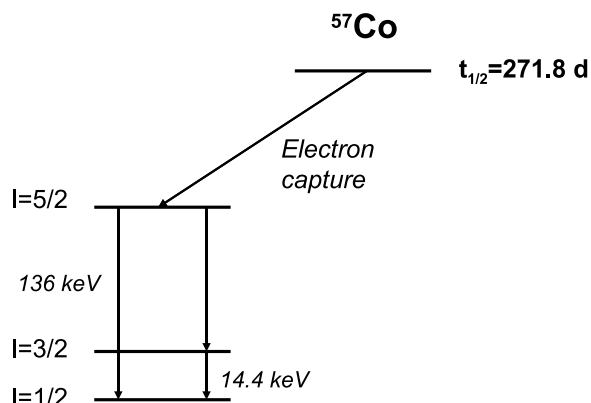


Figure 2.11: Radioactive decay of ^{57}Co

The ^{57}Co is transformed into ^{57}Fe in an excited state via electron capture and has a nuclear spin of $5/2$. The excited state can relax in two possible pathways: directly into the $I=1/2$ groundstate and emitting a 136 keV-photon or indirectly via the metastable $I=3/2$ state and a following relaxation into the ground state under emission of a 14.4 keV photon. The indirect transition is more favorable with a probability of about 85%. A comparatively long half life time of the radioactive isotope, a very small natural linewidth of the 14.4 keV transition and a high Debye-Waller factor makes

Mößbauer spectroscopy very applicable in the field of iron chemistry.

2.1.8 Density Functional Theory

When trying to understand and interpret spectroscopical results, quantum chemical methods offer valuable insights into mechanistic and energetic aspects of virtually ever chemical problem one could imagine. With the ongoing increase in available computing performance, theoretical methods have gained significant attention since the late 1980's. Within all the developed theories and techniques, density functional theory is of special value for the practical chemist, for it is able to deliver reliable results at affordable computational cost which can be compared with spectroscopical results, or can be used to devise reaction mechanisms.

All theoretical models include the Born-Oppenheimer separation and only focus on the electrons of a system, combining the behaviour of all cores in one potential. Wavefunction-based methods are all resulting in approximate results of the Schrödinger-equation. Originating from the work of Douglas Rayner Hartree and Vladimir Alexandrovitch Fock in the late 1920's^[17] this has been named the Hartree-Fock method (HF). The general assumption is that the exact wavefunction of any given system can be approximated by one Slater-determinant, thus a set of coupled equations can be derived to describe the set of orbitals. By solving this set of equations, one yields the HF-wavefunction and the overall energy of the system. The resulting energies (or spectroscopic properties for that matter) are always upper-bounds for the real values, since the HF-approximation completely neglects the electron-electron interactions. This renders the HF-method unfeasible for the examination of transition metal compounds or even biological systems. Nowadays, HF provides merely a starting point for more accurate calculations, for example coupled cluster or configuration-interaction methods. These so-called post-HF methods are very accurate in treating the electron-electron correlation, but for molecules composed of more than around 20-30 atoms, they are far too expensive in terms of calculational costs. In 1998 the Nobelprize in chemistry was awarded to Walter Kohn for his merits in developing the basis of modern density functional theory. In 1964, he and Ho-

hohenberg devised the Hohenberg-Kohn theorems^[18], which are the foundation of virtually all modern theoretical methods applicable to transition metal complexes or bio(in)organic molecules in general. DFT replaces the approximation of the wavefunction of all orbitals with the electron density as foundation, massively cutting down the complexity of the calculation. The electron density is described by only three independent variables for any given system, whereas the description of the wavefunction of any N-atomic system demands 3N variables.

- **First Hohenberg-Kohn-Theorem:** The total energy of any many-electron systems is a unique functional of its electron density.
- **Second Hohenberg-Kohn-Theorem:** The functional of the electron density is a minimum for the electronic ground state.

This way, the problem is reduced from approximating a many-body schrödinger equation to minimising an electron density functional. But a way how to calculate the electron density practically was not described, it was one year later that Kohn and Sham^[19] devised a feasible way to do so. They mapped the system of N interacting electrons onto a potential where the electrons were not interacting any more, thus making the resulting equations far more easy to solve. This was called the *Kohn-Sham-Formulation*.

2.1.9 DFT on Spin Crossover Compounds

The big challenge in the theoretical investigation of spin-crossover compounds is the correct handling of the electronic states. Since the prominent characteristic of compounds able to undergo a thermal spin-crossover is the very small energetic difference of the high-spin and the low-spin state, the electronic ground state is often misspredicted^[20]. The treatment of typical spin-crossover systems with ab-initio methods is too expensive at the moment (with regard to computational costs). Conventional Hartree-Fock calculations strongly favor a maximum number of unpaired electrons. Generalized gradient approximations (e.g. functionals like BP86) normally favor low-spin states. The combination of these gradient density functionals with a certain

amount of HF-exchange leads to a stabilisation of the high-spin states proportional to the percentage of HF-exchange that is taken into account.

2.2 Photoswitchable Systems

2.2.1 Natural Photoswitches

The most prominent photoswitchable molecule that comes to mind is retinal^[21], the aldehyde of vitamin A and the basis for vision in virtually all vertebrates. The process of sight involves a photoinduced *cis-trans* isomerisation of one C-C double bond in the highly light-sensitive 11-*cis*-retinal as an introductory step.

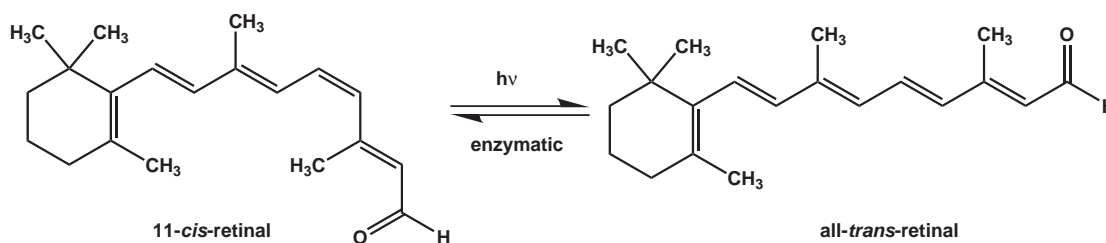


Figure 2.12: Photoisomerization of retinal

The retinal, which itself is coordinated to the enzymatically active site of a photoinactive protein, the opsin, forming the agglomerate rhodopsin. By photoisomerization, the retinal is transformed from the *cis*- to an all-*trans*-state, starting a cascading signal transduction inside the retina. The now bleached rhodopsin is hydrolyzed afterwards into the all-*trans*-retinal and opsin, but regenerated within several minutes by binding another 11-*cis*-retinal molecule. The all-*trans*-retinal is converted back to its 11-*cis*-state by enzymatic processes.

As usual, when dealing with the mimicry of biological processes for technical applications, the system to be explored has to be simplified very much.

2.2.2 LIESST Effect

The course of the spin-transition, regarding the thermal spin-crossover, is always the same, from high-spin at high temperatures to low-spin at lower temperatures.

The ratio of the two states depends only on the current temperature, making this physical phenomenon rather uninteresting in terms of molecular switching processes. But it was shown that by irradiating with intense laser pulses the high-spin state could be populated significantly for a short period of time ($<1\text{ms}$). The relaxation could be decreased significantly by lowering the temperature and thus affording a quantitative population of the high-spin state by irradiation with light in a visible wavelength^{[22][23]}. Keeping the system at low temperature, the created high-spin state was stable for a long period of time. The phenomenon was from now on referred to as **Light-Induced-Excited Spin State Trapping**, abbreviated LIESST-effect.

The effect can be explained with the help of the respective potential diagram.

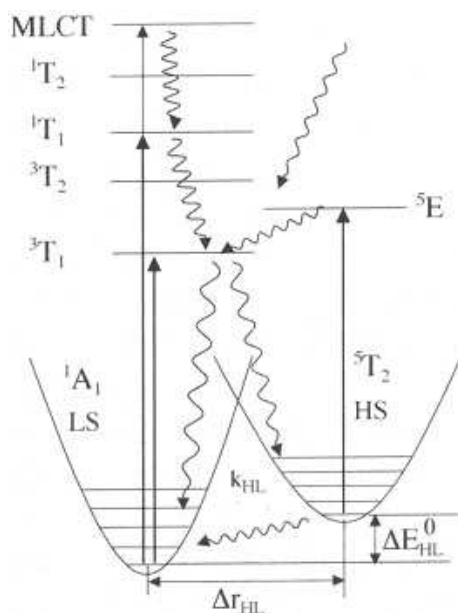


Figure 2.13: Potential wells for the HS and the LS state of an exemplary iron(II)-system

Irradiation with light in the green regime of the visible spectrum into the transition from an 1A_1 state to 1T_1 or 1T_2 , followed by two intersystem crossings into the respective triplett and then quintett state, the 5T_2 is being populated. The relaxation back into the ground state is spin- and parity-forbidden, therefore it cannot take place as a radiative process, but rather as non-adiabatic tunneling through the potential barrier. By exciting the 5T_2 high-spin state with light in the red regime, the 1A_1 state can be repopulated. This effect was designated the reverse-LIESST.

At first glance, this fulfills the prerequisite for an excellent opto-magnetical switch. Magnetic properties can be selectively and quantitatively switched from one state to another. But the big disadvantage is the limitation of all LIESST-processes to temperatures far below room temperature, the highest ever observed being around 130 K with respective lifetimes of well in the second-range. The problem with rising temperatures are the higher vibrational levels of the metastable high-spin state, which are more and more populated, which drastically increases the tunneling rate through the potential barrier.

At first there were only known examples containing iron(II)-centers that exhibited the LIESST effect. It was assumed the smaller changes in bondlength in e.g. Fe(III) or Co(II) spin-crossover compounds result in a much smaller energy barrier between the two states, thus resulting in a much higher tunneling rate from HS back to LS even at low temperatures. The metastable HS state was believed to have a half life time too small to be observable with conventional methods. The system investigated by far the most intensive in this field is $[\text{Fe}(\text{phen})_2(\text{NCS})_2]$. But finally, a Fe(III) spin-crossover compound was synthesized by Sato^[24] that also showed a well observable LIESST effect.

It was later shown that the metastable highspin state could also be populated at low temperatures in vacuum by irradiation with soft x-ray L-shell excitation^[25] (**S**oft-**X**-**R**ay **I**nduced **E**xcited **S**pin-**S**tate **T**rapping). A disadvantage of the SOXIESST apart from the demanding experimental setup is the occurrence of bond-cleavages during irradiation. A similar experiment with the electronic excitation of the K-shell, but at ambient conditions was performed with hard x-rays^[26], this was designated HAXIESST, for **H**ard **X**-**R**ay **I**nduced **E**xcited **S**pin **S**tate **T**rapping. Not only are there no observable bond-breaks after the irradiation, the spatial resolution of the shorter wavelength is increased.

Another way to generate a high-spin state out of seemingly low-spin-only compounds (having a rather strong ligand-field) is induced by the nuclear decay of ^{57}Co . The energy for this process is not generated by an external source, but rather by the energy-release by the transformation of ^{57}Co into ^{57}Fe through electron-capture from

the K-shell of the Co-nucleus^{[27][28]}. A high-spin cobalt(II)-complex was doped with ⁵⁷Co-centers and used as a mössbauer-source against sodium hexacyanoferrate as single-line absorber. At room temperature, the expected Fe high-spin species could be detected, but at lower temperatures, an additional high-spin species was observed. This was assigned to a metastable high-spin state generated by the excitation from the nuclear decay of ⁵⁷Co.

2.2.3 LD-LISC Effect

To make spin-crossover compounds a candidate for molecular switching applications, both states have to be stable at room temperature. In order to achieve this, the location, where the photoexcitation takes place, has to be shifted away from the metal center of the complexes due to aforementioned limitations of LIESST. Roux and Boillot therefore developed spin-crossover systems with ligands containing a photoisomerizable C-C doublebond, which undergoes a *cis-trans* isomerisation upon irradiation^[29]. The change in ligand geometry changes the strength of the ligand-field exerted on the metal center and thus the ligand field splitting of the *d*-orbitals, driving the whole system further towards a low-spin configuration. This was further on designated the **Ligand-Driven Light-Induced Spin-Change** or abbreviated LD-LISC in respective papers. The advantage in the design of such systems is the decoupling of the spin-crossover inducing ligand sphere and the fine-tuning of the optical properties of the photosensitive ligands.

The system investigated by Boillot was composed of four styrylpyridines coordinated via the pyridine nitrogen to an iron(II)-center.

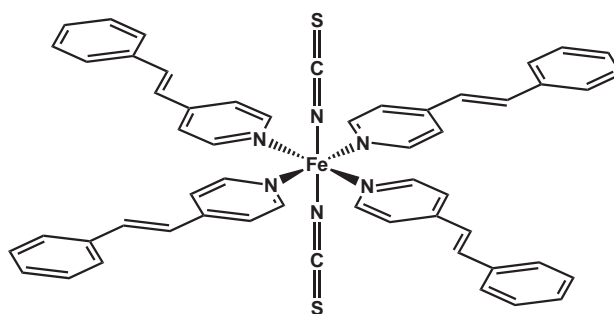


Figure 2.14: Styrylpyridine Complex investigated by Boillot

It was shown that the complex had different spin-transition behaviour when the ligands were properly irradiated and thus changed their geometry from *trans* to *cis*. While the *trans*-form of the complex exhibited a thermal spin-crossover, the irradiated *cis*-form remained in the high-spin state. Several other systems employing this kind of switching were developed afterwards^{[30] [31] [32]}.

2.2.4 Azobenzene-Isomerisation

The azobenzene is considered the archetype of a switchable molecule.

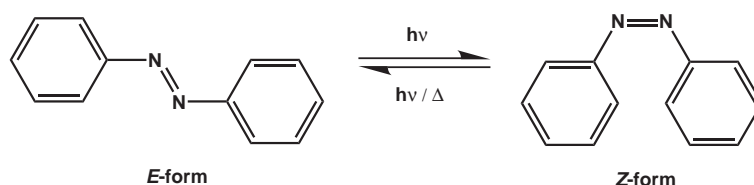


Figure 2.15: E/Z-Isomerization of Azobenzene

While being present in a wide spectrum of possible applications, the exact mechanism of the *cis-trans*-isomerization in azobenzene and its derivatives is not completely understood and a topic of ongoing research. There are three distinct isomerisation pathways that are discussed in the literature^{[33] [34] [35]}.

- **Inversion:** The inversion of the phenylgroup adjacent to one of the azo-nitrogen atoms, similar to the tunneling of the nitrogen atom in ammonia.
- **Concerted Inversion:** The synchronous inversion at both nitrogen atoms via a linear transition state

- **Rotation:** Partial breaking of the N-N double bond and subsequent out-of-plane rotation of one of the phenyl substituents.

2.2.5 Alternatives to the E/Z-Isomerization of Azobenzene

Apart from the *cis-trans* isomerisation of stilbenes or azobenzene-derivatives, there are several other interesting photosensitive functional groups that are under investigation as possible candidates for molecular switching.

A class of molecules suitable for being used as molecular switches are spiropyranes 2.16, which can be switched with light.

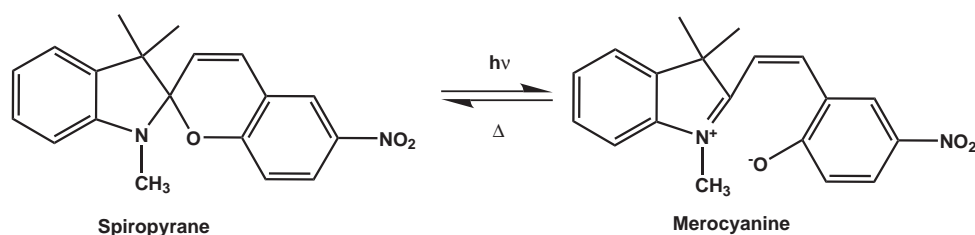


Figure 2.16: Ring-opening in a spiropyran

They undergo an electrocyclic reversible ring-opening, which transforms back to the closed state thermally as well as photoinduced using a different wavelength^{[36] [37] [38] [39]}.

The fulgides shown in figure 2.17 can also be switched between two thermally stable states via light-induced pericyclic reactions^{[40] [41] [42] [43]}.

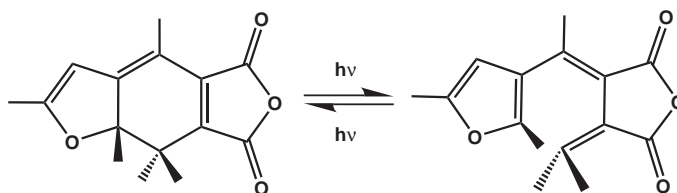


Figure 2.17: Ring-opening in a fulgide

Diarylethenes and Dithienylethenes 2.18 have recently been used as ligands in transition metal complexes^{[44] [45] [46] [47]}.

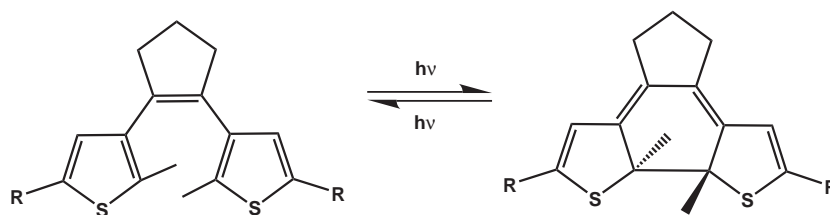


Figure 2.18: Ring-opening in a diarylethene

2.2.6 Organic Paramagnetism

The characteristics of inorganic compounds suitable for switching processes have been discussed in the previous chapters. However, there is also the field of purely organic molecules that exhibit switchable paramagnetic behaviour, which also has to be mentioned when talking about molecular magnetism. This class of organic paramagnets was first reported in 1991^{[48][49]}, basing on nitronyl nitroxides.

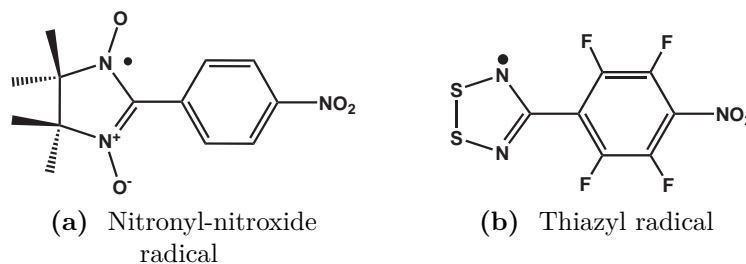


Figure 2.19: Examples for organic ferromagnets

What they have in common with the compounds exhibiting LIESST, back when they were discovered and considered as possible switches, are the very low temperatures, at which the experiments have to be performed. The first reported organic ferromagnet (figure 2.19a) shows bistability at a maximum of 1.5 K. The intense work on this promising field led to a raise in temperature up to about 40 K for sulphur-based radicals (figure 2.19b)^{[50][51]}. The combination of similar organic paramagnets as ligands with transition metal centers is another approach towards the design of molecular-level switching. Detailed reviews covering the field of strictly organic paramagnets have been published^{[52][53]}.

2.3 Molecular Switches

2.3.1 Technical Applications

Almost four decades ago, Intel co-founder Gordon E. Moore predicted the doubling of transistor-density on silicon basis every year for the next years^[54], nowadays often being referred to as **Moore's Law**. Current mass-production of silicon-based microarchitectures have a feature size of 45 nm, and techniques producing even smaller structures are already announced. But this so-called **top-down** approach in the fabrication of electronics, albeit all its breakthroughs in pushing the miniaturization forward, is facing a somewhat natural barrier in the fact, that the production procedures cannot be adapted to generate structures smaller than a certain limit.

For example, the magnetic domains on conventional harddrives cannot be fabricated smaller than a certain size, since they need a minimum domain size to uphold the information. Otherwise, the thermal energy would be already enough to remove the arrangement of the single spins inside the domain, thus erasing the information (*Superparamagnetic Limit*). Or the lithographic processes in producing the circuitry of silicon-based computer-chips are bound to the wavelength of the light, with which the features are molded on the silicon-wafers.

These problems have lead to an increased research interest in the so called *bottom-up* approach, where the desired structures are assembled from the smallest thinkable unit, e.g. polymer chains, molecules or even single atoms.

2.3.2 Switches

The feature all switches, molecular or not, do have in common, is bistability with two distinctive forms, being designated YES or NO, ON or OFF, 1 or 0. In one form the switch must be able to perform a function in that the other form lacks completely. In terms of molecular switching, these two distinct states could be e.g. the occupied and unoccupied form of a receptor molecule, two oxidation-states for redox-active compounds or an acid and its conjugate base, which can be reversibly converted into

each other^[55].

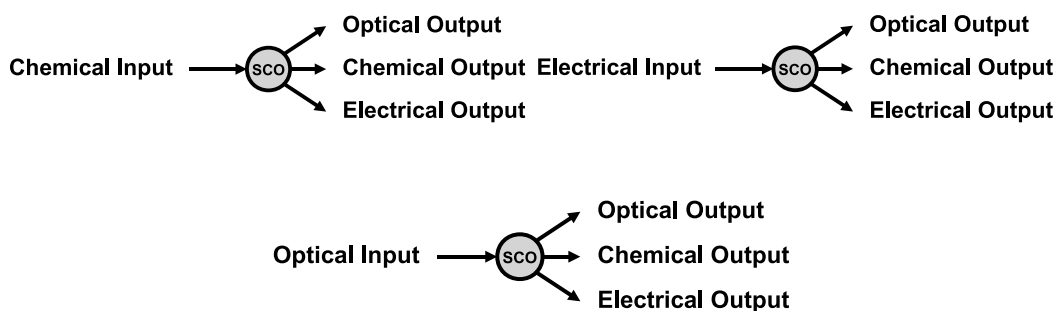


Figure 2.20: Logic Gateways SCO complexes^[55]

This way, it is possible to use such systems as logic NOT gates, that have one input and one output (figure 2.20). There is a number of studies dealing with the usage of such systems, e.g.^[56] ^[57]. A huge number of systems are suitable for being used as a NOT gate, but have not been tested extensively for their switching behaviour.

2.3.3 Displays

Especially transition metal complexes that relax with high quantum yields from the lowest triplet-state to the singlet ground-state. These *triplet-emitters* are promising candidates for their use in light emitting diodes^[58] (*OLED*), since their luminescence-efficiency is (at least in theory with neglect of radiationless deactivation of the excited state) up to four times higher than the conventional singlet-emitters used in standard OLEDs using purely organic emitters.

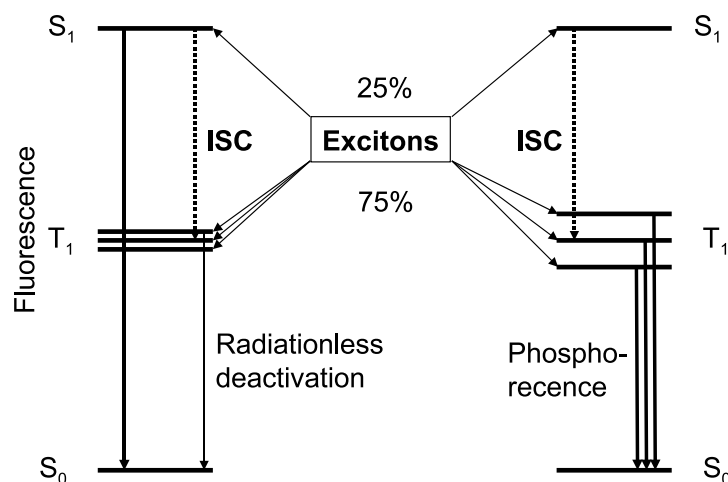


Figure 2.21: Jablonski-diagram of organic and organometallic LED^[58]

Comparing the spin statistics of exciton-relaxation in a purely organic emitter (left side) with an emitter that has a transition metal incorporated (right side), the advantage in using such systems which show phosphorescence can be explained. The recombination of an electron and the corresponding hole inside the diode (=exciton) leads to 25% population of the singlet-state ($S=0$, $M_S=0$) and 75% of the triplet-state ($S=1$, $M_S=0, \pm 1$). The pure organic systems thus convert 75% of the energy to heat, since only fluorescence from the singlet-state is possible. Due to the faster inter-system-crossing of the organometallic system, 100% of the exciton-energy is converted to light. Spin-Crossover compounds have a huge potential in this field, since their electronics is rather well understood, and the gap between the different electronic states can be effectively tuned by choosing the proper ligand setup.

3 Coordinated Azo-functions

3.1 Switching Concept

The first step in synthesizing a switchable coordination-compound was to gain better understanding of the different coordination modes of azo-ligands. Since the azo-group itself is capable of coordinating to metal-centers, the coordination of pyridine and phenolates as additional coordination sites in *ortho*-position to the azo-function were investigated. As phenolate-donors, the ligands 4-methyl-2-(phenyldiazenyl)phenol (*azocresol*) and 4-methyl-2-(phenyldiazenyl)naphthol (*azonaphthol*) were to be synthesized and coordinated to iron.

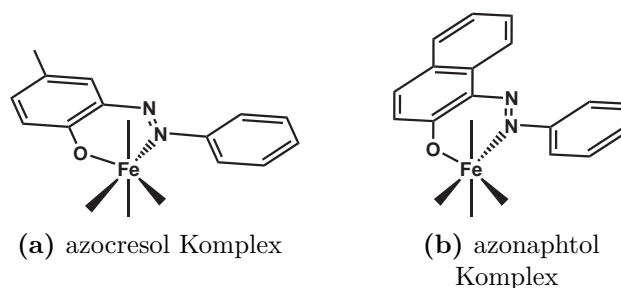


Figure 3.1: Azophenol Ligands

In addition to these phenolates, the ligand 2-(phenyldiazenyl)pyridine was synthesized and coordinated as well.

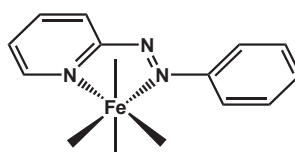


Figure 3.2: Complex with 2-phenylazopyridine

The ligand 2-pyridylazoresorcinol has the phenolate- and the pyridine-donor site combined and provides the additional possibility of influencing the coordination number of the metal-center.

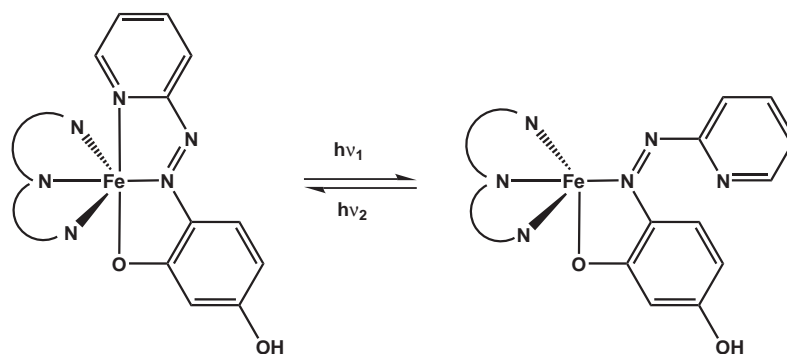


Figure 3.3: Phenylazoresorcinol-based Switch

The other coordination sites unoccupied by the photoswitches were to be filled with photoinactive pyridine-donors such as bipyridine, phenanthroline or terpyridine, since these ligands are well known to likely form spin-crossover compounds.

3.2 Design

As laid out in the introduction, to be suitable for any switching application, the system has to bear a photosensitive functionality somewhere in the ligand sphere, and it should undergo a thermal spin transition, so that way, the optical stimulus of irradiation can be connected to a magnetic information, since complexes where the difference between the two possible spin-states is in the order of magnitude of the thermal energy, the probability of successfully switching the magnetic state of the central atom is far higher than in standard highspin- or lowspin-compounds.

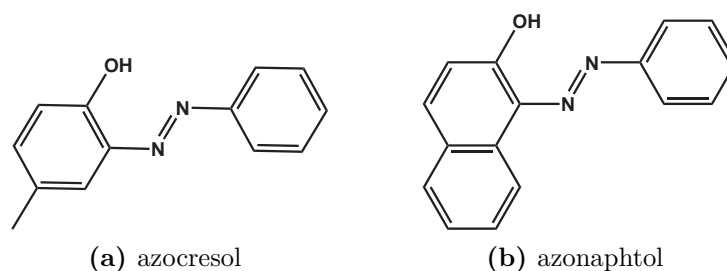


Figure 3.4: Azophenol Ligands

The azophenol-ligands were synthesized using a standard azo-coupling of an *in-situ* generated diazonium-cation and an activated aromatic system. The iron(II)-complexes were prepared by reacting three equivalents of the deprotonated ligands (deprotonated with sodium methoxide) with freshly prepared iron(II) chloride tetrahydrate in methanol. The compounds precipitated and were pure according to Mößbauer-spectra and elemental analysis.

Since electron-deficient aromatic systems like pyridines are not susceptible to the azo-coupling via the diazonium-cation, a different reaction had to be used.

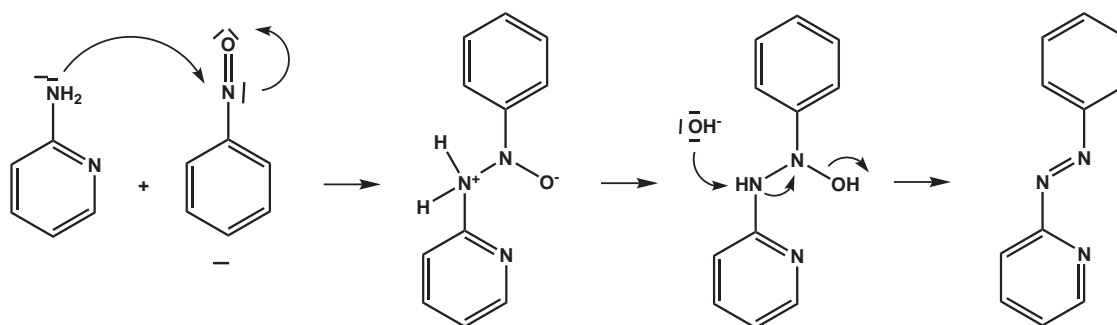


Figure 3.5: Base-catalyzed azocoupling of nitroso-and amino group

The "Mills-Reaction" couples an aromatic amine with an adequately functionalized nitroso-derivative. The nitroso-function is initially attacked by the amine in a nucleophilic fashion. This intermediate rearranges to a substituted hydrazone, which is able to eliminate water under alkaline as well as under acidic conditions, thus leading to the desired azobenzene-derivative.

Another switchable system was designed using 4-(2-pyridylazo)-resorcinol (Figure 3.6), in analogy to the similar coordination sphere iron(III)-complex that was first proven to exhibit LIESST.

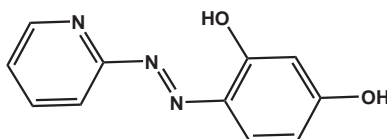


Figure 3.6: Phenylazoresorcinol-Ligand

A homoleptic iron(II)-complex was synthesized by reacting 2 equivalents of the py-

ridylazoresorcinol with iron(II)-hexaaquo-tetrafluoroborate in acetonitrile. The phenols were deprotonated with sodium methoxide. Also the synthesis of a heteroleptic compound with photoinactive coligands was attempted, using terpyridine, 2,2'-bipyridine and 1,10-phenanthroline as coligands. But according to elemental analysis and Mößbauer spectroscopy, no defined products were obtained, but rather mixtures of several possible combinations,

Since the Mößbauer-spectra of the homoleptic iron(II)-compound showed an unusual residue at low temperatures, which indicated some kind of by-product formed during the complex synthesis, it was tried to selectively methylate the second phenolate-function of the PAR-ligand, so coordination or the oxidation to the diketone would be hindered.

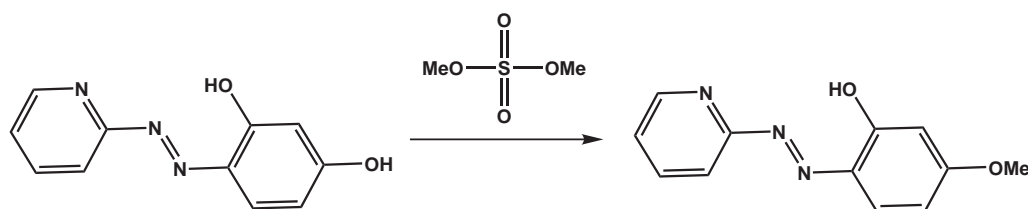


Figure 3.7: Methylation of the phenolate trans to the azofunction

The "unnecessary" phenol-function was to be reacted with dimethyl sulfate^[59] selectively in *trans*-position to the azo-group. The spectroscopical analysis of the reaction product showed no selective methylation of the phenol *trans* to the azo-function, but rather a mixture of not substituted and one- and two-fold substituted products which were unseparable with the chromatographical methods at hand.

3.3 Results

3.3.1 Optical Switching

Ligand Switching

The UV-irradiation experiments with 2-phenylazopyridine have already been performed elsewhere^[60]. For the synthesized azophenol-ligands, the UV-spectra of the

azocresol-derivative are depicted representatively, since the switching behaviour of azocresol and azonaphtol is virtually the same.

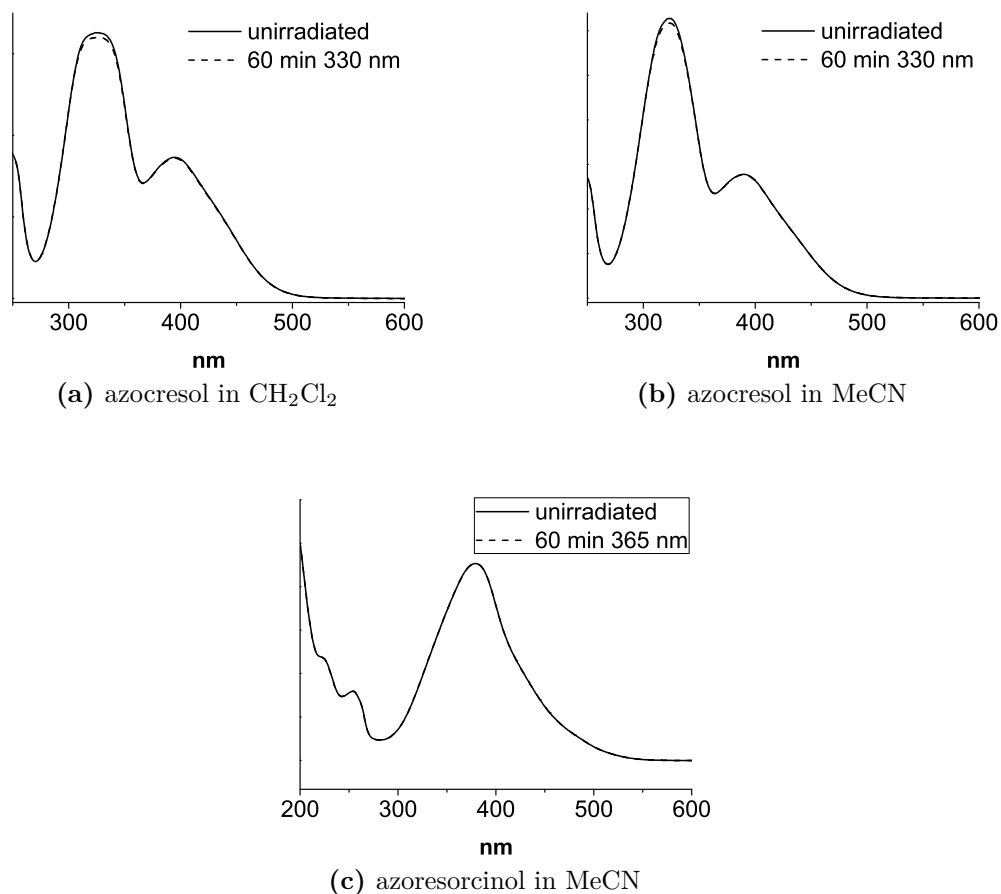


Figure 3.8: UV/Vis-spectra of azophenol-ligands

The three azophenols all showed very little (azocresol, azonaphtol) or no (azoresorcinol) effects upon irradiation. Other solvents did not change this fact. The poor switchability is probably due to the fact that one of the two lone-pairs of the azo-group is pre-oriented towards the phenol-function and thus blocking effectively the isomerisation process.

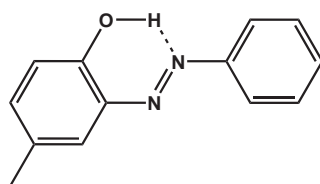


Figure 3.9: Hydrogen-bonding in azophenols

The azoresorcinol-ligand could not be influenced by irradiation at all, its spectra remained completely unchanged.

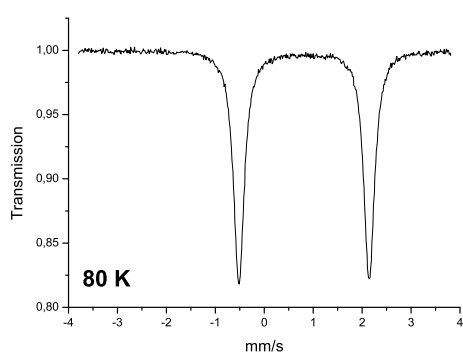
Complex Switching

The complexes were irradiated despite the rather small switching effects observed in pure ligand solutions, to investigate if the deprotonated, coordinated azophenol-ligands would be more susceptible towards irradiation.

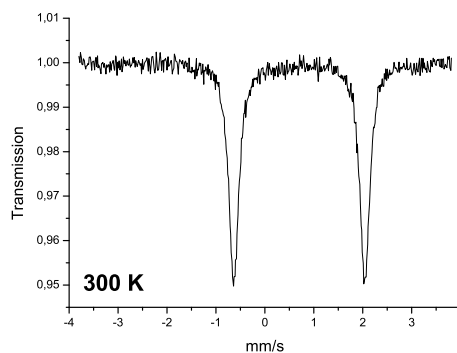
The complexes all showed no switchability at all in the UV/Vis spectra. The samples were dissolved in various solvents and irradiated with the wavelengths of the π - π^* -transitions of the coordinated azo-ligands.

2-(phenyldiazenyl)pyridine-complexes

The spectra of the two-fold substituted iron(II)-2-(phenyldiazenyl)pyridine showed a high-spin-state at room temperature as well as at liquid nitrogen temperature. No signs of an onsetting thermal spin crossover were detected.



(a) $\delta_{IS}=0.92\text{mm/s}$; $\Delta_{EQ}=2.66\text{mm/s}$



(b) $\delta_{IS}=0.82\text{mm/s}$; $\Delta_{EQ}=2.68\text{mm/s}$

Figure 3.10: Mössbauer-spectra of $[\text{Fe}(\text{pap})_2\text{Cl}_2]$

The homoleptic three-fold substituted iron(II)-complex is a pure lowspin-complex at both measured temperatures, leaving no possibility of a thermal spin crossover at lower temperatures.

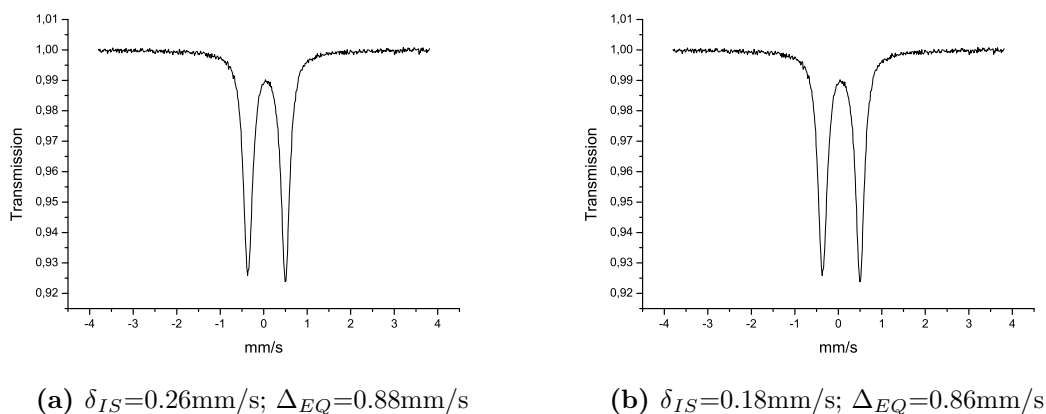


Figure 3.11: Mößbauer-spectra of [Fe(pap)₃](BF₄)₂

Phenylazoresorcinol

The homoleptic iron(II)-complex with phenylazoresorcinol shows a typical iron(II)-lowspin doublet with a small quadrupole splitting.

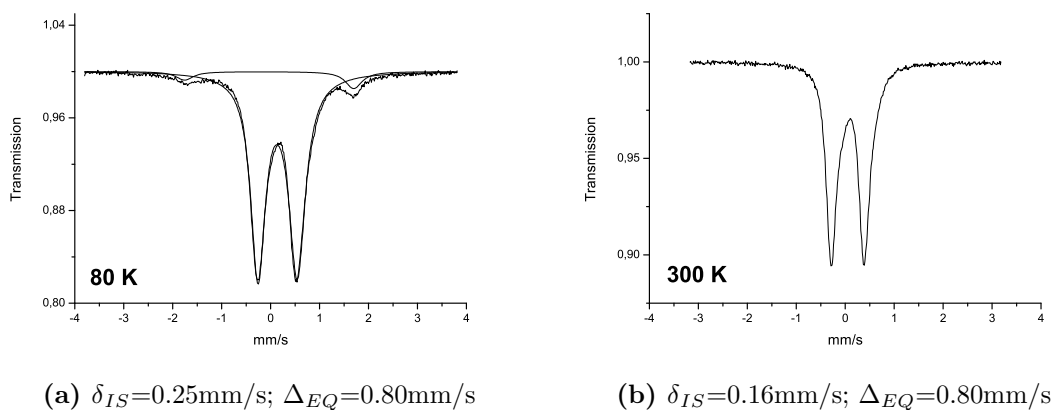


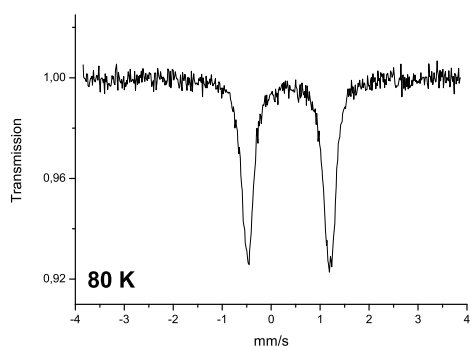
Figure 3.12: Mößbauer-spectra of [Fe(PAR)₂]

The additional signal at 80 K was assigned to an iron(III)-lowspin species, possibly formed during synthesis. The fact that the signal is invisible at room temperature also supports this assumption, since iron(III)-compounds show a fast relaxation and

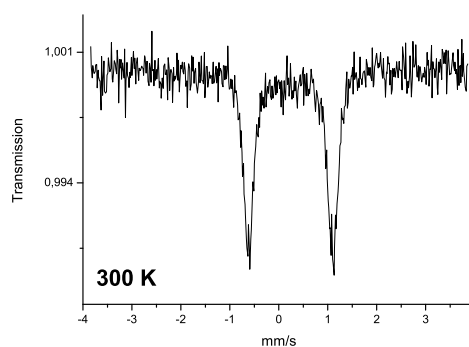
therefore very broad signals at higher temperatures.

Phenyldiazenyl-phenolates

The spectra of the two azophenolate-compounds also show now spin-transition at all.



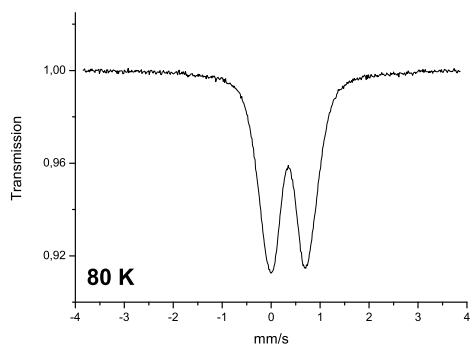
(a) $\delta_{IS}=0.47\text{mm/s}$; $\Delta_{EQ}=1.68\text{mm/s}$



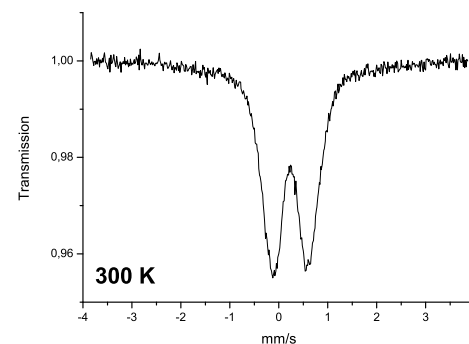
(b) $\delta_{IS}=0.36\text{mm/s}$; $\Delta_{EQ}=1.72\text{mm/s}$

Figure 3.13: Mößbauer-spectra of $[\text{Fe}(\text{azonaph})_3]$

Both complexes show the same temperature-dependent increase in the isomer-shift, while the quadrupole-splitting remains the same. The azonaphthol-complex is in the lowspin-state, while the azocresol-complex is an iron(III)-highspin. The larger aromatic system in the naphthol-derivative is already enough to change the spin-state of its complex.



(a) $\delta_{IS}=0.48\text{mm/s}$; $\Delta_{EQ}=0.74\text{mm/s}$



(b) $\delta_{IS}=0.35\text{mm/s}$; $\Delta_{EQ}=0.74\text{mm/s}$

Figure 3.14: Mößbauer-spectra of $[\text{Fe}(\text{azocresol})_3]$

The systems investigated in this chapter all proved to be not suitable for switching purposes. The irradiation of the complexes was unsuccessful in all conducted experiments. This leads to the conclusion that the switching-function must not be otherwise occupied in chemical bonds, since this completely eliminates the isomerisation-process.

3.4 Syntheses

3.4.1 Synthesis of 4-methyl-2-(phenyldiazenyl)phenol



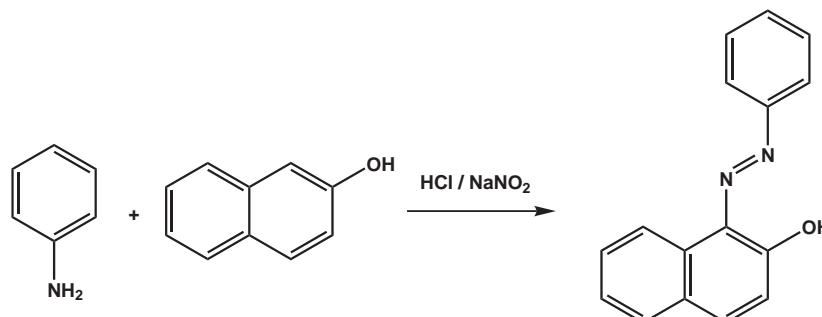
3.7 g aniline were dissolved in 20 mL of half-concentrated hydrochloric acid. 2.8 g of sodium nitrite were dissolved in the minimum amount of water. 2.6 mL (2.7 g) *p*-cresol were dissolved in 20 mL of 10% aqueous sodium hydroxide. All solutions were cooled to 0°C with an ice-bath. The sodium nitrite solution was slowly added to the aniline under vigorous stirring and cooling. The mixture was stirred at 0°C for 30 min. The freshly diazotised aniline was now added dropwise to the *p*-cresol. The mixture was stirred for another 30 min and allowed to warm to room temperature. The precipitate was filtered off and washed twice with water.

Elemental analysis	C	H	N
Calculated	66.66	4.73	11.96
Found	66.02	4.55	12.28

^1H NMR (400 MHz, CD_2Cl_2) δ = 12.57 (s, 1H), 7.87 (ddd, J = 4.8, 3.9, 2.2 Hz, 2H), 7.77 – 7.73 (m, 1H), 7.57 – 7.45 (m, 3H), 7.18 (dd, J = 8.4, 2.3 Hz, 1H), 6.94 – 6.89 (m, 1H), 2.38 (s, 3H).

^{13}C NMR (110 MHz, CD_2Cl_2) δ = 209.43, 150.63, 137.06, 134.29, 132.88, 131.06, 129.35, 122.12, 117.72, 20.00.

3.4.2 Synthesis of 4-methyl-2-(phenyldiazenyl)naphthol



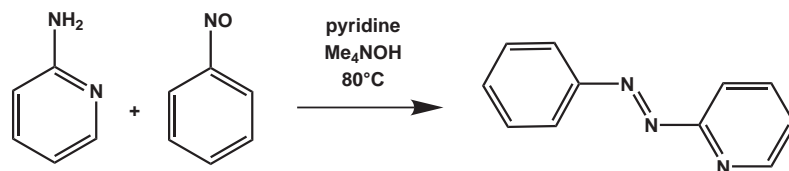
The synthesis was carried out in analogy to the described procedure for 4-methyl-2-(phenyldiazenyl)-phenol, but instead of *p*-cresol, a solution of 5.76 g of β-naphthol in 20 mL of 10% aqueous sodium hydroxide was used as coupling partner for the diazotised aniline.

Elemental analysis	C	H	N
Calculated	71.11	4.10	10.37
Found	70.24	3.88	11.02

¹H NMR (400 MHz, CD₂Cl₂) δ = 8.55 (d, J = 8.3 Hz, 1H), 7.74 (ddd, J = 16.3, 8.6, 5.2 Hz, 3H), 7.64 – 7.44 (m, 4H), 7.38 (tdd, J = 7.1, 1.2, 0.6 Hz, 1H), 7.35 – 7.27 (m, 1H), 6.84 (d, J = 9.4 Hz, 1H).

¹³C NMR (110 MHz, CD₂Cl₂) δ = 170.36, 145.35, 139.57, 133.55, 129.93, 129.54, 128.74, 128.56, 128.13, 127.58, 125.60, 124.34, 121.58, 118.75.

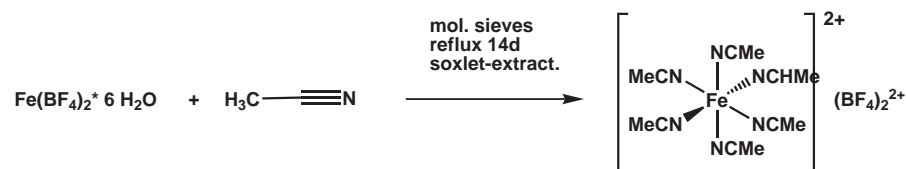
3.4.3 Synthesis of 2-(phenyldiazenyl)pyridine



To a solution of 25 mL of a 60 wt % of tetramethylammoniumhydroxide and 2.00 g 2-aminopyridine in 25 mL of pyridine was added over a period of 60 min a solution of 3.00 g nitrosobenzene in 50 mL of pyridine at a temperature of about 80° C. After that, the solution was allowed to cool to room temperature. The mixture was extracted three times with 50 mL of toluene each. The organic extracts were dried over natriumsulphate and the solvent was removed *in vacuo*. The product was purified by column chromatography using silica gel and a 2:1 mixture of cyclohexane and ethylacetate as eluent. The phenylazopyridine was observable as a deep-red fraction on the silicagel, so no TLC was necessary to distinguish the product from impurities.

Elemental analysis	C	H	N
Calculated	72.11	4.95	22.94
Found	71.67	5.06	23.24

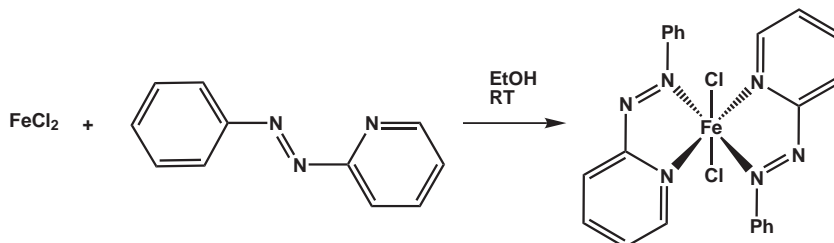
¹H NMR (400 MHz, CDCl₃) δ = 8.74 (dd, *J* = 4.7, 1.0 Hz, 1H), 8.09 – 8.02 (m, 2H), 7.94 – 7.87 (m, 1H), 7.83 (d, *J* = 8.0 Hz, 1H), 7.59 – 7.48 (m, 3H), 7.44 – 7.37 (m, 1H).

3.4.4 Synthesis of $[\text{Fe}(\text{CH}_3\text{CN})_6](\text{BF}_4)_2$ 

4.9 g of iron(II)-hexaaquo tetrafluoroborate were dissolved in 120 mL of dry and degassed acetonitril inside a soxleth-aparatus. The extractor was filled with freshly activated molecular sieves (pore size 4A). The solution was then refluxed for 10 days under inert conditions. The volume of the solution was reduced *in vacuo* to about half of its original volume. 50 mL of fry diethylether were added, and a slight green solid precipitated, which was filtered, washed three times with diethylether and dried several hours in vacuum.

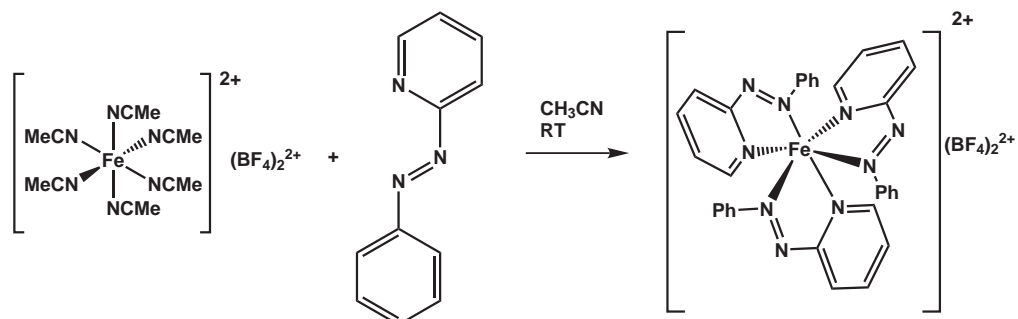
Elemental analysis	C	H	N
Calculated	30.29	3.81	17.66
Found	24.25	3.69	13.99

3.4.5 Synthesis of $[\text{Fe}(2\text{-(phenyldiazenyl)pyridine})_2\text{Cl}_2]$



127 mg iron(II) chloride and 366 mg 2-phenylazopyridine were dissolved in 5 mL ethanol each. The ligand was added dropwise to the well stirred iron chloride solution. Stirring was continued at room temperature over night, when a dark green solid precipitated, which was filtered, washed with cold ethanol and dried in vacuum for several hours.

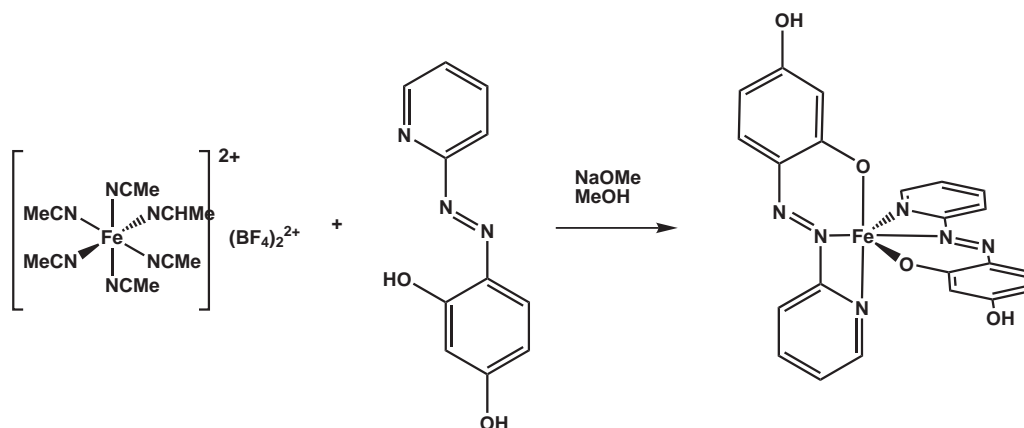
Elemental analysis	C	H	N
Calculated	53.58	3.68	17.04
Found	53.19	3.79	17.13

3.4.6 Synthesis of $[\text{Fe}(\text{2-(phenyldiazenyl)pyridine})_3](\text{BF}_4)_2$ 

714 mg of iron(II)-hexakisacetonitrile tetrafluoroborate were dissolved in 10 mL of dry acetonitrile. To this, a solution of 2-phenylazopyridine dissolved in 10 mL of acetonitrile was added dropwise. The mixture was stirred for two hours, the volume of the solvent was reduced and diethylether was added. The mixture was stored at -40°C over night, when a blue solid precipitated, which was filtered and dried in vacuum for several hours.

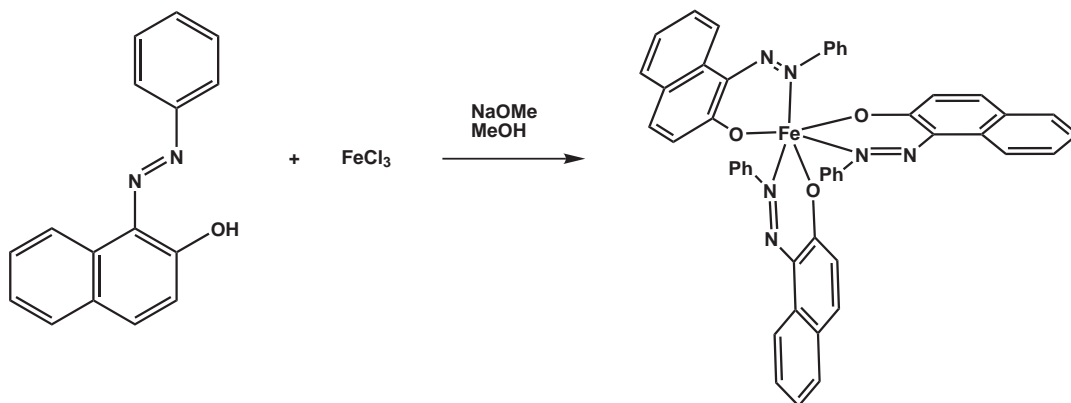
Elemental analysis	C	H	N
Calculated	50.87	3.49	16.18
Found	50.28	3.34	16.19

3.4.7 Synthesis of $[\text{Fe}(4\text{-(pyridin-2-yl diazenyl)-resorcinol})_2]$



430 mg iron(II)-hexakisacetonitrile tetrafluoroborate were dissolved in 20 mL of acetonitrile. 430 mg 2-pyridylazoresorcinol were suspended in 50 mL methanol and treated with 216 mg sodium methanolat in 15 ml of methanol. The ligand solution was added dropwise to the iron-solution and stirred at room temperature over night. The solution was evaporated to dryness and taken up in 10 mL of ethanol. After addition of 30 mL diethylether, a green solid precipitated, which was washed with diethylether and dried several hours in vacuum.

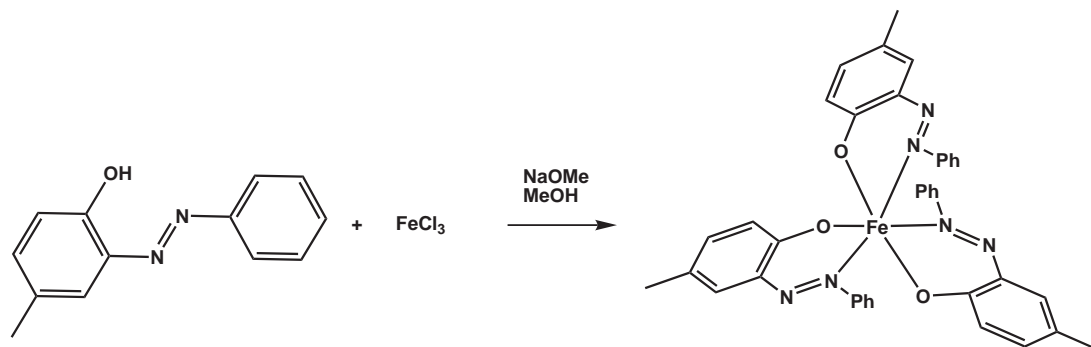
Elemental analysis	C	H	N
Calculated	54.57	3.33	17.35
Found	55.89	4.01	16.51

3.4.8 Synthesis of [Fe(4-methyl-2-(phenyldiazenyl)naphtol)₃]

745 mg of 4-methyl-2-(phenyldiazenyl)-1-naphthol were suspended in 30 mL of methanol. 70 mg metallic sodium were dissolved in 20 mL methanol and subsequently added to the ligand and stirred for an hour. 160 mg iron (III) chloride were meanwhile dissolved in 10 mL methanol. The deprotonated ligand was added dropwise to the metal solution. A brown precipitate formed, which was filtered off and dried in vacuum.

Elemental analysis	C	H	N
Calculated	72.28	4.17	10.54
Found	71.87	3.98	11.02

3.4.9 Synthesis of [Fe(4-methyl-2-(phenyldiazenyl)phenol)₃]



The synthesis was carried out analog to the procedure with the naphthol-based azo-ligand. This time, 640 mg of 4-methyl-2-(phenyldiazenyl)-phenol were suspended in 30 mL of methanol. 70 mg metallic sodium were dissolved in 20 mL methanol and subsequently added to the ligand and stirred for an hour. 160 mg iron (III) chloride were meanwhile dissolved in 10 mL methanol. The deprotonated ligand was added dropwise to the metal solution. A dark brown precipitate formed, which was filtered off and dried in vacuum.

Elemental analysis	C	H	N
Calculated	67.93	4.82	12.19
Found	68.52	5.61	11.49

4 Azopyridines

4.1 Design of a switchable SCO-complex

4.1.1 Salten-type complexes

A different approach towards the preparation of molecular switches presented in this work was inspired by a family of spin crossover compounds described in the literature. First synthesized in 1985 by Maeda et al.^[61], the five-coordinate ligand 4-azaheptamethylene-1,7-bis(salicylideneimine) (**salten**) offers the possibility of selectively substituting one position at an iron(III)-center, the others being occupied by the photochemically inert salten-ligand. When the sixth coordination-site is substituted with a pyridine-ligand, the iron(III)-compounds exhibit thermal spin crossover.

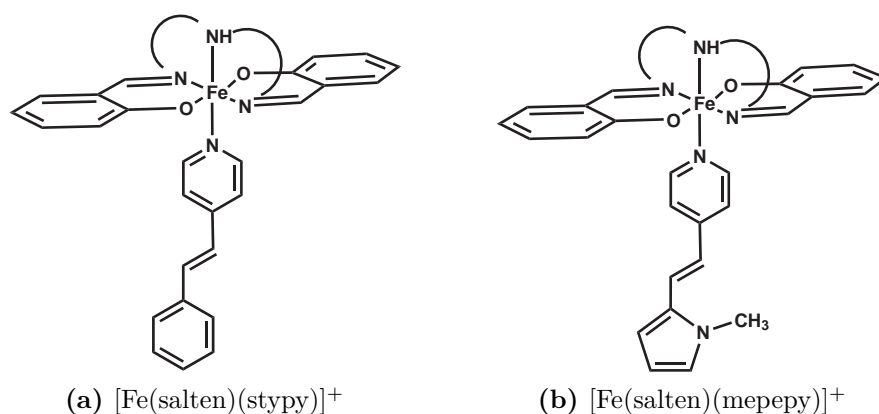


Figure 4.1: Literature-known Systems

If the pyridine is carrying a photoswitchable compound, the ligand-field of the iron-

center can be influenced by irradiation. This was done with two stilbenes (see figure 4.1, the 4-styrylpyridine (**stypy**)^[29], and the 4-(2-(1-methyl-pyrrol-2-yl)-vinyl)-pyridine (**mepepy**)^[30], as shown in figure 4.1. Using a salt-metathesis with sodium tetraphenylborate in methanol, the chloride-ligand from e.g. [Fe(salten)Cl] can be readily exchanged with the desired neutral pyridine.

In analogy to the aforementioned systems, the azopyridine-analogons of the styrylpyridines were chosen as photoswitches, for their well known photoisomerisation properties as well as their chemical stability.

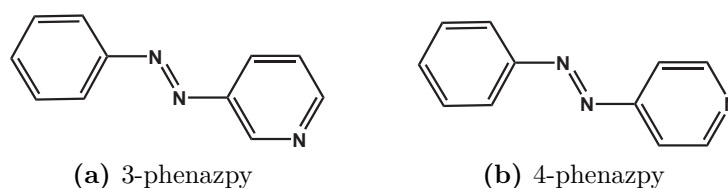


Figure 4.2: Synthesized Photoswitchable Ligands

The ligands 3-phenylazopyridine and 4-phenylazopyridine were synthesized according to previously used procedures (see figure 3.5). The appropriate 3-aminopyridine and 4-aminopyridine were condensed under alkaline conditions with nitrosobenzene dissolved in pyridine and the product was extracted with toluene. After column chromatography and vacuum-drying, the products were proven to be pure by NMR and elemental analysis. In addition to the two azopyridines, optical switching experiments were also carried out with non-functionalized pyridine and a methyl-substituted azopyridine.

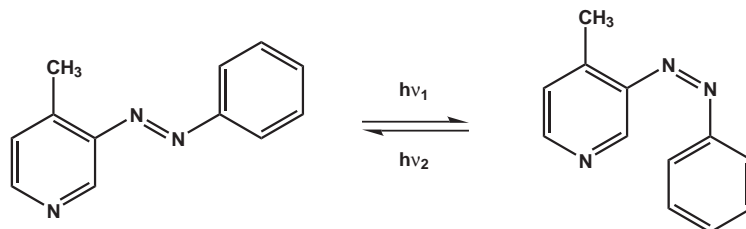


Figure 4.3: Sterically hindered azopyridine for photo-decoordination

The methyl-group directly adjacent to the azo-group should make coordination for the ligand more difficult when it is isomerized to the *cis*-conformation. This system was

chosen to compare the effect of ligand-isomerisation in solution with the sterically non-hindered azopyridines and to check if the measured effects are caused by the *cis-trans*-isomerisation of the azo-group, a simple photo-induced decoordination or re-coordination of the N-N group itself towards the metal center, which would render the ligand inert towards the backswitching into the initial *trans*-geometry.

4.2 Thermal Spin Crossover

4.2.1 Mößbauer-Spectra

The iron(III)-compounds investigated in this chapter all showed different Mößbauer-spectra from those in the previous chapter.

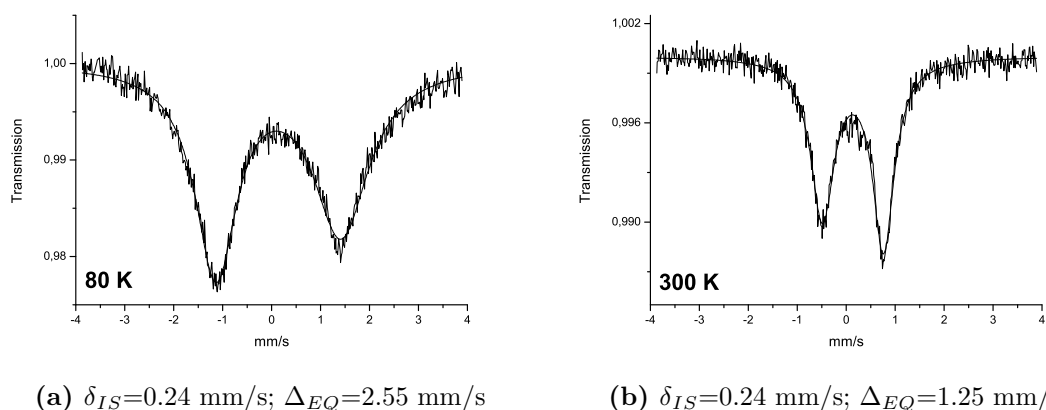


Figure 4.4: Mößbauer-spectra of [Fe(salten)pyridine]BPh₄

The salten-complex with an unsubstituted pyridine shows a rather high quadrupole-splitting for an iron(III)-highspin compound, which indicates a very asymmetric ligand-field even in the more symmetric highspin-state, where all *d*-orbitals are singly populated. The isomer-shift is constant throughout the measured temperature range, the quadrupole-split roughly doubles its value.

The next two pages show the spectra of the two salten-azopyridine compounds at eight different temperatures, showing the course of the spin-transition.

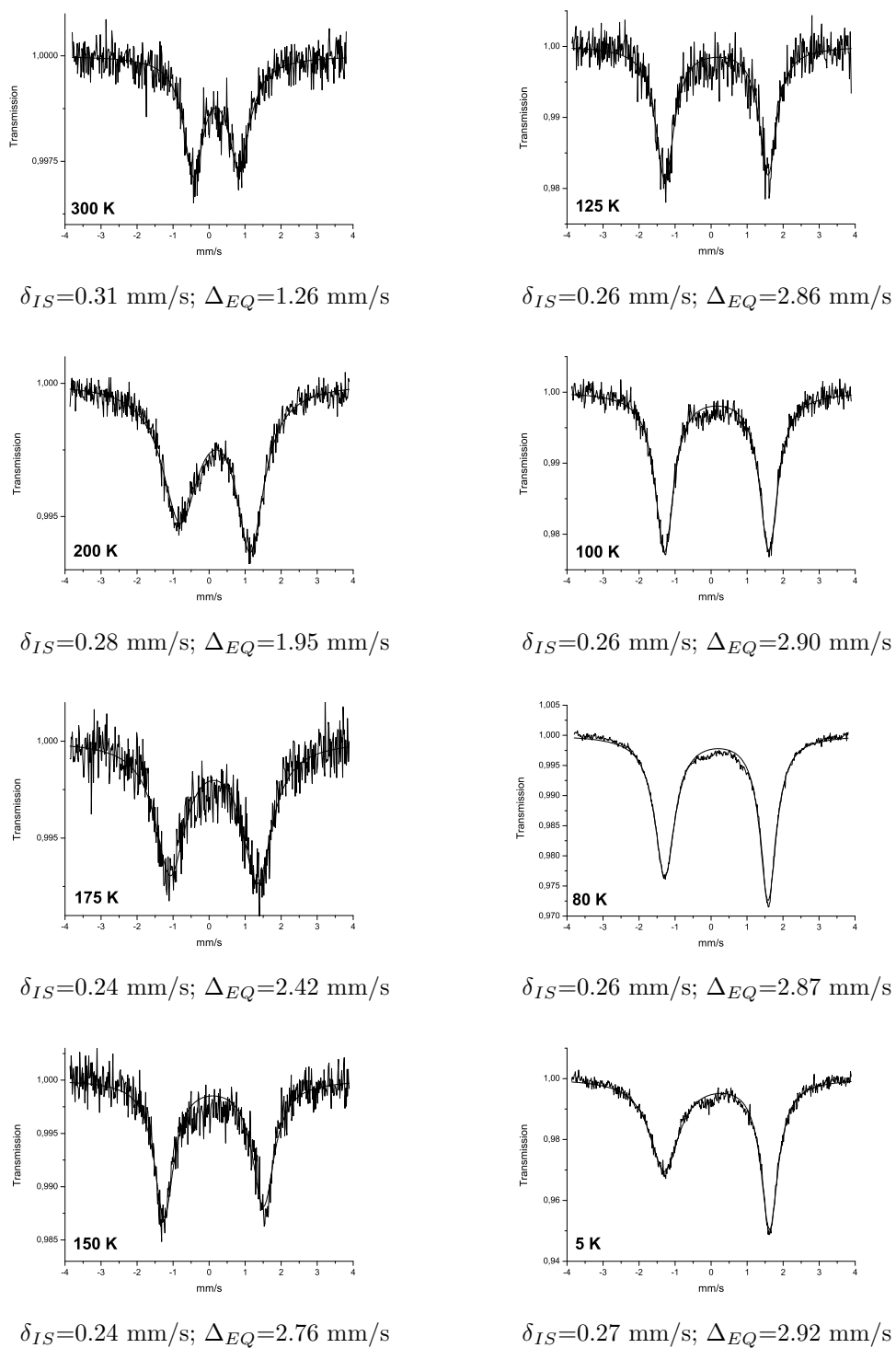
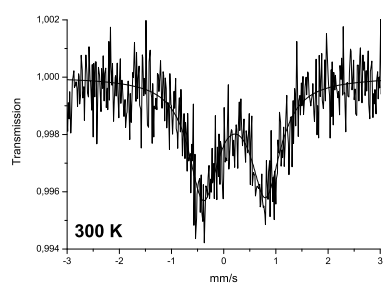
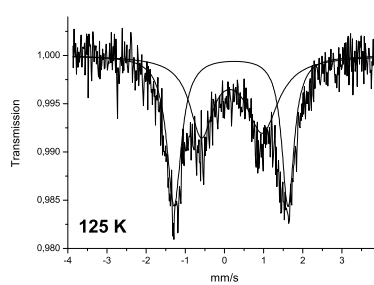


Figure 4.5: Mössbauer-Spectra of $[\text{Fe}(\text{salten})_3\text{-phenazpy}]\text{BPh}_4$

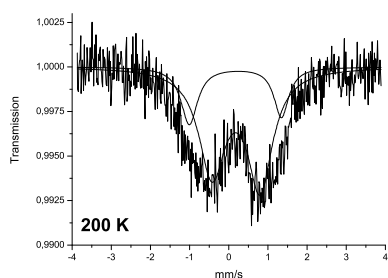


$$\delta_{IS}=0.32 \text{ mm/s}; \Delta_{EQ}=1.19 \text{ mm/s}$$



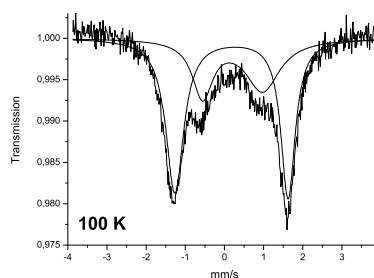
$$\delta_{IS}=0.30 \text{ mm/s}; \Delta_{EQ}=1.56 \text{ mm/s}$$

$$\delta_{IS}=0.28 \text{ mm/s}; \Delta_{EQ}=2.91 \text{ mm/s}$$



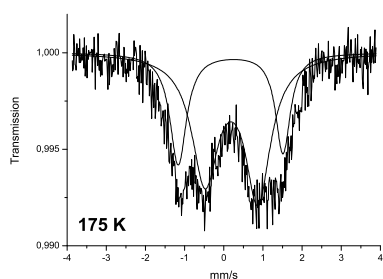
$$\delta_{IS}=0.30 \text{ mm/s}; \Delta_{EQ}=1.23 \text{ mm/s}$$

$$\delta_{IS}=0.28 \text{ mm/s}; \Delta_{EQ}=2.35 \text{ mm/s}$$



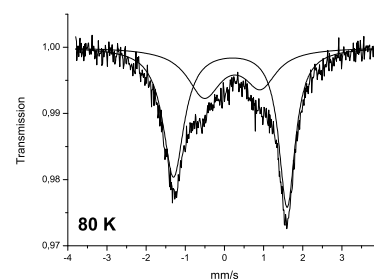
$$\delta_{IS}=0.32 \text{ mm/s}; \Delta_{EQ}=1.53 \text{ mm/s}$$

$$\delta_{IS}=0.29 \text{ mm/s}; \Delta_{EQ}=2.89 \text{ mm/s}$$



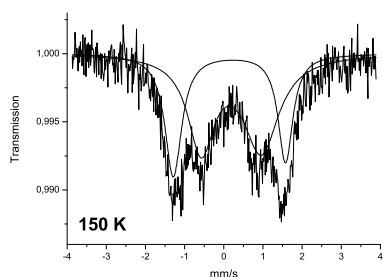
$$\delta_{IS}=0.31 \text{ mm/s}; \Delta_{EQ}=1.35 \text{ mm/s}$$

$$\delta_{IS}=0.29 \text{ mm/s}; \Delta_{EQ}=2.68 \text{ mm/s}$$



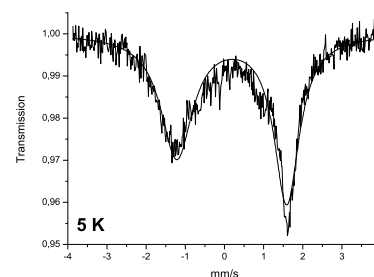
$$\delta_{IS}=0.30 \text{ mm/s}; \Delta_{EQ}=1.51 \text{ mm/s}$$

$$\delta_{IS}=0.26 \text{ mm/s}; \Delta_{EQ}=2.90 \text{ mm/s}$$



$$\delta_{IS}=0.30 \text{ mm/s}; \Delta_{EQ}=1.53 \text{ mm/s}$$

$$\delta_{IS}=0.25 \text{ mm/s}; \Delta_{EQ}=2.87 \text{ mm/s}$$



$$\delta_{IS}=0.30 \text{ mm/s}; \Delta_{EQ}=2.81 \text{ mm/s}$$

Figure 4.6: Mössbauer-spectra of $[\text{Fe}(\text{salten})_4\text{-phenazpy}]\text{BPh}_4$

The two investigated compounds are nice examples of the two different ways in which the spin-crossover shows up in Mößbauer-spectroscopy. The spectra of the 3-phenazpy complex, depicted in figure 4.5 show a gradual change in the quadrupole-splitting of the complex. This means that the relaxation between the two spin-states occurs on a faster timescale than the Mößbauer-excitation itself. It is impossible to distinguish two different species, one observes rather an averaged signal. In the 4-phenazpy compound, the subspectra of the two spin-states are clearly distinguishable, and intensity is transferred from the low-spin to the high-spin signal while increasing the temperature. The relaxation between the two spin-states is hereby slightly slower than the Mößbauer-excitation.

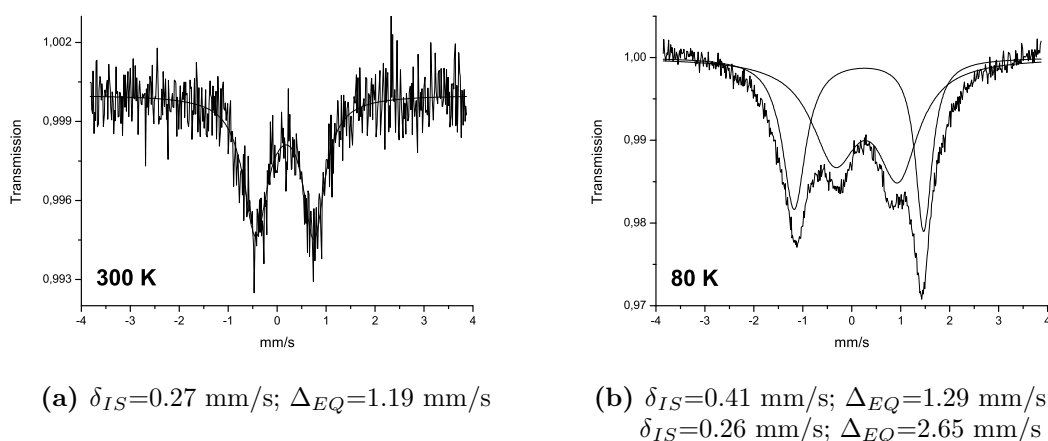


Figure 4.7: Mößbauer-spectra of $[\text{Fe}(\text{salten})4\text{-methyl-3-azopyridine}]^+$

The complex $[\text{Fe}(\text{salten})3\text{-methylazopyridine}]$ shows, similar to the complex formed with 4-phenazpy, two clearly distinguishable signals at liquid nitrogen temperature. In all investigated compounds, the quantity of the Mößbauer-effect is significantly decreased while the measurement-temperature is increased.

To check for an impurity of unreacted $[\text{Fe}(\text{salten})\text{Cl}]$, which was the precursor for all synthesized compounds, it was also characterized.

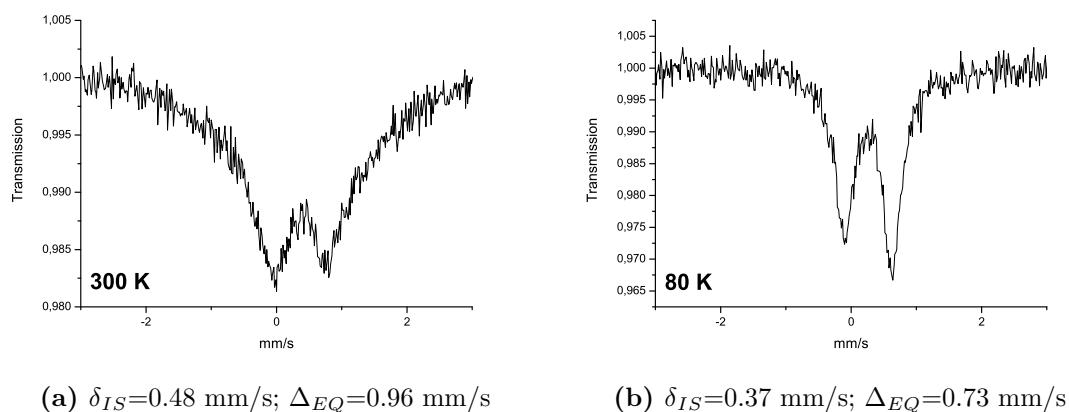


Figure 4.8: Mößbauer-spectra of [Fe(salten)Cl]

Both spectra show a typical singular iron(III)-lowspin species with a very broad signal at room temperature. The Mößbauer-spectra of the pyridine-substituted iron-salten compounds all showed a thermal spin crossover behaviour.

4.2.2 Magnetic Measurements

The susceptibility measurements of the salten-phenazpy (figure 4.9) compounds show a gradual and incomplete spin transition.

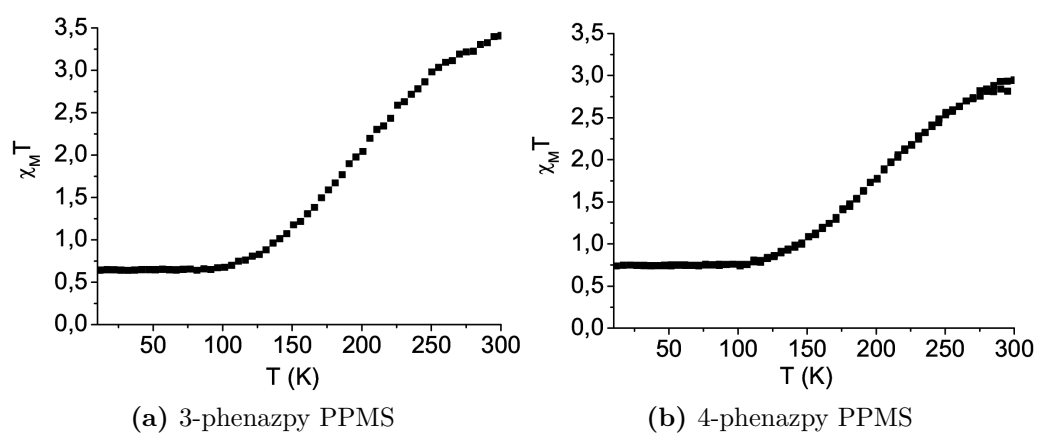


Figure 4.9: Magnetic Susceptibilities of 3-phenazpy and 4-phenazpy complexes

4.3 Photoinduced Switching

4.3.1 Optical Switching

To check if the coordinated azo-compound is still accessible for a *cis-trans* isomerisation of the azo-group, solutions of the uncoordinated ligand as well as the synthesized complexes were investigated with UV/Vis-spectroscopy. The two distinct absorption bands of the azo-function, the $\pi - \pi^*$ and the $n - \pi^*$ transition were taken as a guide to choose the appropriate wavelength for the irradiation experiment.

Ligand Switching

The two ligands 3-phenylazopyridine and 4-phenylazopyridine were dissolved in ethanol, UV/Vis spectra were recorded, the solutions irradiated with 310 nm wavelength for 30 minutes and another spectrum was taken.

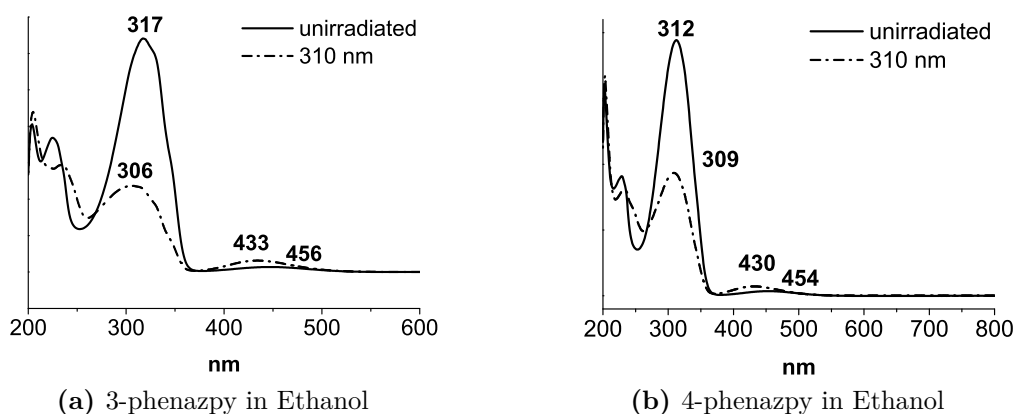


Figure 4.10: Switching of 3-phenazpy and 4-phenazpy

The same procedure was repeated with toluene, dichloromethane and acetonitrile, but the effect of the irradiation as well as the reversibility of the switching was at a maximum in ethanol.

Complex Switching

The two synthesized phenazpy-complexes were dissolved in ethanol, irradiated and measured. Ethanol was chosen after pre-testing the solubility in various solvents, which showed to be highest in alcohols, acetonitrile and acetone. Acetone had to be omitted for the irradiation experiments for its high self-absorption in the region of the $\pi - \pi^*$ transition at about 320nm. Acetonitrile, while having a good transmittance in the wavelength region of interest, was ignored due to the high affinity to coordinate to a transition metal center, thus minimizing the possibility of ligand-exchange.

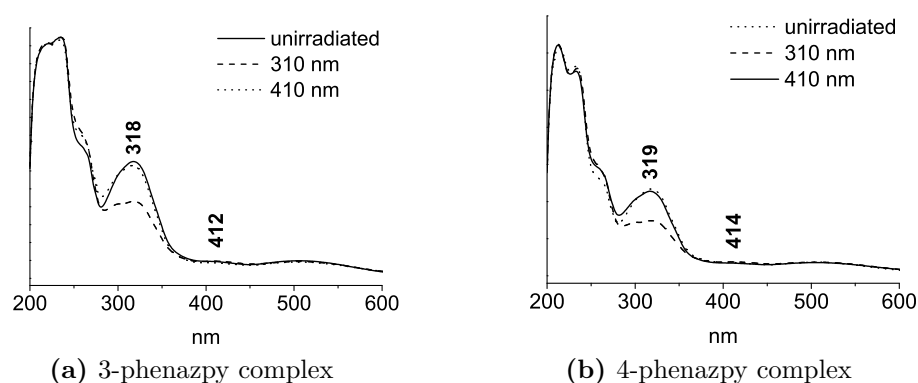


Figure 4.11: Irradiation of 3-phenazpy and 4-phenazpy complexes

The switching in dimethylsulfoxid was also investigated, but the effect of the irradiation on the two bands of interest in the corresponding UV/Vis-spectra was significantly smaller than that observed in ethanol. Ethanol and methanol were therefore chosen as solvents for the subsequent magnetic measurements in solution.

4.3.2 Evans Measurements

To investigate the influence of the ligand-isomerization in solution quantitatively, irradiation experiments were conducted using the shifting of proton-resonances in a paramagnetic environment. This method was first developed by Evans in 1959^[62] and subsequently named after him.

Two coaxial NMR-tubes are used, the inner one containing a mixture of the solvent and a small portion of an inert reference substance (e.g. tetramethylsilane or *tert*-butanol), while the outer tube contains the sample substance dissolved in the exact same solvent/reference solution used in the inner tube.

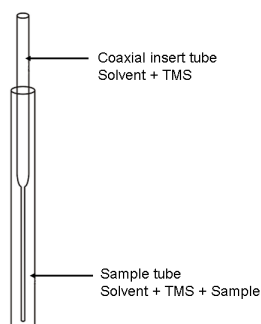


Figure 4.12: NMR-tube with coaxial insert

Due to the different magnetic environment generated by the paramagnetic sample, the proton-signals of the reference are shifted to higher frequencies

$$\chi_g = \frac{3 \cdot \Delta f}{4 \cdot \pi \cdot f \cdot m} + \chi_{g,Solvent} - \chi_{g,diamagn.} \quad (4.1)$$

Δf	frequency shift of reference	[Hz]
f	absolute frequency of NMR instrument	[Hz]
m	sample mass	[g]
$\chi_{g,Solvent}$	susceptibility of solvent	[cm ³ g ⁻¹]
$\chi_{g,diamagn.}$	diamagnetic correction	[cm ³ g ⁻¹]

The resulting values have to be corrected for the diamagnetism of the sample. This is done by adding the increments for the different bonds-types and atoms using Pascals' constants^[63].

The effective magnetic moment in terms of Bohr magnetons is calculated as followed:

$$\mu = 2.828 \cdot \sqrt{\chi_m \cdot T} \quad (4.2)$$

Especially when dealing with spin-crossover compounds, that change their magnetism

completely from diamagnetic to paramagnetic, the paramagnetic shift is a very sensitive and accurate spectroscopic probe. The crucial step in the preparation of the measured samples is the accurate determination of the concentration of the solution.

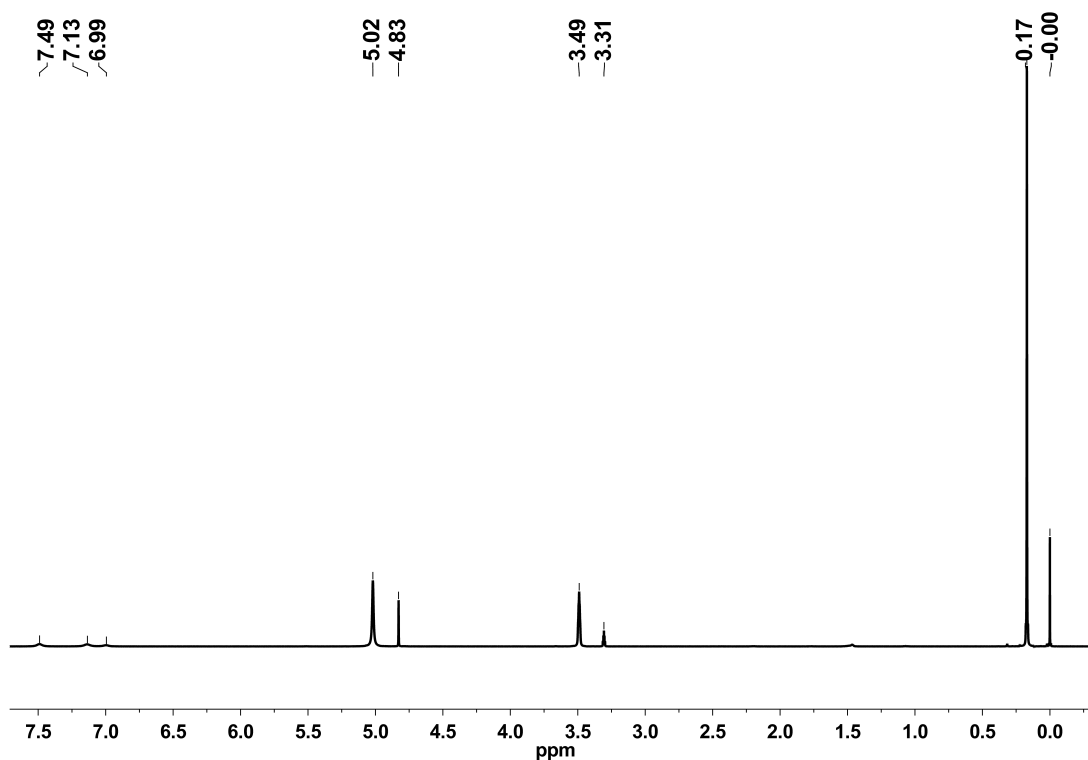


Figure 4.13: ^1H -NMR-spectrum of an Evans-measurement of $[\text{Fe}(\text{salten})\text{pyridine}]\text{BPh}_4$

In figure 4.13 the complete proton-spectrum of the complex $[\text{Fe}(\text{salten})\text{pyridine}]\text{BPh}_4$ dissolved in $\text{MeOH-}d_4$ is shown as an example. The most intense peaks are tetramethylsilane at around 0 ppm, methanol at 3.31 ppm and the residual water at 4.83 ppm. The paramagnetic shift is clearly observable on these three signals, since they are all doubled and shifted to higher frequency than the respective literature values. The use of tetramethylsilane as reference is nevertheless essential, since it is the least likely candidate to chemically interact with the sample, which would interfere with the measurement.

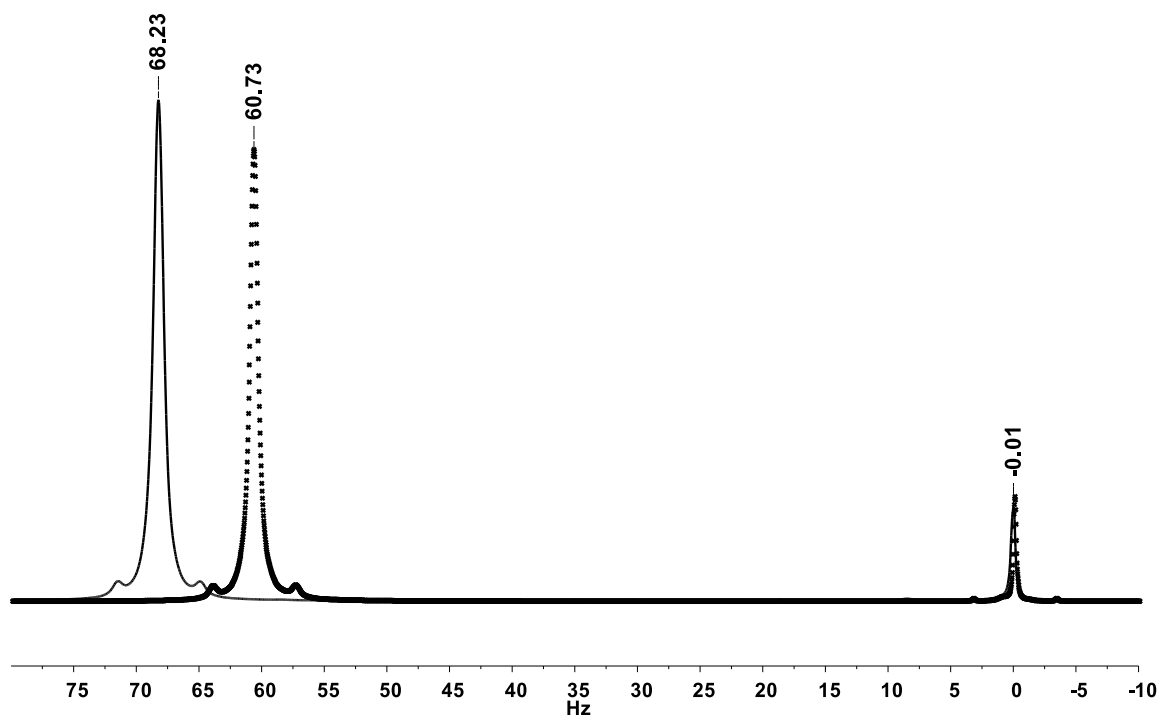


Figure 4.14: Overlay of two NMRs before (straight line) and after (dotted line) irradiation of $[\text{Fe}(\text{salten})\text{pyridine}]\text{BPh}_4$, TMS-peaks magnified

In figure 4.14 the TMS-signal is magnified and the two measurements before and after irradiation are overlaid.

In table 4.1 and 4.2 the results of the salten-phenazpy compounds in ethanol as solvents are collected.

Sample	[mmol/L]	Δf [Hz]	χ_m	μ_{eff} .
not irradiated	2.509	54.086	0.0128	5.55
60 min 310 nm	2.509	48.300	0.0114	5.24

Table 4.1: $[\text{Fe}(\text{salten})4\text{-phenazpy}]^+$ in $\text{EtOH-}d_6$

The ethanol used for the measurements was delivered in sealed ampoules and was not dried before use.

Sample	[mmol/L]	Δf [Hz]	χ_m	μ_{eff} .
not irradiated	3.429	67.135	0.0116	5.29
60 min 310 nm	3.429	61.263	0.0106	5.05

Table 4.2: $[\text{Fe}(\text{salten})3\text{-phenazpy}]^+$ in $\text{EtOH-}d_6$

Both compounds show a decrease of their magnetic moment of about 0.25 Bohr magnetons. The measurement was repeated with the addition of excess ligand to the solution. In addition to this, measurements were done with the 4-methyl-substituted 3-phenazpy ligand (see figure 4.3) to check the differences in the ligand-field strength. The methyl-substituted azopyridine is likely to de-coordinate in its *cis*-conformation, so an excess of free ligand was added to the solution.

Sample	[mmol/L]	Δf [Hz]	χ_m	μ_{eff} .
not irradiated	1.837	37.801	0.0122	5.42
60 min 310 nm	1.837	30.480	0.0099	4.87
60 min 440 nm	1.837	31.424	0.0101	4.93

Table 4.3: $[\text{Fe}(\text{salten})4\text{-methyl-3-azopyridine}]^+$ in $\text{MeCN-}d_3$ with excess ligand

The measurement in acetonitrile was done after several synthetic attempts to substitute the $[\text{Fe}(\text{salten})]$ unit with several nitrile donors failed, so it could safely be assumed that the tendency of acetonitrile coordinating to the iron-center was neglectable. The effect of the irradiation was bigger than the effect has been on the unsubstituted phenazpy-ligands.

Sample	[mmol/L]	Δf [Hz]	χ_m	μ_{eff} .
in CD_2Cl_2 not irradiated	1.22	26.287	0.0129	5.56
in CD_2Cl_2 60 min 310 nm	1.22	26.355	0.0129	5.57

Table 4.4: $[\text{Fe}(\text{salten})4\text{-methyl-3-azopyridine}]^+$ in CD_2Cl_2 with excess ligand

The results surprisingly showed no irradiation effect at all in dichloromethane as solvent, so it had to be assumed that the measured effect in acetonitrile was mainly due to ligand-decoordination. In order to verify this, the experiment with 4-phenazpy was repeated with an excess of free ligand in alcoholic and dichloromethane solutions.

Sample	[mmol/L]	Δf [Hz]	χ_m	$\mu_{eff.}$
not irradiated	1.924	43.085	0.0134	5.66
60 min 310 nm	1.924	42.163	0.0131	5.60

Table 4.5: $[\text{Fe}(\text{salten})4\text{-phenazpy}]^+$ in $\text{MeOH-}d_4$ with excess ligand

With the addition of additional ligand, so the solution was virtually saturated, the change is greatly reduced. The change becomes neglectable when the same procedure is done in pre-dried dichloromethane (table 4.6).

Sample	[mmol/L]	Δf [Hz]	χ_m	$\mu_{eff.}$
not irradiated	1.599	27.191	0.0102	4.95
60 min 310 nm	1.599	27.099	0.0102	4.94

Table 4.6: $[\text{Fe}(\text{salten})4\text{-phenazpy}]^+$ in CD_2Cl_2 with excess ligand

Again, the irradiation had no effect on the solution in dried dichloromethane. This left the possibility of the methyl-substituent on the 3-methylazopyridine being responsible for the photodecoordination, not the volatility of the pyridine-iron bond itself. To investigate this, the $[\text{Fe}(\text{salten})]$ was substituted with mere pyridine as sixth ligand and the irradiation experiment was repeated.

Sample	[mmol/L]	Δf [Hz]	χ_m	$\mu_{eff.}$
in $\text{MeOH-}d_4$ not irradiated	3.398	68.246	0.0121	5.38
in $\text{MeOH-}d_4$ 60 min 310 nm	3.398	60.744	0.0108	5.09

Table 4.7: $[\text{Fe}(\text{salten})\text{pyridine}]^+$ in $\text{MeOH-}d_4$

Obviously, the change in paramagnetism to this point did not result from the *cis-trans*-isomerisation of a coordinated azo-unit, since it is also present with a non-switchable substituent. To verify that the cause of the change was indeed an photodecoordination of the attached pyridine, the measurement was repeated in deuterated pyridine as solvent, in analogy to the addition of excess ligand in the previous measurements.

Sample	[mmol/L]	Δf [Hz]	χ_m	μ_{eff}
in Pyridine- d_5 not irradiated	3.67	48.848	0.0081	4.40
in Pyridine- d_5 60 min 310 nm	3.67	49.235	0.0081	4.42

Table 4.8: $[\text{Fe}(\text{salten})\text{pyridine}]^+$ in Pyridine- d_5

A proof of this assumption, the irradiation of the sample in pyridine brought no change in paramagnetism. It thus can be safely assumed that the reduction of the magnetic moment observed in some measurements is not a switching effect of the azopyridines. Since a coordination of a solvent molecule like ethanol would decrease the ligand field with respect to the pyridine-donor it replaces, there are two plausible scenarios why the magnetic moment is in fact decreased in some irradiation experiments.

The $[\text{Fe}(\text{salten})]$ -unit could form some kind of μ -oxo-bridged dimers (see figure 4.15) by reacting with residual water molecules in the deuterated NMR-solvents.

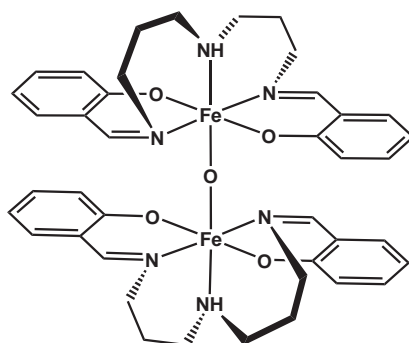


Figure 4.15: μ -oxo-bridged $[\text{Fe}(\text{salten})]$ -dimer

This is supported by the fact that the magnetic moments does not change when pre-dried, non-hygroscopic solvents like dichloromethane are used for the measurements. On the other hand, the effect would have to be orders of magnitude higher in non-dried methanol, since there are several equivalents of water available with respect to the low complex concentration. The bridged dimer would have to be antiferromagnetically coupled, so the resulting dimer should almost be diamagnetic.

The alternative explanation is coordination of the azo-group to the metal-center in its *cis*-conformation (figure 4.16. As shown in previous chapters, this would render

the azopyridine inert towards an isomerisation back into the *trans*-state.

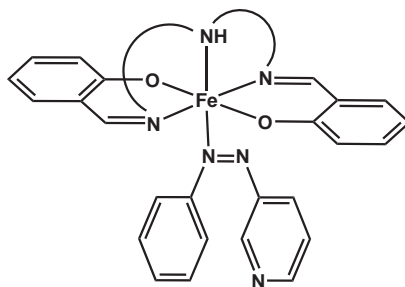


Figure 4.16: Coordination via the azo-group

DFT-calculations showed this to be quite possible for all investigated azopyridines, but the proof of this hypothesis would include the synthesis of the pure azocoordinated $[\text{Fe}(\text{salten})\text{phenazpy}]$ complex. This is rather unlikely, for the azoligands cannot be switched into their *cis*-conformation quantitatively.

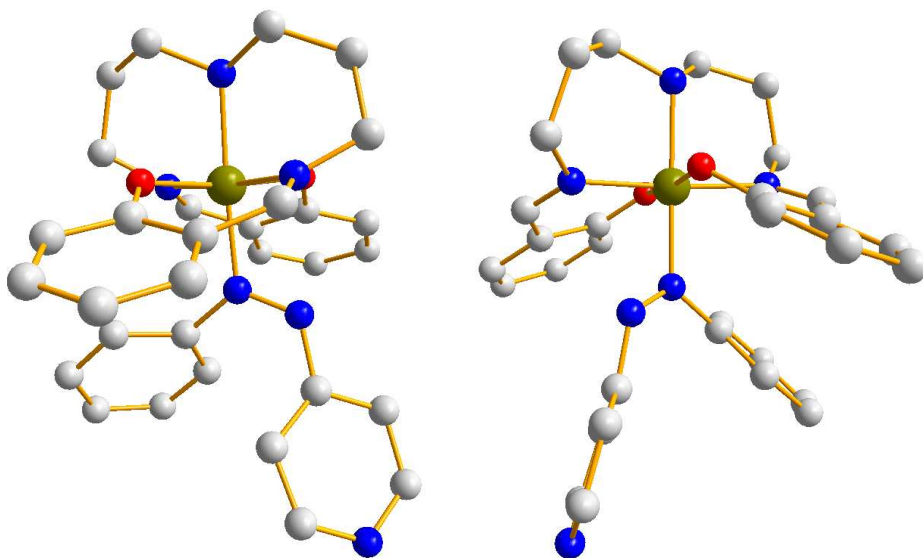


Figure 4.17: Optimised geometry of the proposed *cis*-azocoordination

The proof with infrared-spectroscopy in solution would also be unsuccessful, since the azo-group does not provide an intense and distinguishable band in the spectra. To check if the isomerisation of the attached ligand indeed would not change the magnetic moment of the complex, even if no decoordination took place, the compounds were studied further with density functional theory.

4.4 Quantum-chemical Analysis

4.4.1 Calculations

The influence of the *cis-trans* isomerisation of photoswitchable ligands imposed on the metal center was to be investigated qualitatively, since the energies resulting from similar singlepoint-calculations on different compounds can not be compared directly. The first approach to take a look at the electronic changes would be to compare the energies of the d-orbitals. From the crystal structure determination the coordination of the iron-center can be assumed as octahedral. So the difference between the two orbital sets t_{2g} and e_g would be the ligand-field splitting $10Dq$ and could be taken directly as a measure of the ligand-field strength and its change. Unfortunately, the orbitals generated by density functional theory cannot be taken as representations of the true wavefunction of the investigated system, since this function simply is not available in density functional theory.

The other way to evaluate the energetic differences was the comparison of the total energies of the respective compounds. The big advantage of this approach is that the singlepoint-energy calculations are much less demanding than geometry optimisations and subsequent frequency calculations, therefore they can be run with much larger basis-sets and different functionals.

For the geometry optimisations, the single crystal structure of $[\text{Fe}(\text{salten})\text{stypy}]^+$ in *cis* as well as in the *trans* conformation, was used as starting point, replacing the stilbenes with the respective azopyridine-derivative. The geometries were pre-optimised with the Hartree-Fock method and the 6-31g pople-style basis-set. Full optimisation was carried out using either the B3LYP hybrid-functional or the BP86 gradient functional with TZVP basis, since this combinations have been proven to yield reliable results for transition metal complexes^[64]. The calculated bondlengths of the styrylpyridine-complex were in good agreement with the measured crystal-structure (see table 4.9 and table 4.10)

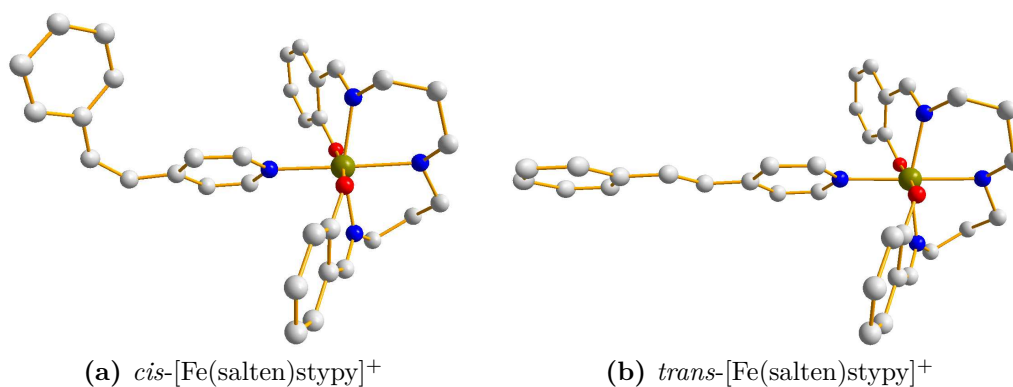


Figure 4.18: Optimised geometries of [Fe(salten)stypy]⁺

Bond length	measured	B3LYP/TZVP	BP86/TZVP
Fe-Pyridine	2.0531	2.0383	2.0152
Fe-Amine	2.0625	2.0703	2.0683
Fe-Phenolate 1	1.9232	1.9144	1.9037
Fe-Phenolate 2	1.9130	1.8864	1.8985
Fe-Imine 1	1.9632	1.9842	1.9584
Fe-Imine 2	1.9972	2.0048	1.9645

Table 4.9: Comparison of bondlengths in *cis*-[Fe(salten)stypy]

The angle between the two aromatic systems in the stilbene-derivatives was taken from the crystal structure determination. In the azo ligand, it was initially set to 45°. The correct angle is not critical, since the goal was to understand the influence on the electronic structure of the iron-center when the conjugation of the two aromatic rings in the attached pyridine-ligands is disturbed.

Bond length	measured	B3LYP/TZVP	BP86/TZVP
Fe-Pyridine	2.1457	2.0354	2.0119
Fe-Amine	2.1269	2.0704	2.0681
Fe-Phenolate	1.9184	1.9139	1.9026
Fe-Phenolate 2	1.9080	1.8887	1.9007
Fe-Imine 1	2.0396	1.9836	1.9585
Fe-Imine 2	2.0596	2.0038	1.9631

Table 4.10: Comparison of bondlengths in *trans*-[Fe(salten)stypy]

The calculated structures were both in good agreement with the crystal-structure parameters. The structures of the stypy and mepepy complexes were calculated the

same way.

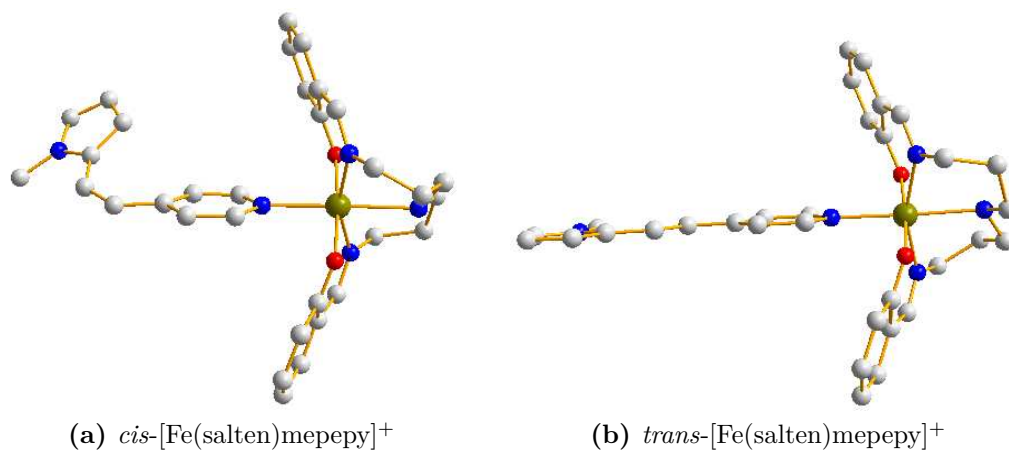


Figure 4.19: Optimised geometries of [Fe(salten)mepepy]⁺

The rotational angle of the pyridine-substituent and the salten-unit differs in each calculation, since the rotational barrier of the pyridine-iron bond is very small.

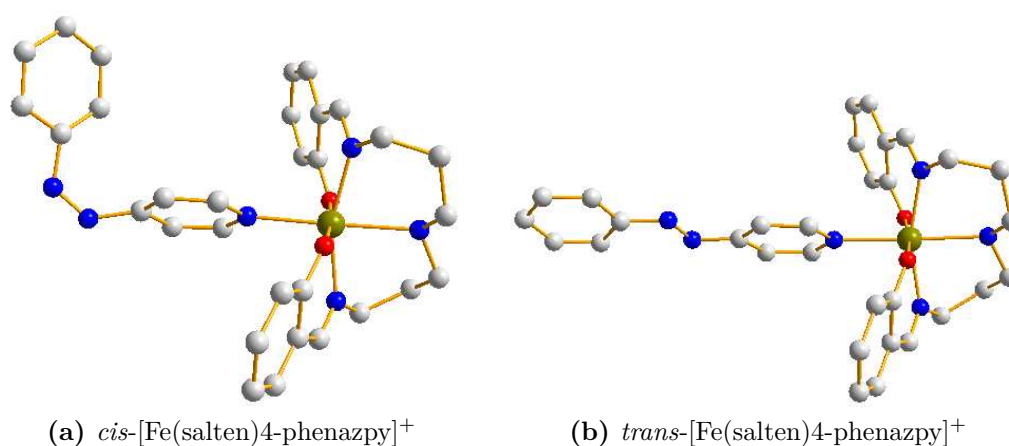


Figure 4.20: Optimised geometries of [Fe(salten)4-phenazpy]⁺

The BP86-functional correctly predicted the low-spin-state to be lower in energy (as it is in all compounds able to undergo a thermal spin-transition), so the subsequent single-points were carried out using the optimised geometry from the BP86/TZVP runs. The total energies without zero-point correction were subtracted to determine the groundstate.

Molecule	B3LYP	TPSSH	MPW2PLYP	BP86	BP86
Spin State	TZVP	def2-TZVPP	def2-TZVPP	TZVP	def2-QZVP
stypy <i>cis</i>	HS (0.07)	LS (2.39)	HS (6.05)	LS (21.64)	LS (19.47)
stypy <i>trans</i>	LS (0.09)	LS (2.39)	HS (6.02)	LS (21.80)	LS (19.54)
mepepy <i>cis</i>	LS (0.13)	LS (2.44)	HS (6.13)	LS (21.72)	LS (19.47)
mepepy <i>trans</i>	LS (0.18)	LS (2.49)	HS (6.16)	LS (21.69)	LS (19.41)
azpy <i>cis</i>	HS (0.37)	LS (2.12)	HS (6.16)	LS (21.55)	LS (19.26)
azpy <i>trans</i>	LS (0.01)	LS (10.61)	HS (5.95)	LS (21.94)	LS (20.70)

Table 4.11: Calculated ground-states for the compounds and difference to other state

Only the calculations with B3LYP/TZVP and BP86/TZVP were carried out as full geometric optimisations, the others were single-point calculations on the BP86/TZVP optimised structures. Only the functionals TPSSH and BP86 were able to correctly predict the low-spin-groundstate of the three complexes, however in the case of BP86 with a too large difference between the two states. Since BP86 has no HF-exchange at all, and TPSSH only applies 10% exchange, this seems to be the cause for the incorrect energetics of the other calculations.

Subsequent frequency calculations proved the calculated structures to be the global minimum, for there were no negative frequencies in the calculated spectra. From the frequency-runs the zero-point-energy was obtained and used to correct all single-point energies.

Molecule	$\Delta E + \text{ZPE}[\text{kcal}]$	$\Delta H[\text{kcal}]$	$\Delta S[\text{cal}]$
stypy <i>cis</i>	18.92	17.38	14.68
stypy <i>trans</i>	19.16	17.67	14.42
mepepy <i>cis</i>	18.97	17.40	14.32
mepepy <i>trans</i>	19.07	17.62	14.75
azpy <i>cis</i>	18.76	17.19	16.00
azpy <i>trans</i>	19.00	17.34	16.47

Table 4.12: Thermochemical differences between HS and LS states

The values in table 4.12 show the thermochemical differences between the high-spin and the low-spin state in the respective conformations. The values are taken from

frequency calculations with the BP86 functional and the TZVP basis-set.

With the thermochemical data gained from the respective frequency calculations, ΔG for the spin-transition was calculated for each compound in the respective conformation, with energies resulting from various single-point calculations.

Molecule conformation	B3LYP TZVP	TPSSH def2-TZVPP	MPW2PLYP def2-TZVPP	BP86 TZVP	BP86 def2-QZVP
stypy <i>cis</i>	-7.30	-6.25	-14.68	13.01	10.84
stypy <i>trans</i>	-7.32	-6.03	-14.44	13.37	11.12
mepepy <i>cis</i>	-7.34	-6.15	-14.73	13.13	10.87
mepepy <i>trans</i>	-6.20	-5.96	-14.62	13.23	10.95
azpy <i>cis</i>	-8.24	-5.12	-15.29	12.42	10.13
azpy <i>trans</i>	-7.89	1.10	-15.46	12.43	11.18

Table 4.13: ΔG values (in [*kcal*]) for the transition from LS to HS

For spin-crossover compounds it is typical that the entropic contribution to the free energy is bigger than the difference in the inner energies. But the energetic difference calculated by the BP86/TZVP combination is too large to be compensated by the entropy term.

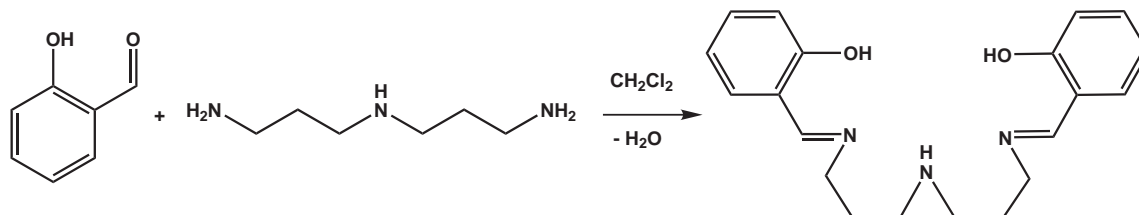
4.5 Results and Discussion

The projected complexes $[\text{Fe}(\text{salten})_4\text{-phenazpy}]^+$, $[\text{Fe}(\text{salten})_3\text{-phenazpy}]^+$ and $[\text{Fe}(\text{salten})\text{methyl-3-phenazpy}]^+$ were successfully synthesized and characterized. All showed to be spin-crossover compounds with a photoswitchable unit in their ligand sphere. However, the coordination via only one pyridine-donor to the iron-center seems to be too weak to get access to a truly bistable molecule in solution. The DFT-studies in the complexes all showed no clear tendency, which conformer of the coordinated switch would yield the stronger ligand-field. The differences of the energetic distance between the high-spin and the low-spin state in the respective conformation of the investigated compound was neglectible.

4.6 Syntheses

4.6.1 Synthesis of

4-azaheptamethylene-1,7-bis(salicylideneimine)

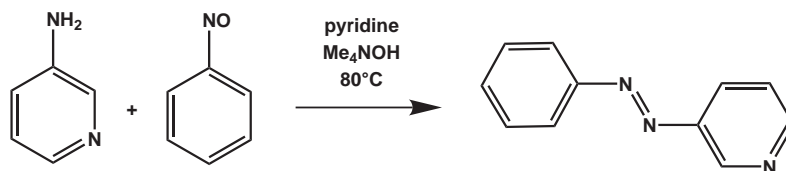


8.6 mL salicylaldehyde and 5.7 mL of di-(2-aminopropyl)-amine were dissolved in 40 mL dichloromethane. The mixture was refluxed for two hours using a Dean-Stark-Trap to remove the emerging two equivalents of water. The solution was allowed to cool to room temperature. The solvent was removed *in vacuo* to yield the yellow highly viscous product. The ligand was used without further purification.

¹H NMR (400 MHz, CD₂Cl₂) δ = 13.33 (s, 2H), 8.34 (s, 2H), 7.26 (m, 4H), 6.85 (m, 4H), 3.64 (m, 4H), 2.68 (m, 4H), 1.84 (m, 4H).

¹³C NMR (110 MHz, CD₂Cl₂) δ = 165.03 (s), 161.24 (s), 131.95 (s), 131.21 (s), 118.94 (s), 118.38 (s), 116.69 (s), 57.39 (s), 47.38 (s), 31.28 (s).

4.6.2 Synthesis of 3-(phenyldiazenyl)pyridine



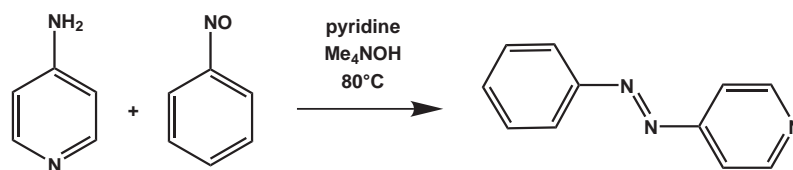
To a solution of 25 mL of a 60 wt % of tetramethylammoniumhydroxide and 2.00 g 3-aminopyridine in 25 mL of pyridine was added over a period of 60 min a solution of 3.00 g nitrosobenzene in 50 mL of pyridine at a temperature of about 80° C. After that, the solution was allowed to cool to room temperature. The mixture was extracted three times with 50 mL of toluene each. The organic extracts were dried over natriumsulphate and the solvent was removed *in vacuo*. The product was purified by column chromatography using silica gel and a 2:1 mixture of cyclohexane and ethylacetate as eluent. The phenylazopyridine was observable as a deep-red fraction on the silicagel, so no TLC was necessary to distinguish the product from impurities.

Elemental analysis	C	H	N
Calculated	72.11	4.95	22.94
Found	71.67	5.06	23.24

¹H NMR (400 MHz, CD₂Cl₂) δ = 9.18 (dd, *J* = 2.4, 0.7 Hz, 1H), 8.70 (dd, *J* = 4.7, 1.6 Hz, 1H), 8.16 (ddd, *J* = 8.2, 2.4, 1.6 Hz, 1H), 8.00 – 7.93 (m, 2H), 7.61 – 7.51 (m, 3H), 7.47 (ddd, *J* = 8.2, 4.7, 0.8 Hz, 1H).

¹³C NMR (110 MHz, CD₂Cl₂) δ = 152.57 (s), 151.82 (s), 147.85 (s), 147.17 (s), 131.69 (s), 129.20 (s), 126.74 (s), 123.94 (s), 122.95 (s).

4.6.3 Synthesis of 4-(phenyldiazenyl)pyridine



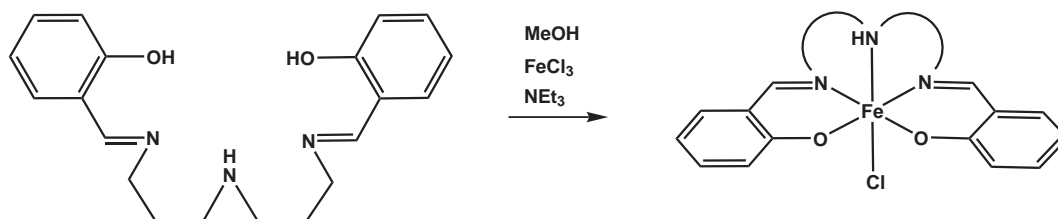
To a solution of 25 mL of a 60 wt % of tetramethylammoniumhydroxide and 2.00 g 4-aminopyridine in 25 mL of pyridine was added over a period of 60 min a solution of 3.00 g nitrosobenzene in 50 mL of pyridine at a temperature of about 80° C. After that, the solution was allowed to cool to room temperature. The mixture was extracted three times with 50 mL of toluene each. The organic extracts were dried over natriumsulphate and the solvent was removed *in vacuo*. The product was purified by column chromatography using silica gel and a 2:1 mixture of cyclohexane and ethylacetate as eluent. The phenylazopyridine was observable as a deep-red fraction on the silicagel, so no TLC-monitoring was necessary to distinguish the product from impurities.

Elemental analysis	C	H	N
Calculated	72.11	4.95	22.94
Found	71.67	5.06	23.24

¹H NMR (400 MHz, CD₂Cl₂) δ = 8.81 (dd, J = 4.5, 1.6 Hz, 1H), 8.02 – 7.96 (m, 1H), 7.72 (dd, J = 4.5, 1.6 Hz, 1H), 7.61 – 7.56 (m, 2H).

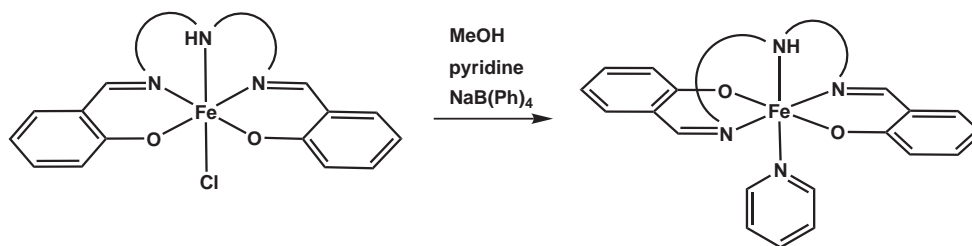
¹³C NMR (101 MHz, CD₂Cl₂) δ = 157.17 (s), 152.42 (s), 151.38 (s), 132.35 (s), 129.27 (s), 123.29 (s), 116.06 (s).

4.6.4 Synthesis of [Fe(salten)Cl]



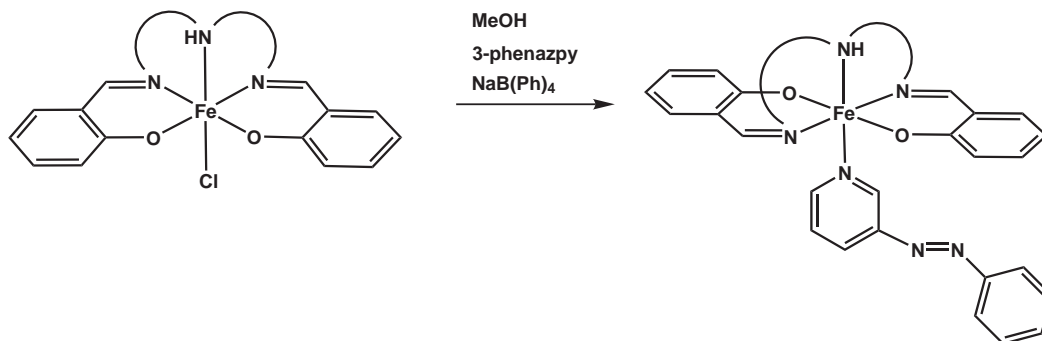
To 3.4 g of salten-ligand in 50 mL of methanol, a solution of 1.62 g anhydrous iron(III)chloride in 50 mL of methanol was added. The mixture was stirred for 10 min at roomtemperature. Then 2.79 mL of triethylamine was added. The reaction was heated at 50°C for one hour, then allowed to cool to roomtemperature. The black precipitate was removed using a glas frit, washed three times with diethylether and dried *in vacuo*.

Elemental analysis	C	H	N
Calculated	56.03	5.41	9.80
Found	57.13	5.48	10.32

4.6.5 Synthesis of $[\text{Fe}(\text{salten})\text{py}]\text{BPh}_4$ 

To a solution of 0.98 g of $[\text{Fe}(\text{salten})\text{Cl}]$ in 50 mL of methanol was added a solution of 0.45 ml pyridine in 5 mL of methanol. The solution was stirred at 60°C for one hour and immediately filtered. To the filtrate was added a solution of 0.75 g of sodiumtetraphenylborate in 10 mL of methanol. The mixture was stirred at 60°C for ten minutes, then allowed to cool to roomtemperature over night. The precipitate was filtered of using a glas frit and washed one time with pre-cooled methanol and several times with diethylether to remove uncoordinated pyridine and dried *in vacuo*.

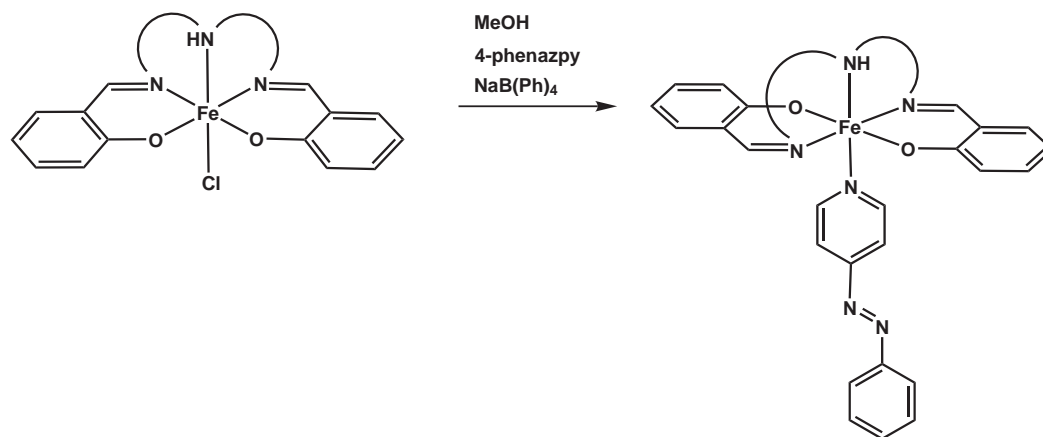
Elemental analysis	C	H	N
Calculated	74.35	6.11	7.08
Found	74.19	6.20	7.21

4.6.6 Synthesis of $[\text{Fe}(\text{salten})_3\text{-(phenyldiazenyl)py}]\text{BPh}_4$ 

To a solution of 0.98 g of $[\text{Fe}(\text{salten})\text{Cl}]$ in 50 mL of methanol was added a solution of 0.45 g 3-azopyridine in 5 mL of methanol. The solution was stirred at 60°C for one hour and immediately filtered. To the filtrate was added a solution of 0.75 g of sodiumtetrakisphenylborate in 10 mL of methanol. The mixture was stirred at 60°C for ten minutes, then allowed to cool to roomtemperature over night. The precipitate was filtered of using a glas frit and washed one time with pre-cooled methanol and several times with diethylether to remove uncoordinated 3-azopyridine and dried *in vacuo*. The chlorine analysis showed that not all of the chlorides had been exchanged with the azopyridine ligand, so the raw product was dissolved in 25 mL methanol again. To this a solution of 0.28 g of sodiumtetrakisphenylborate and 0.23 g of 3-azopyridine were added. The mixture was stirred at 70°C for one hour and then stored in a freezer for four days. The precipitate was filtered of, washed several times with diethylether and dried *in vacuo*. The chlorine content was not measureable any more.

Elemental analysis	C	H	N	Cl
Calculated	73.75	5.85	9.38	0.00
Found 1	72.52	6.27	8.40	4.50
Found 2	73.15	5.85	9.29	n.a.

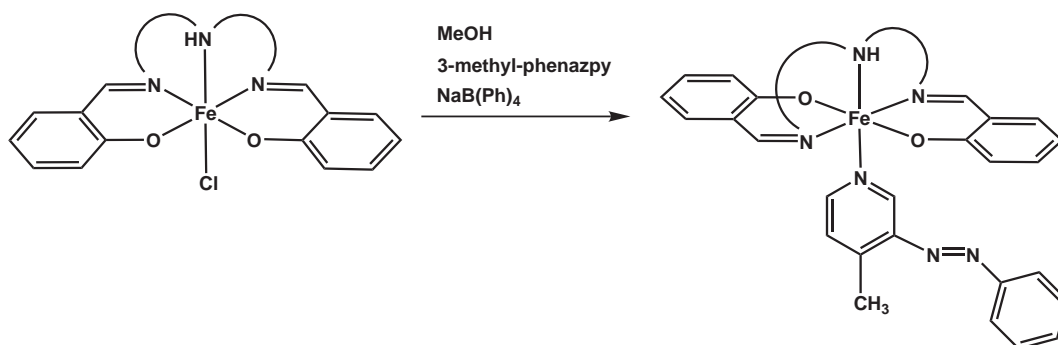
4.6.7 Synthesis of [Fe(salten)4-(phenyldiazenyl)py]BPh₄



The synthesis was carried out analog to the synthesis of [Fe(salten)3-azopyridine]. This time, the recrystallization with additional sodiumtetrphenylborate and azopyridine was immediately executed afterwards.

Elemental analysis	C	H	N
Calculated	73.75	5.85	9.38
Found	72.69	5.87	9.27

4.6.8 Synthesis of

[Fe(salten)4-methyl-3-(phenyldiazenyl)py]BPh₄

The synthesis was carried out analog to the synthesis of [Fe(salten)3-azopyridine]. This time, the recrystallization with additional sodiumtetraphenylborate and azopyridine was immediately executed afterwards.

Elemental analysis	C	H	N
Calculated	73.93	5.98	9.59
Found	75.78	6.24	8.27

5 Azochelates

5.1 The non-coordinating azo-group

It has been shown that the directly coordinated azo-function is no longer susceptible to optical *cis-trans* isomerisation, since the lone-pairs of the two nitrogens are no longer free to rotate due to the coordination to the transition metal. Also the coordination via only one aromatic nitrogen-donor such as pyridine is rather susceptible towards photo-decoordination. Therefore, to minimise the risk of decoordination and still have a switchable function present in the ligand, a new system had to be devised, this time using chelating photoswitchable ligands.

5.2 Ligand Design and Synthetic Routes

5.2.1 Substituted Phenanthrolines and Bipyridines

Since most spin-crossover compounds are bearing several aromatic nitrogen-donors in their ligand sphere, this substitution pattern had to be preserved, so the new strategy involved the substitution of such units as bipyridine and phenanthroline with a photosensitive functional group.

Geometric considerations, derived from low-level optimizations of conceivable model systems, led to the choice of substituting the aromatic backbone in 5-position (bipy) or 3-position (phen) (figure 5.1) to achieve a good switchability (the *trans*-isomer had to likely form a stable complex, while it still should be able to switch the azo-function to the *cis*-state).

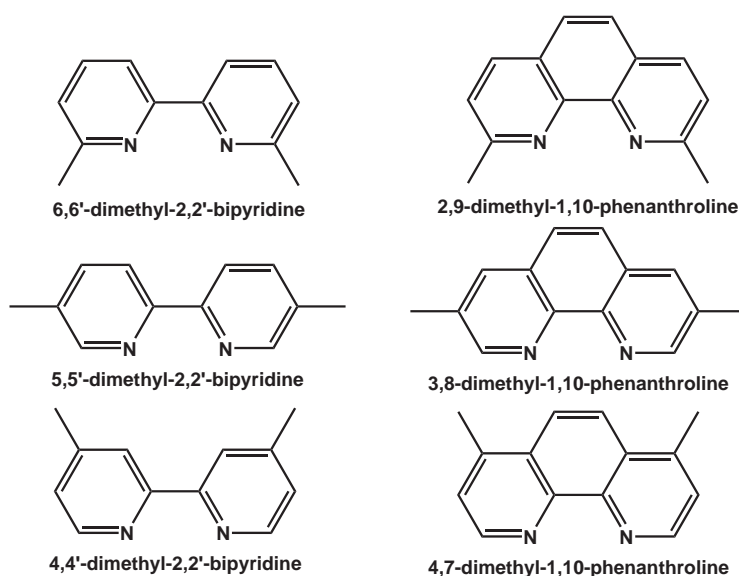


Figure 5.1: Substitution patterns for Bipyridine and Phenanthroline

First candidate is obviously 1,10-phenanthroline as backbone, since it is also present in the most prominent representative of synthetic spin-crossover systems, the aforementioned $[\text{Fe}(\text{phen})_2(\text{NCS})_2]$, shown in figure 2.3. There are only few publications dealing with the substitution of phenanthroline selectively in the desired positions^{[65][66][67]}, and they all involve harsh reaction conditions while giving rather unsatisfactory yields.

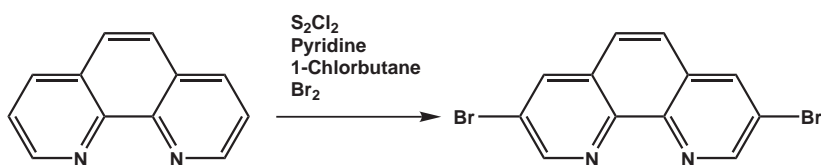


Figure 5.2: Bromination of Phenanthroline

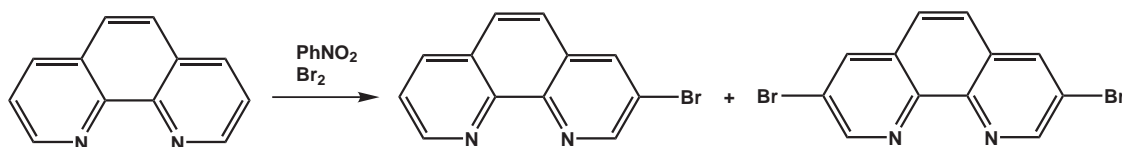


Figure 5.3: Bromination of Phenanthroline in Nitrobenzene

The only example of a selective 3,8-substitution of 1,10-phenanthroline is the bromination in these positions. Virtually all derivatives of 1,10-phenanthroline in literature

are of a 2,9-substitution pattern^[68]. Since phenanthroline is not as likely to be functionalized in a feasible way, the choice was the substitution of bipyridine. From this backbone, two possible ligands suitable for forming a switchable molecule, were derived.

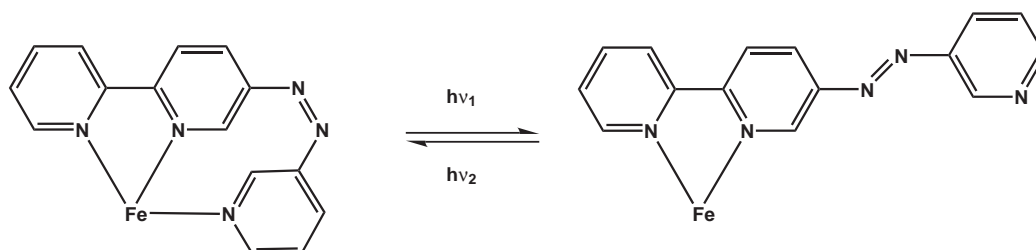


Figure 5.4: Projected switchable Azoterpy-ligand

A monosubstituted bipyridine with one switchable function (figure 5.4), and the symmetrical disubstituted azobipyridine (figure 5.5).

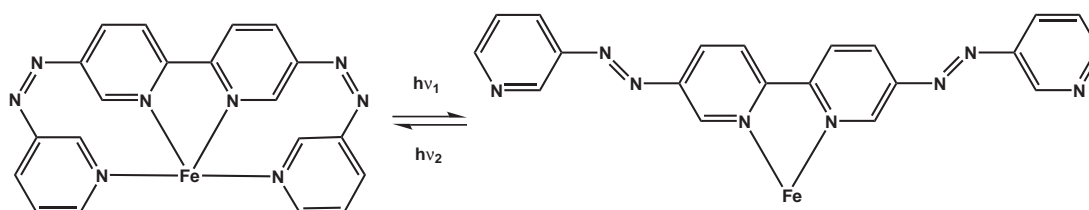


Figure 5.5: Projected switchable Azoquadpy-ligand

The azocoupling was to be achieved by using the Mills-reaction described in a previous chapter (figure 3.5). The two building blocks for the projected photoswitchable ligands are therefore the suitable bipyridine backbone, and the 3-nitrosopyridine.

5.2.2 Symmetrically and asymmetrically substituted bipyridines

The apparently most feasible way to gain access to the desired substitution-pattern of the bipyridine-backbone is by utilizing a metal-mediated coupling of the appropriate building blocks. Several methods are described in the literature so far, most of them using modified Negishi-couplings under the use of palladium-catalysts.

The first method used was developed by Janiak^[69]. Commercially available 5-nitro-2-aminopyridine was reduced using tin chloride in concentrated hydrochloric acid

at 0°C, giving pure 5-amino-2-chloropyridine quantitatively^[70]. This was dissolved in dried and degassed dimethylformamide. The coupling agent was formed *in-situ* by the reaction of nickel chloride with triphenylphosphine and subsequent reduction of the Ni(II) to zerovalent nickel. After heating, the reaction was quenched with concentrated ammonia solution and stirred for several hours, but after the workup, only trace amounts of the desired compound were detectable by NMR-spectroscopy.

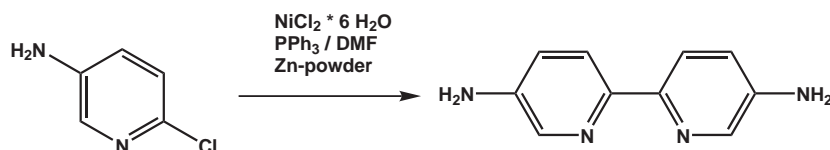


Figure 5.6: Direct coupling of 2-chloro-5-aminopyridine

A slight modification of the reaction conditions^[71], gaseous ammonia was added several times to maintain the saturation level of the quenched reaction mixture, but this didn't lead to better results.

The next possible method to form the desired bipyridine was a coupling with a protected amino-function. The 5-amino-2-chloropyridine was reacted with 2,5-hexanedion prior to the coupling reaction. With this building block, the synthesis of the symmetrical 5,5'-diamino-2,2'-bipyridine (figure 5.7), as well as an asymmetrical coupling, using similar conditions but leading to 5-monoamino-2,2'-bipyridine (figure 5.8), was tried.

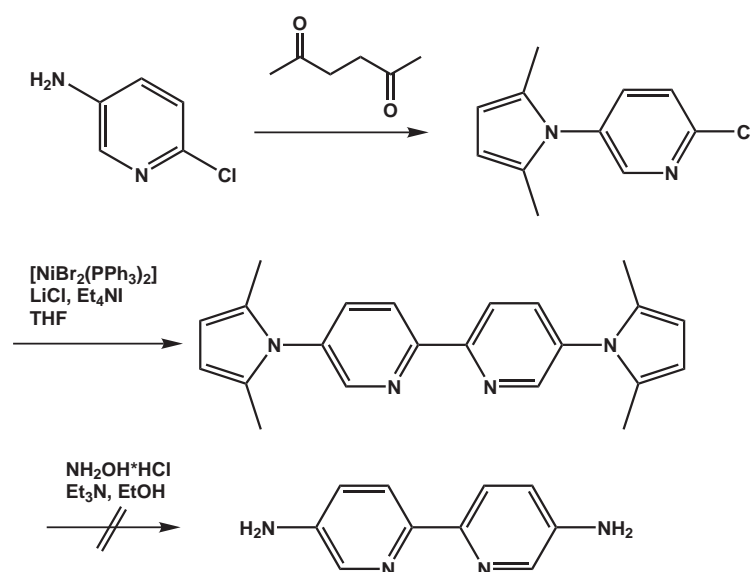


Figure 5.7: Coupling of symmetrical Pyrrol-protected bipyridine^[72]

The protection of the amino-group was achieved in good yields. The Ni(II)-based coupling catalyst was prepared according to a literature procedure^[73] by reacting nickelbromide with an excess of triphenylphosphine in boiling butanol. Subsequent coupling in tetrahydrofuran yielded the pyrrole-protected, disubstituted bipyridine (according to NMR analysis), but the deprotection of the amino-function failed completely. Varying the reaction conditions did not change this outcome.

It was also tried to synthesize the mono-substituted bipyridine by means of an asymmetric coupling. This reaction (figure 5.8) coupled the pyrrole-protected chloropyridine with 2-bromopyridine.

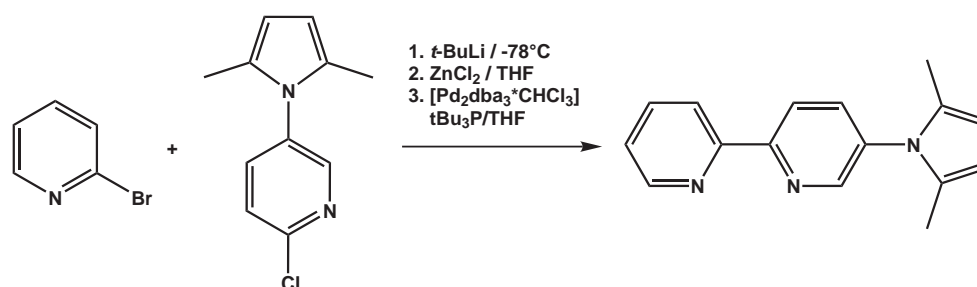


Figure 5.8: Coupling of an asymmetrical Pyrrol-protected bipyridine^[74]

Bromine being the better leaving group, it should clearly favor the formation of the monosubstituted product. The coupling was tried with freshly synthesized^[75] tris-(di-

benzylidene-acetone)-Pd(O) \cdot CHCl₃ as catalyst in the presence of zinc chloride and tributylphosphine in tetrahydrofuran, starting with the lithiation of the bromopyridine at -78°C and subsequent addition of the coupling reagents. Several variations of the reaction parameters (time and temperature) lead to no reproducible results.

Since there was no coupling product detectable in most of the preparations, the bromine was exchanged as a leaving group with trimethyltin. This procedure was earlier described^[76] for the palladium-catalysed coupling of unsymmetrical heterobiaryls.

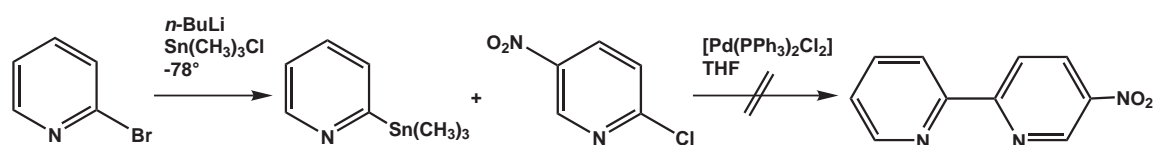


Figure 5.9: Coupling with trimethylstannyl-derivative

The preparation of the 2-(trimethyltin)-pyridine was achieved by reacting 2-bromopyridine and trimethyltinchloride in tetrahydrofuran with preceding lithiation of the bromopyridine at -78°C . Subsequent distillation of the mixture yielded pure 2-(trimethylstannyl)-pyridine. The coupling step involved the use of bis-(triphenylphosphine)-palladium-(II)-chloride as catalyst. The unreduced 5-nitro-2-chloropyridine was used for the coupling, since the amino-derivative was reported to give no detectable reaction at all. The reduction was planned to be carried out after successful isolation of the coupling product.

The last known coupling method that resulted in the correctly substituted bipyridine unit is a reductive coupling using either raney-nickel^[77] or palladium on activated charcoal^[78].

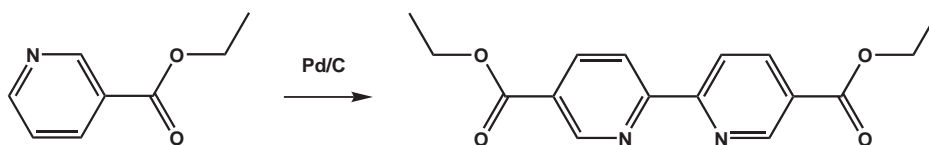


Figure 5.10: Reductive Coupling of neat ethyl nicotinate

Neat ethyl nicotinate was refluxed with about 10% palladium on carbon for several days. After dilution with *n*-hexane and extraction of the filtered catalyst in a Soxhlet-

extractor no product could be obtained after removal of the solvent and residual ethyl nicotinate.

5.2.3 Curtius Rearrangement

Since the attempts to obtain the mono- and diaminosubstituted bipyridine in reasonable yields from metal-mediated coupling reactions were irreproducible at best, a more conventional way had to be employed. Whittle et al. devised a way of modifying readily substituted bipyridines.

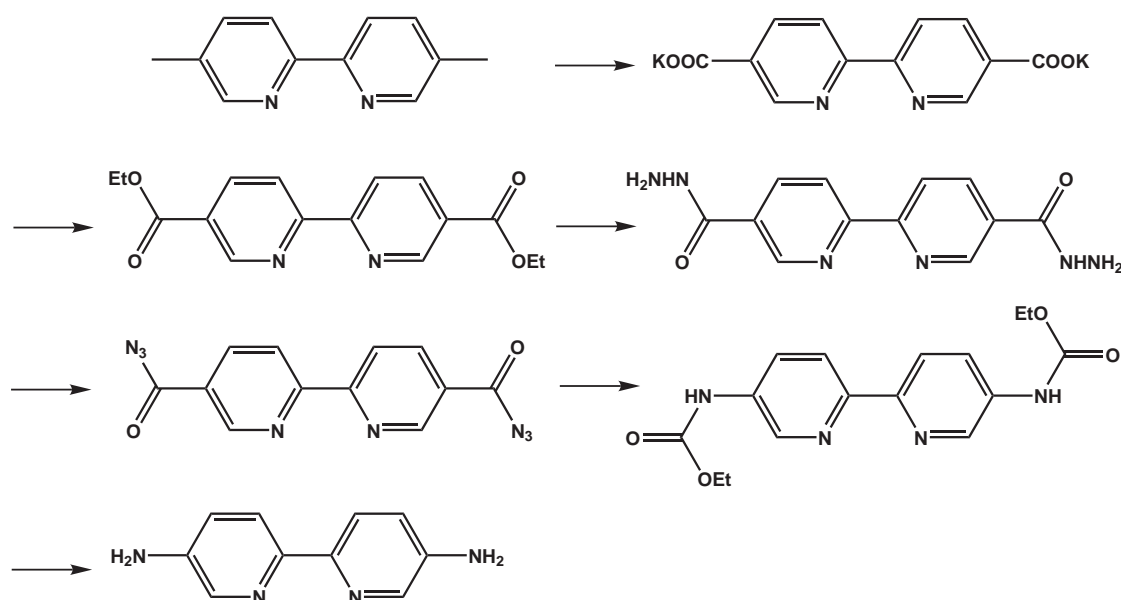


Figure 5.11: Diaminobipyridine after Whittle et al.^[79]

Starting from the 5,5'-dimethyl-substituted bipyridine, the methyl-groups were oxidised using either an aqueous solution of several equivalents of potassium permanganate or a mixture of potassium dichromate in concentrated sulfuric acid (as describe in^[79]). While the oxidation with dichromate resulted in a slightly better yield (72% compared to 58%), the more convenient work-up (removal of the solid MnO₂ and acidifying with half-concentrated hydrochloric acid) and the toxicity and carcinogenicity of chromium-trioxide made the oxidation with permanganate-solution the preferred way.

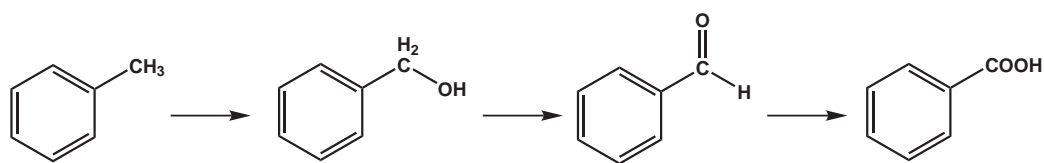


Figure 5.12: Reaction intermediates of the side-chain oxidation

The oxidation of side-chains of aromatic systems includes several single-electron-transfers from the permanganate to the aromatic ring, subsequently resulting in benzyl alcohol and benzaldehyde as intermediates and finally benzoic acid. Since the intermediates are all more reactive than the initial reactant, so the intermediates cannot be isolated. Since the resulting potassium salt of the diacid (and the following products as well) were practically insoluble in common solvents, the spectroscopic characterization with NMR had to be omitted, and the identity of the products had to be verified with elemental analysis and infrared spectroscopy only. For this reaction step, the appearance of the characteristic infrared-bands for a carboxylate group at 1691 cm^{-1} delivered the evidence for the success of the oxidation, since there are no other possible causes for this absorption band. The elemental analysis was also unsatisfactory, since the product was precipitated from water, which could not be removed completely.

The dicarboxylate of the oxidised bipyridine was esterified several hours under reflux with excess ethanol and concentrated sulfuric acid as water-removing reagent. It was also tried to use a dean-stark-trap for the reaction, but due to the poor solubility in either toluene or chloroform, this did not succeed. The shift in the IR-band of the carbonyl-stretching vibration to higher wavenumbers and the elemental analysis proved this reaction to work correctly.

The ester of the bipyridine was hydrazinolysed with a slight excess of an 80% aqueous hydrazinehydrate-solution under reflux in ethanol. The dicarbohydrazide was transformed to the diazide by suspending it in concentrated hydrochloric acid at 0°C and the slow addition of sodium nitrite. Upon dilution with copious amounts of water, the diazide precipitated. Again, the identification relied only on the IR-band of the azide-group and elemental analysis.

With the azide, it is now possible to generate the desired amine by means of a Curtius rearrangement. This reaction pathway of azides was named after its discoverer Theodor Curtius^[80].

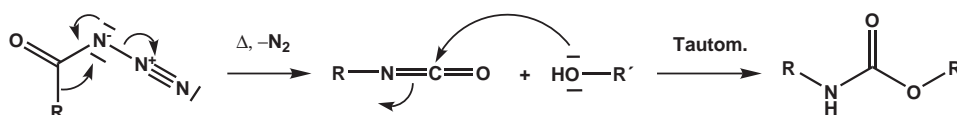


Figure 5.13: Proposed mechanism of the Curtius rearrangement

The diazide is thermally unstable and, under the release of nitrogen, is rearranging to the corresponding isocyanate. When an inert solvent like benzene is used for the reaction, the isocyanate can be isolated. But in the presence of a nucleophile like water or alcohols, it tautomerises directly to the carbamate. A consecutive mechanism with an intermediate highly reactive nitren-species was also discussed, but up until now there is now spectroscopic evidence of the existence of such an intermediate, so the concerted mechanism as shown in figure 5.13 is more accepted.

The resulting carbamate had now to be cleaved using sodium hydroxide under reflux, and after acidification the hydrochloride of the desired amine was obtained.

5.2.4 Formation of Nitrosopyridine

As with the phenylazopyridines mentioned above, the same problem arises when dealing with bipyridines. These systems are not accessible with standard azocoupling reactions due to their electron deficiency, so once again the method of condensating an aminogroup and a nitrosofunction had to be employed (figure 3.5).

The common method for the generation of nitroso-functionalized molecules is the reduction of the corresponding nitro-derivatives. Although pyridine is not very susceptible for an electrophilic substitution due to its electron deficiency, the desired 3-nitropyridine is rather easily accessible through direct nitration of pyridine in trifluoroacetic anhydride^[81]. This method has the advantage that there is no need for dinitrogen pentoxide handling prior to the reaction (dinitrogen pentoxide in sulfur dioxide solution being the only electrophile that has been reported to substitute pyri-

dine in reasonable yield^[82]).

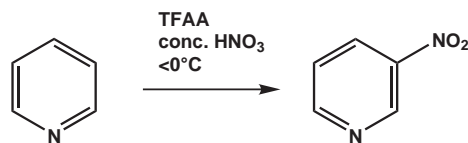


Figure 5.14: Direct Nitration of Pyridine

After quenching the reaction mixture with one equivalent sodium metabisulfite in aqueous solution, neutralization with sodium hydroxide and extraction with dichloromethane, the 3-nitropyridine was purified with column chromatography over silica gel to yield 80% 3-nitropyridine. The nitro-group was now to be oxidised to the nitroso-function. The mechanism is exemplified in figure 5.15.

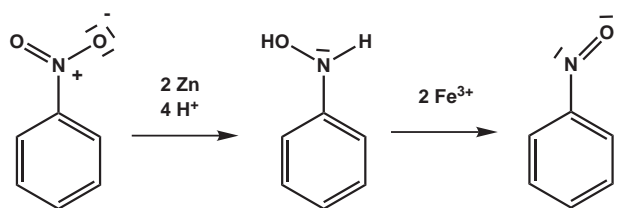


Figure 5.15: Reduction of a nitrofunction to nitroso

In a slightly acidic solution, the nitrobenzene is reduced by the uptake of four electrons to the hydroxylamine. The addition of iron(III)chloride oxidises the hydroxylamine to nitrosobenzene^[83]. This published procedure was transferred to the corresponding nitropyridine, with no success. 3-nitrosopyridine was not to be gained from the reduction with zinc.

Another way to generate the 3-nitrosopyridine by reducing 3-nitropyridine was published by Kirpal in 1925^[84]. It used freshly synthesized amalgamated aluminium in diethylether at 0°C, higher temperatures supposedly lead directly to the undesired aminopyridine. Aluminium turnings were freed of their oxide surface by rinsing with sodium hydroxide and water, and afterwards amalgamated with a mercurynitrate solution.

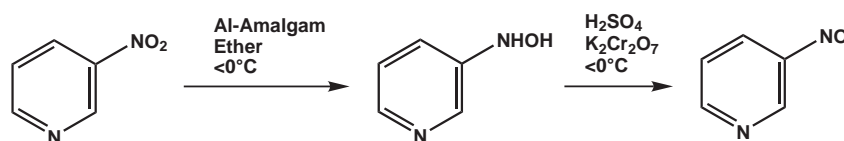


Figure 5.16: Synthesis of Nitrosopyridine from Nitropyridine

After 10 minutes reaction the now formed 3-pyridylhydroxylamine was to be separated from the aluminiumhydroxide by extraction of the precipitate with diethylether. The formation of the precipitate was observable, but after extracting with copious amounts of ether no pyridylhydroxylamine remained after removal of the solvent under reduced pressure. Supposedly the pyridine was adsorbed very strongly into the gel-like aluminiumhydroxide to be extracted. The following reaction with potassium dichromate in sulfuric acid could thus not be carried out.

In 1970, Bartlett published a procedure to substitute a trialkyl-stannyl leaving group on an aromatic ring with nitrosyl chloride to yield the corresponding nitrosoderivative^[85]. Although nitrosyl chloride is commercially available in its gaseous form, the handling of larger amounts of this corrosive and toxic gas is quite delicate. It is far more convenient to either generate the nitrosyl-cation *in-situ* e.g. with sodium nitrite in concentrated hydrochloric acid, or to freshly synthesize the desired amount when needed. Several methods are described in the literature, mostly involving the reaction of an alkyl-nitrite with hydrochloric acid, drying and collecting the gaseous nitrosyl chloride in a cooling trap (e.g.^[86])

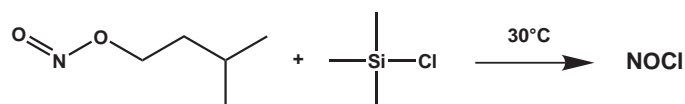


Figure 5.17: Synthesis of nitrosyl chloride

The 3-trimethylstannylpyridine was prepared in analogy to 2-stannylpyridine by first lithiating the 3-bromopyridine, subsequent reaction with trimethyltinchloride and distillation of the product. The synthetic procedure had to be adapted a little due to the different reactivity of the 3-bromopyridine compared to the 2-bromopyridine^[87].

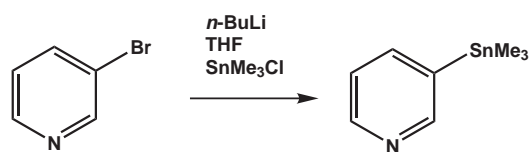


Figure 5.18: Synthesis of 3-stannylpyridine

The temperature had to be as low as possible (about -100°C) to prevent an undesired de-protonation of the 3-bromopyridine^[88], so instead of solid carbon dioxide in acetone, liquid nitrogen was used to freeze the acetone solid, which results in a bath-temperature of -95°C . But still, only small amounts of 3-stannylpyridine were collected from the reaction mixture.

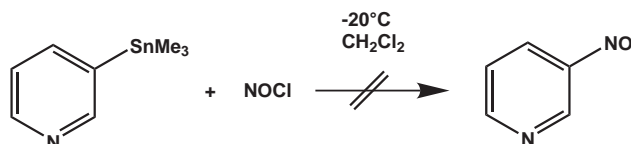
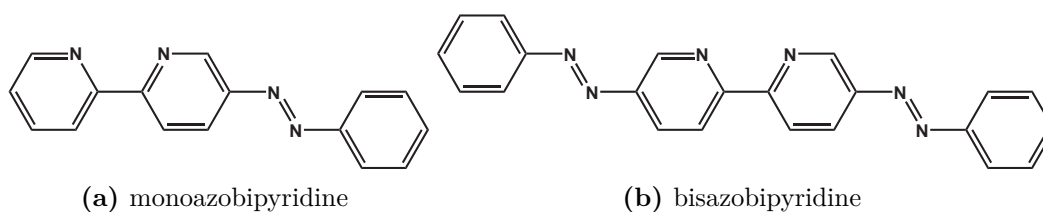


Figure 5.19: Substituting the trimethylstannyl-group with NO

Attempts to react the trimethylstannylpyridine with nitrosyl chloride, at different temperatures and with either subsequent addition of the two reactants or as a one-pot-synthesis, were all unsuccessful. Instead of nitrosyl chloride in dry solvents (dichloromethane and chloroform), the reaction was also attempted with nitrosonium tetrafluoroborate, with no other outcome.

Since all attempts to generate and characterize the 3-nitrosopyridine, the only way around was to proceed with nitrosobenzene instead of nitrosopyridine, thus omitting the switchable decoordination sites at the iron center.



5.2.5 Asymmetrically substituted bipyridine

Newkome published a synthetic protocol^[78] that does not transform both ethylcarboxylate groups simultaneously, but due to a lower reaction temperature should lead selectively to the monocarbohydrazide and leave the second ethylcarboxylate-group unchanged.

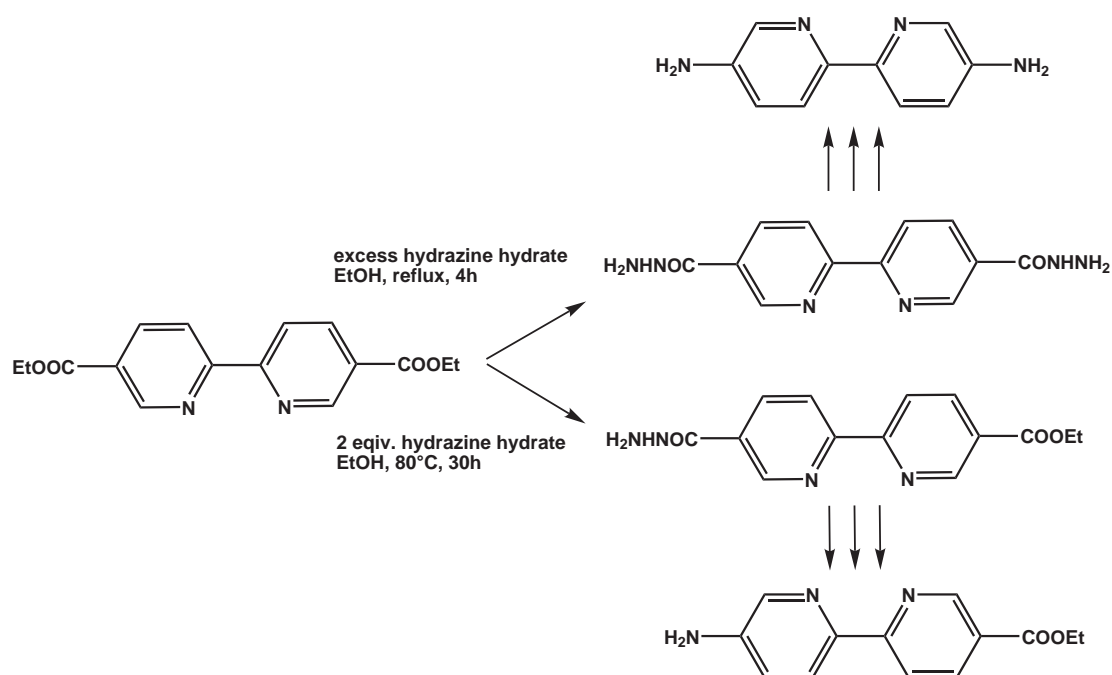


Figure 5.20: Selective asymmetric Rearrangement after Newkome

Unfortunately, the reaction lead to a mixture of mono- and disubstituted bipyridine, which could not be separated due to the bad solubility of the compounds. An other way of gaining access to 5-methyl-2,2'-bipyridine was published by Chung^[89] as a two-step reaction, starting from 2-acetylpyridine, which was transformed to the corresponding iodide-salt by reaction with elemental iodine in pyridine.

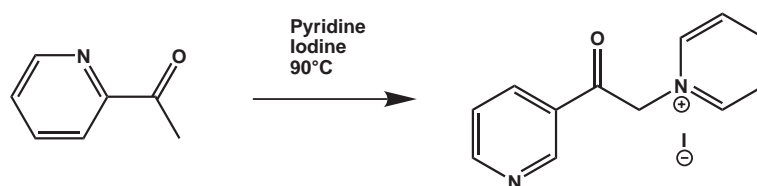


Figure 5.21: Acetylpyridiniumiodide

The pyridine deprotonated the acidic proton in the 2-acetylpyridine and the iodide immediately precipitated from the solution. After removal of residual pyridine from the product with activated charcoal in ethanol, the 2-acetylpyridinium iodide was obtained in good yield. The intermediate was dissolved in dry and degassed formamide and subsequently mixed with ammonium acetate and methacrolein.

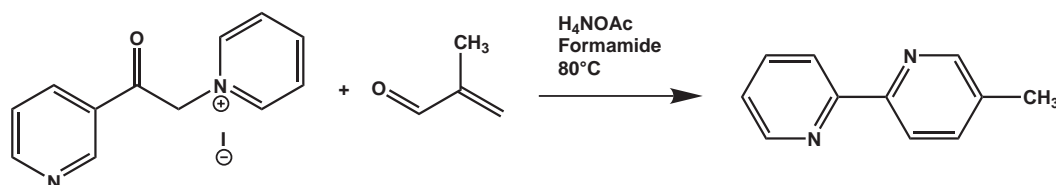


Figure 5.22: Monomethylbipyridine

The formamide was purchased in the highest available quality prior to the synthesis, degassed and stored inside a glove box, since earlier attempts with formamide already stored for some time resulted in very low yields (around 10%). The same synthesis with dried solvents and fresh formamide was virtually quantitative (>90%). After extraction with diethylether and column chromatography 5-methyl-2,2'-bipyridine was obtained in great quantities, which was necessary, for the following reaction steps all resulted in rather low yields.

The synthesis was then continued in analogy to the diamino-substituted bipyridine^[79], with oxidation of the methyl-group to the potassium carboxylate.

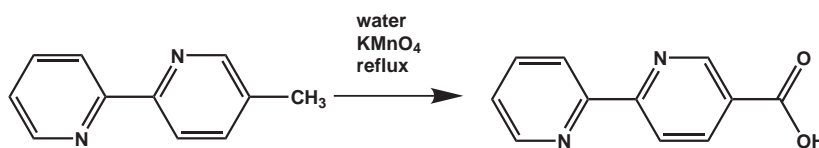


Figure 5.23: Oxidation with permanganate

Again, the oxidation with permanganate in aqueous solution was preferred to other oxidation methods. After removal of the manganese dioxide, the solution had to be reduced to a quarter of its original volume to force precipitation of the carboxylic acid. The identity of the product was once again checked with IR-spectroscopy, as for NMR-studies, the compound is insoluble in common solvents, and though the compound was dried several hours in high vacuum and was pestled several times, it

could not be freed completely of water, so the elemental analysis was unsatisfactory. But the IR-spectrum showed a distinct band at 1721 cm^{-1} , which is assigned to the carbonyl-stretch of the newly-formed carboxylate.

The esterification with excess ethanol and sulfuric acid however did not give any result, and the use of a dean-stark-trap for water-removal was still impossible, so another way had to be used.

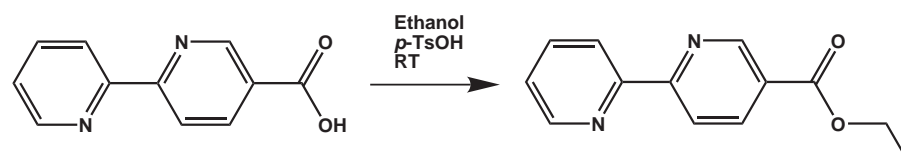


Figure 5.24: Esterification

Paratoluenesulfonic acid, which is used in standard esterifications only in catalytic amounts, was added in five-fold excess to a suspension of the bipyridine-monoacid in ethanol and stirred for 24 hours at roomtemperature. After concentration of the mixture and pH-adjustment to 8 with saturated sodium hydrogencarbonate solution, the desired product was extracted from the mixture with large quantities of ethyl acetate. Despite a high number of extractions, the yield was rather poor.

Having the ethylester of the 5-carboxy-2,2'-bipyridine in larger quantities ($>10\text{g}$), the synthesis progress analogous to the earlier synthesized 5,5'-diamino-2,2'-bipyridine.

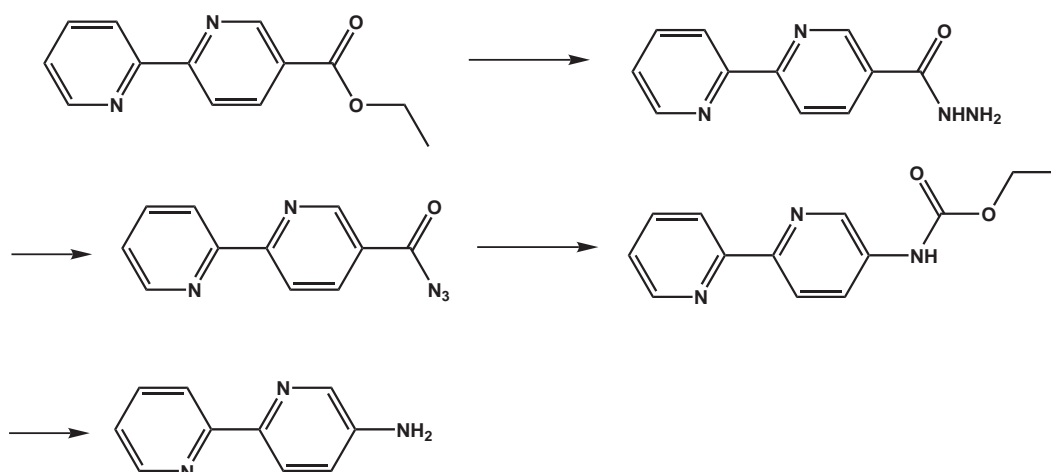


Figure 5.25: Further progression after Whittle^[79]

All synthetic steps were successful, but the yield was low compared to the synthesis

of the symmetrically substituted bipyridine.

5.2.6 Azocoupling

The final step towards the switchable ligand was the azocoupling via the aforementioned Mills-reaction (figure 3.5).

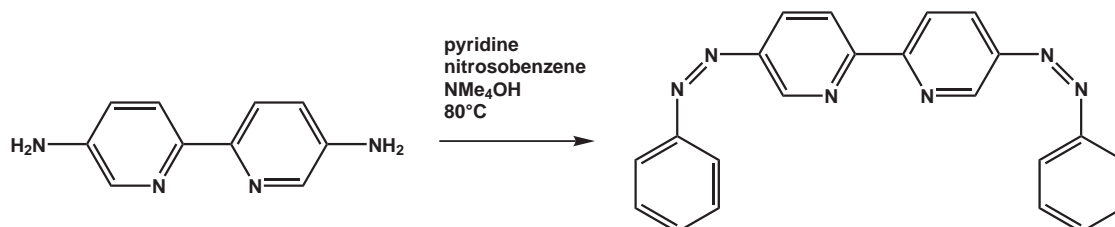


Figure 5.26: Bisazobipyridine

The final product had not to be extracted from the reaction mixture, it readily precipitated during the reaction. After washing with acetone several times to remove adsorbed pyridine, the compound was obtained. A recrystallization however was not possible due to the insolubility in all common solvents. The recorded ¹H-NMR spectrum (figure 5.27) in dimethylsulfoxid is of rather poor quality, since only roughly about 3-4 mg could be dissolved.

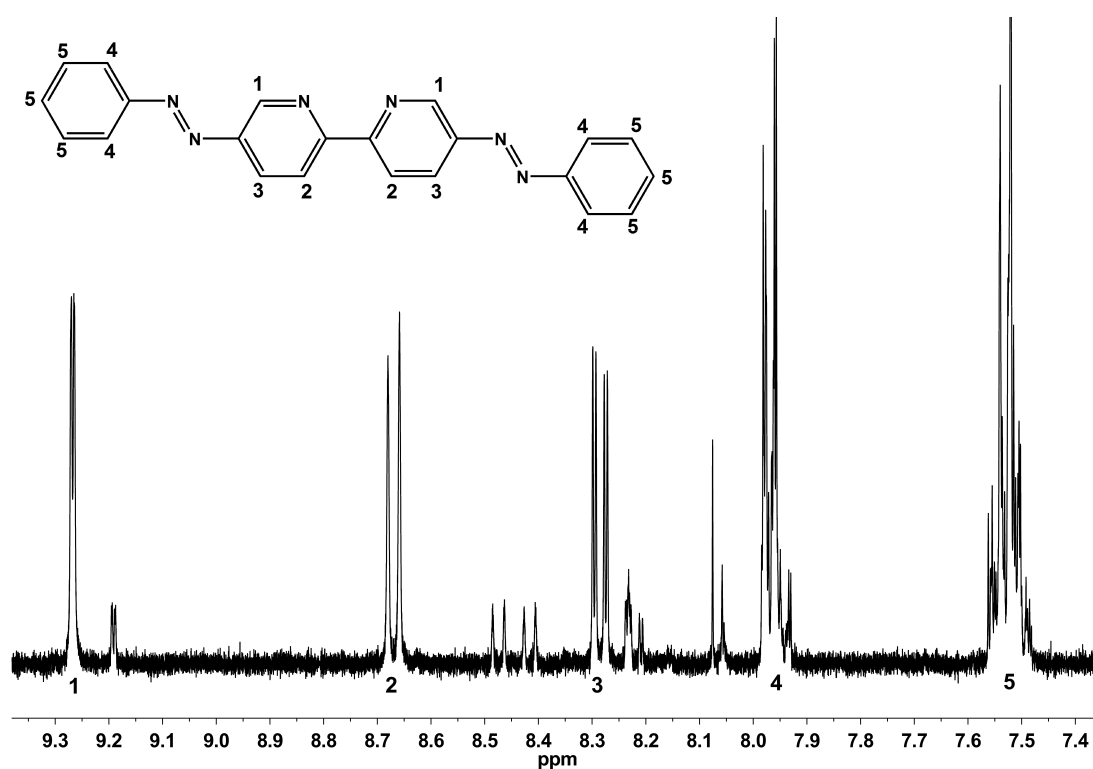


Figure 5.27: $^1\text{H-NMR}$ of Bisazobipyridine

The proton-signals of the bisazobipyridine could be assigned. However, several additional signals from impurities were also observed, which could not be removed by additional work-ups. The dissolved amount of substance also was insufficient for $^{13}\text{C-NMR}$ spectroscopy. To verify the identity of the obtained product, mass spectra were recorded with either electron-impact- or chemical ionisation measurements.

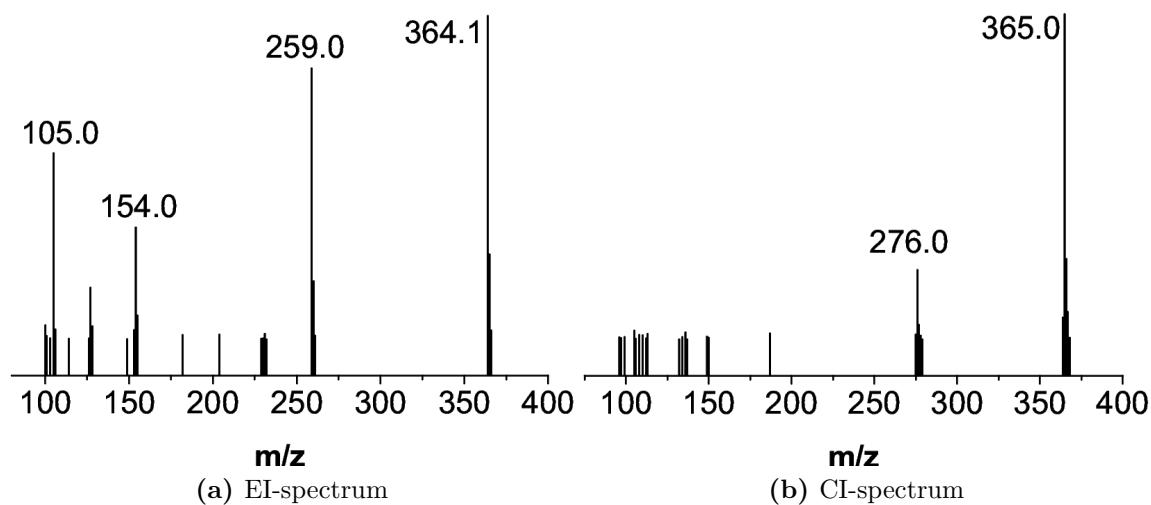


Figure 5.28: Mass-spectra of Bisazobipyridine

Both spectra show the molecule peak of the bisazobipyridine at $m/z=364.1$ (EI-spectrum, M^+) and 365 (CI-spectrum, $M-H^+$), respectively. The most prominent detectable fragments are the phenyldiazoniumcation at $m/z=105$, the unsubstituted bipyridine-core at $m/z=154$ and the monophenylazo-substituted bipyridine (259) and monoaminobipyridine with one remaining phenylazofunction at $m/z=276$.

The measured infrared- and raman-spectra of bisazobipyridine were compared with the calculated spectra (level of theory: B3LYP/6-311++g**).

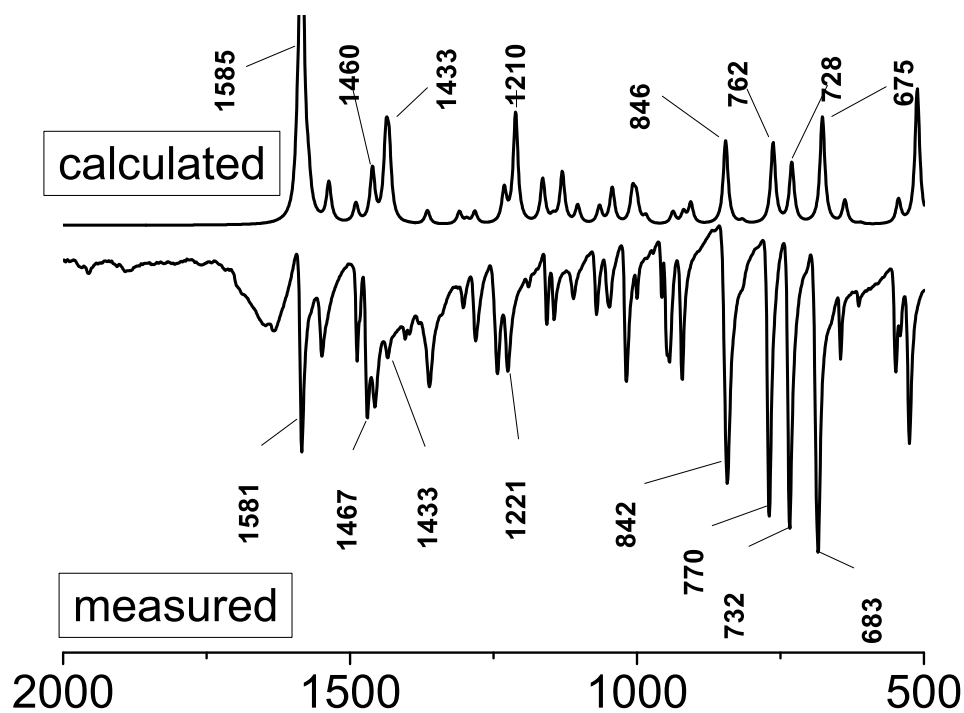


Figure 5.29: IR-spectra of bisazobipyridine

The calculated infrared-spectrum is in good agreement with the experimental spectrum. No distinctive azo-band is observable, the vibrational modes with at least minimal participation of the N-N double-bond are summed up in table 5.1.

measured [cm^{-1}]	calculated [cm^{-1}]	vibrational mode
1581	1585	ν_{108} symm. C-C deformation
1467	1460	ν_{99} symm. C-C deformation
1433	1433	ν_{95} symm. C-C deformation

Table 5.1: IR-active Azo-Bands in bisazobipyridine

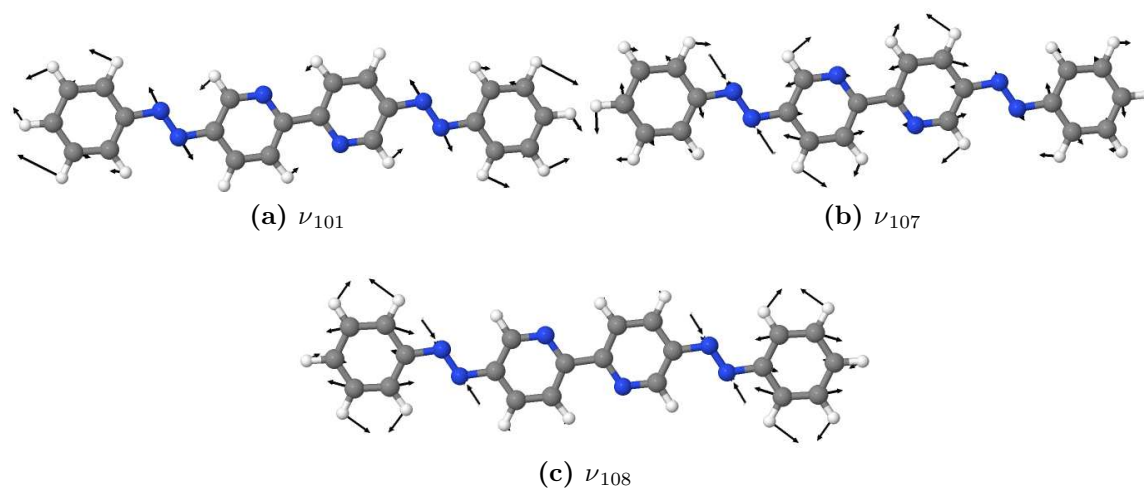


Figure 5.30: Vibrational modes of the azo-group in *trans*-bisazobipyridine

Only the bands with significant participation of the N-N double bond are further depicted, since all other bands are highly unlikely to be of any value when investigating the isomerisation process with vibrational spectroscopy.

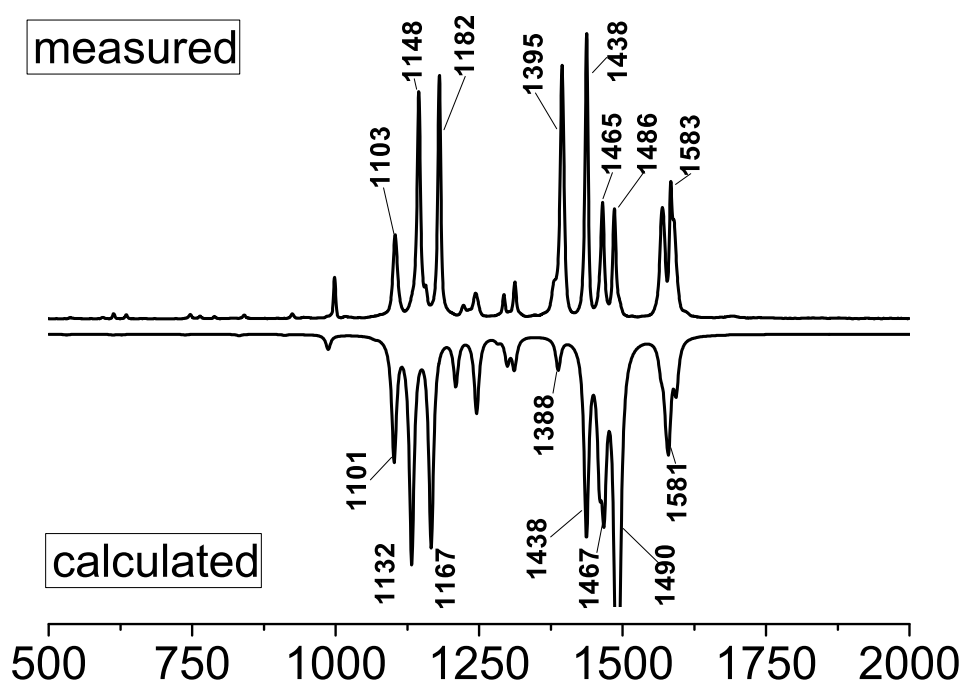


Figure 5.31: Raman-spectra of bisazobipyridine

measured [cm^{-1}]	calculated [cm^{-1}]	vibrational mode
1465	1467	ν_{100} asym. C-C-deformation
1486	1490	ν_{101} asym. C-C-deformation
1583	1581	ν_{107} asym. C-C-deformation

Table 5.2: Assignment Raman-Azobands Bisazobipyridine

All the simulated spectra are in very good agreement with the measured ones after correction of the wavenumbers.

The asymmetric ligand was obtained in a similar way, but the repeated washing was omitted since the ligand was soluble in most solvents. This difference can be explained by the higher symmetry of the disubstituted molecule, which has no dipole moment at all.

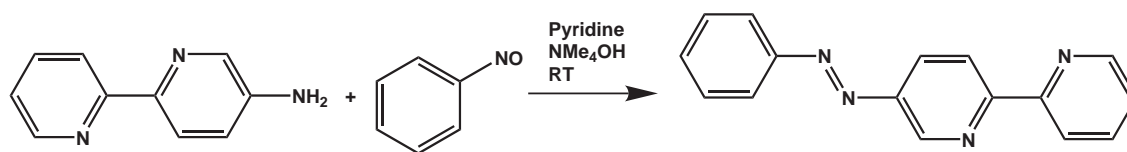


Figure 5.32: Synthesis of monoazobipyridine

Analysis with NMR was achieved, the compound was sufficiently pure after washing once with cold ethanol.

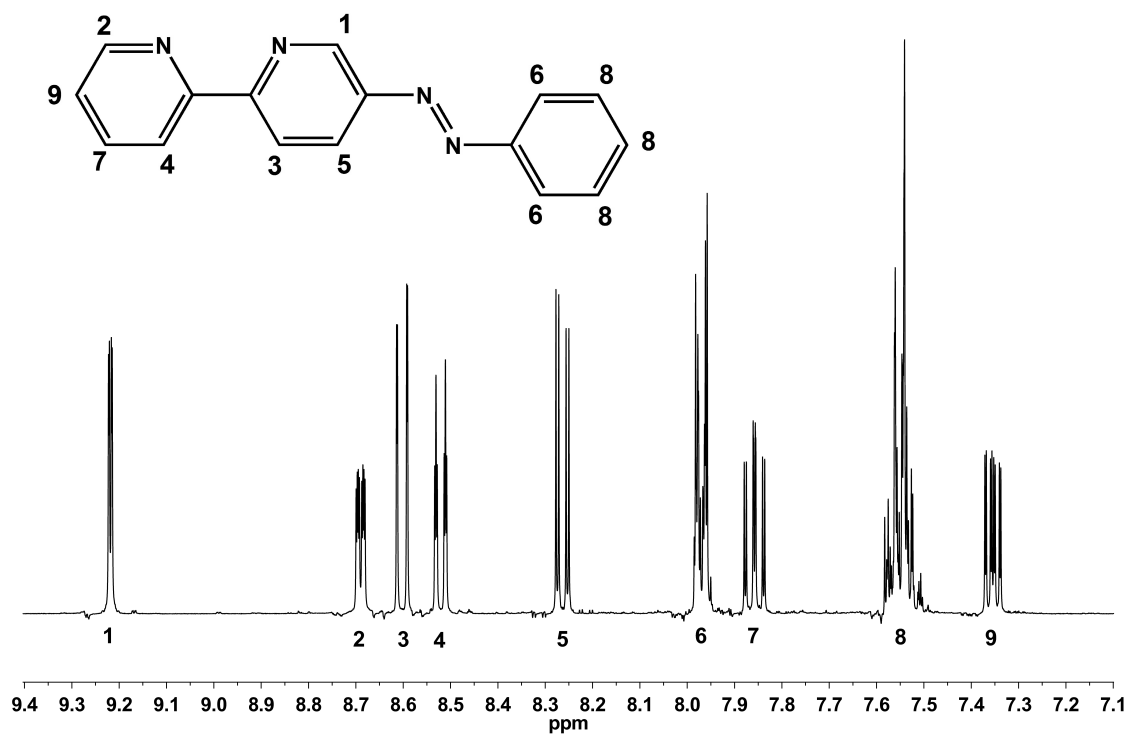


Figure 5.33: ¹H-NMR of monoazobipyridine

The signals were assigned to the corresponding atoms in figure 5.33 and figure 5.34.

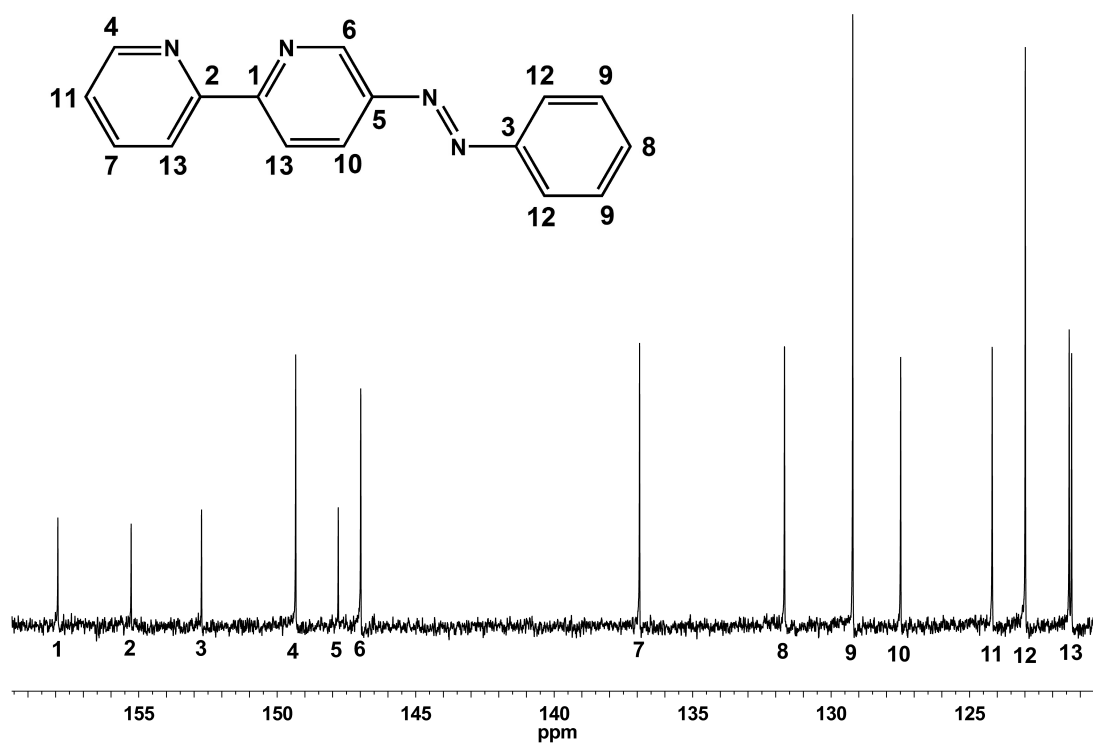


Figure 5.34: ^{13}C -NMR of monoazobipyridine

The measured infrared and raman spectra of the monophenylazo-bipyridine were also compared to the calculated ones, on the same theoretical level as for the bisazobipyridine.

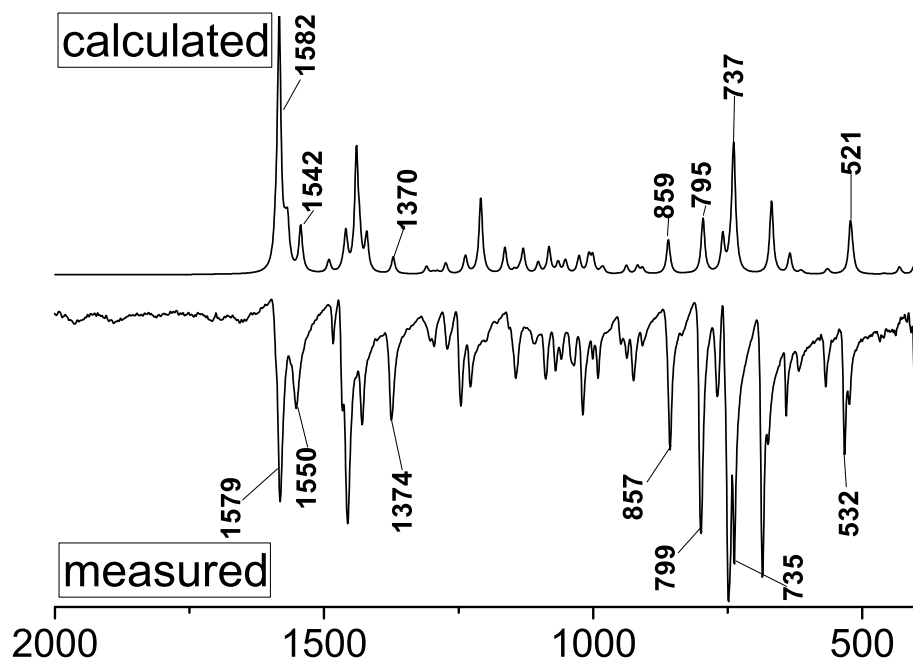


Figure 5.35: IR-spectra of monoazobipyridine

The most prominent bands were assigned. Again, no azo-only band can be observed in the infrared-spectrum.

measured [cm^{-1}]	calculated [cm^{-1}]	vibrational mode
1579	1582	ν_{77}
1555	1542	ν_{73}

Table 5.3: Assignment IR-Bands Monoazobipyridine

As before, in the monoazobipyridine-ligand, the azo-group only shows significant vibrational bands in the raman-spectrum.

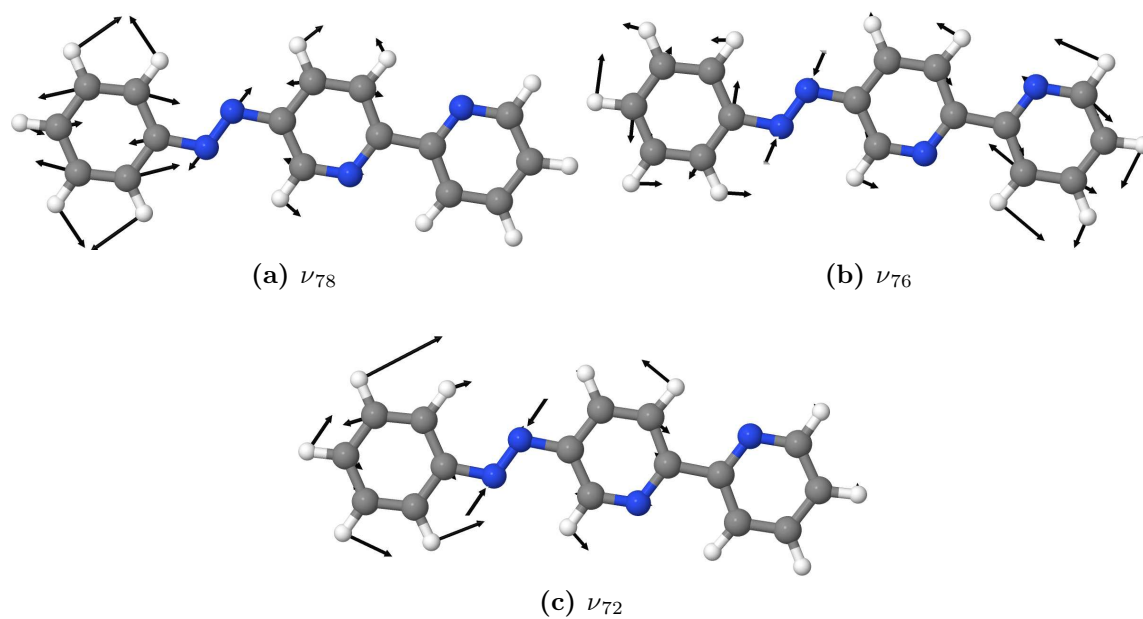


Figure 5.36: Vibrational modes of the azo-group in *trans*-monoazobipyridine

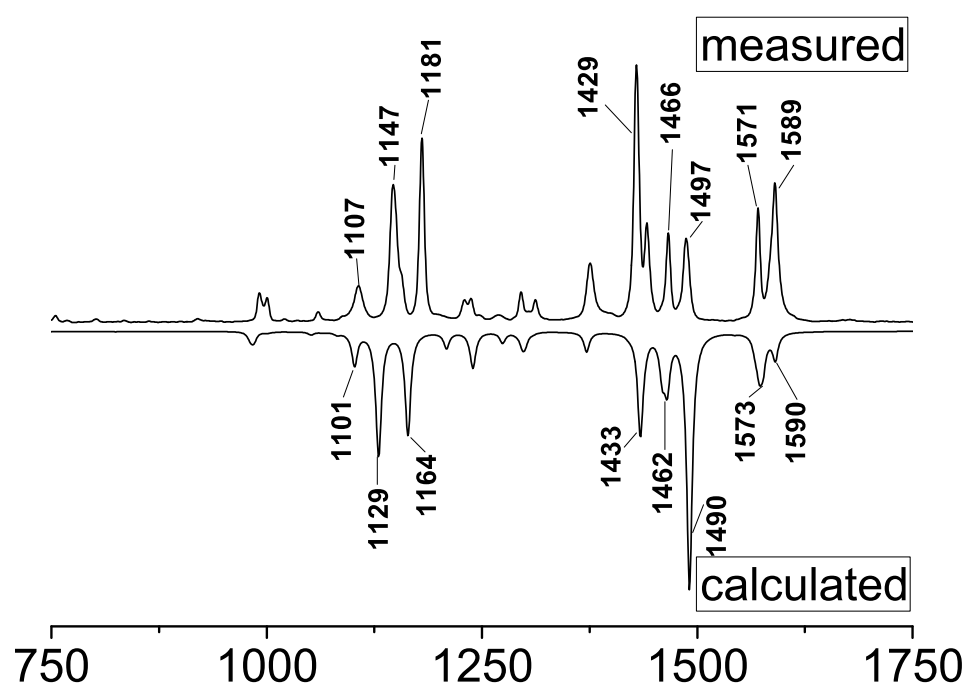


Figure 5.37: Raman-spectra

measured [cm^{-1}]	calculated [cm^{-1}]	vibrational mode
1589	1590	ν_{78}
1571	1573	ν_{76}
1497	1490	ν_{72}

Table 5.4: Assignment IR-Bands Monoazobipyridine

5.3 Switchable Complexes

5.3.1 Iron-chloride precursors

To get access to a suitable molecular switch, the projected molecules all should possess the ability to undergo the thermal spin transition, for their strongly increased sensitivity towards even the slightest changes in the strength of the ligand field. To minimise the number of possible photoswitchable conformers of the same compound, only heteroleptic complexes were to be investigated, bearing a photoinactive co-ligand to occupy the other coordination sites of the iron-center.

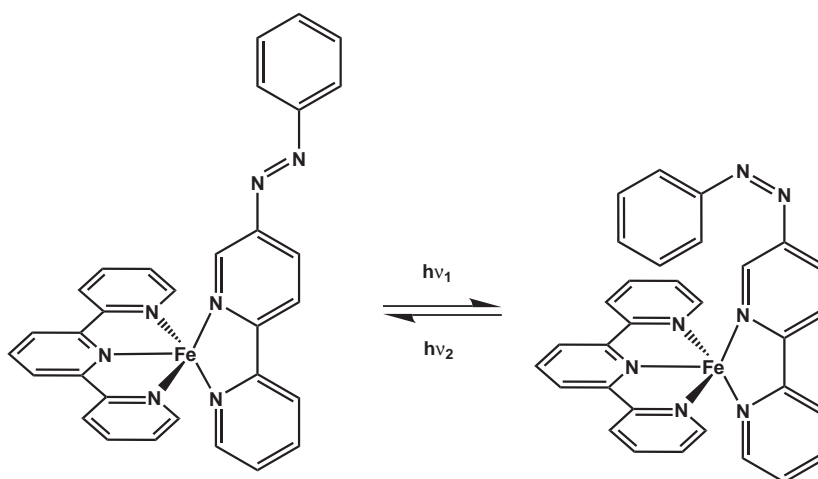


Figure 5.38: Switching of monoazobipy-switch with terpyridine-coligand

Since all of the photoinactive ligands known to form spin-crossover compounds are chelating aromatic N-donors, the synthesis of adequate precursors was rather delicate. The iron chloride tetrahydrate was freshly prepared from fine ground iron powder dissolved in hydrochloric acid, which is far more reactive than the water-free

iron-halides commercially available. Also, the iron had to be used in 10-fold excess (dissolved in degassed ethanol) and the reaction-time had to be rather short (10 min) to suppress the formation of iron-complexes that bear two or three (for bipyridine and phen) equal substituents.

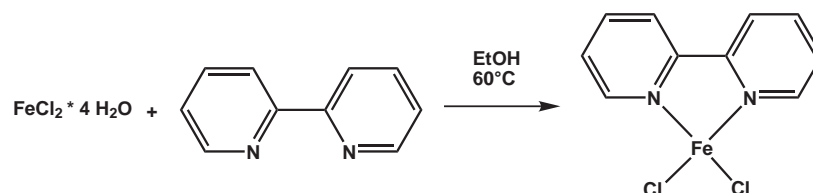


Figure 5.39: Monosubstituted Iron(II)chloride

With this method (exemplified for bipyridine in Figure 5.39) the following compounds were prepared. Since not only aromatic N-donor systems are known to produce thermal spin-crossover systems, also two diphosphine ligands known to form iron(II)-complexes with SCO capability^{[90] [91]}, the 1,2-bis(diphenylphosphino)ethane (dppe) and the *ortho*-bis(diphenylphosphino)benzene (opdp) were coordinated to iron(II)-chloride.

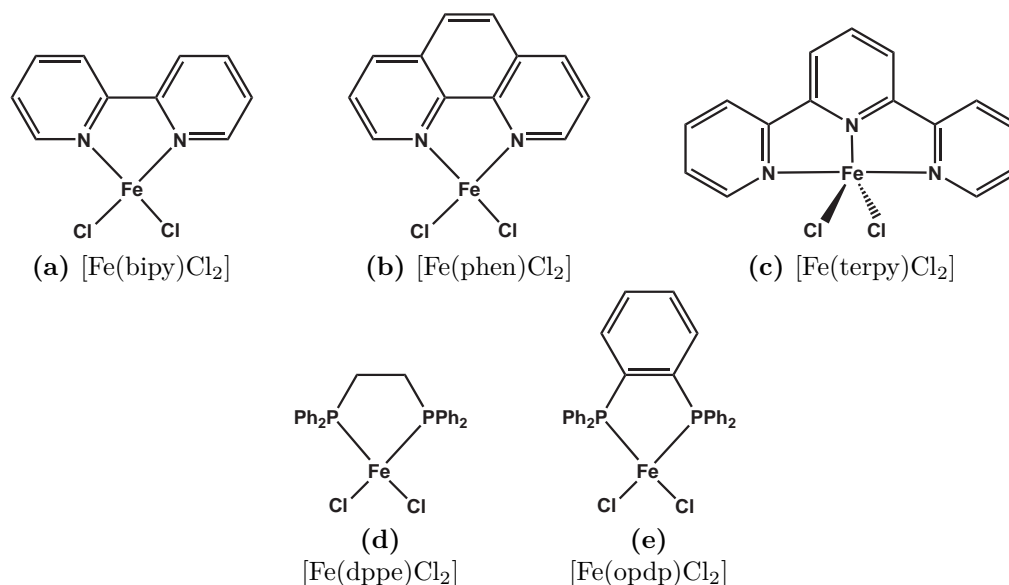


Figure 5.40: Monosubstituted Iron Complexes

Starting from these precursors, it was attempted to exchange the chloride-ligands with

unfunctionalized bipyridine (for direct treatment with the photoswitchable ligands, these were far too time-consuming to synthesise, so the commercially available 2,2'-bipyridine was used instead).

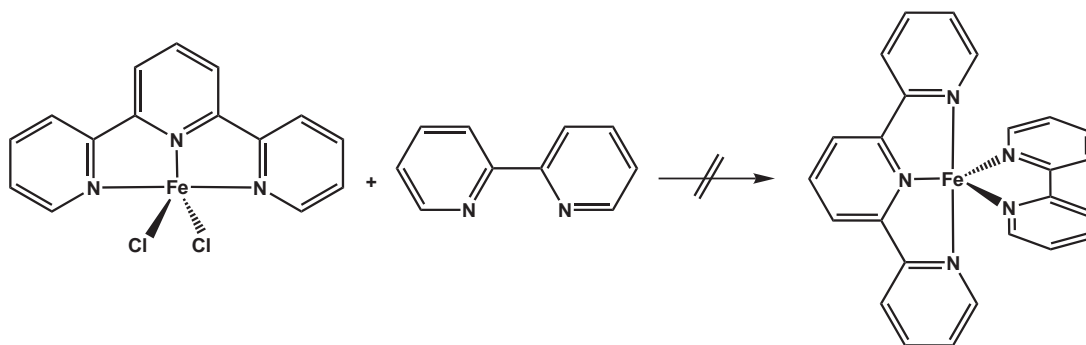


Figure 5.41: Mixed heteroleptic compound

The substitution reactions had to be carried out fast, so the probability of ligand-dissociation and rearrangement was kept low. Either precursor and additional ligand were used in stoichiometric amounts, or one of the two components was used in excess, it was impossible to get a clean and reproducible product from these exchange attempts. Elemental analysis and Mößbauer-spectra always showed the generation of a mixture of products, which is not hard to explain, since all of these chelating ligands are well known to form bis- and tris-substituted iron(II)-complexes.

5.3.2 Bispyrazolylborate

A better alternative than trying to subsequently attach the photoswitch and the inactive ligand to the central atom would of course be either to exchange a rather weakly-bound leaving group on a photoinactive complex with the photoswitchable ligand or to create an intermediate four-coordinated iron-center and immediately afterwards react this compound with the photoswitchable bipyridine which occupies two coordination sites. Following the latter concept, Real et al. published a neutral iron(II)-complex that fulfilled all demands for a suitable switch^[92]. They used two negatively charged bispyrazolylborate and 2,2'-bipyridine (1,10'-phenanthroline) to synthesize an air-stable (in solid) spin-crossover compound.

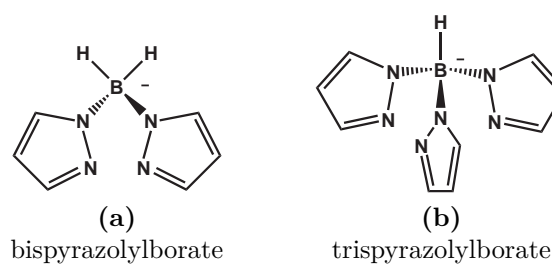


Figure 5.42: Pyrazolylborate Ligands

Conventionally, the two pyrazolborate-derivatives with two or three attached pyrazole-units are synthesized by reacting tetrahydroborate with molten pyrrazole and thus gaining a mixture of two- and threefold substituted borates. By careful adjustment of temperature and reaction time the formation of one of the two could be favored. But by reacting potassium borohydride with an 2-fold excess of pyrrazole in boiling toluene selectively the bis-substituted borate could be synthesized in practically quantitative yields.



Figure 5.43: Synthesis of KH₂BPz₂

The potassium salt of the borate crystallized readily from the still warm toluene-solution. Two equivalents of the bispyrazolylborate were now reacted with iron(II)-perchlorate in methanolic solution, from which the potassium perchlorate immediately precipitated and could be filtered of. The colourless solution now contained the neutral, four-coordinate iron-bispyrazolylborate complex. To this a solution of the desired two-coordinate ligand had to be added, and the neutral six-coordinate complex readily precipitated from the solution upon cooling.

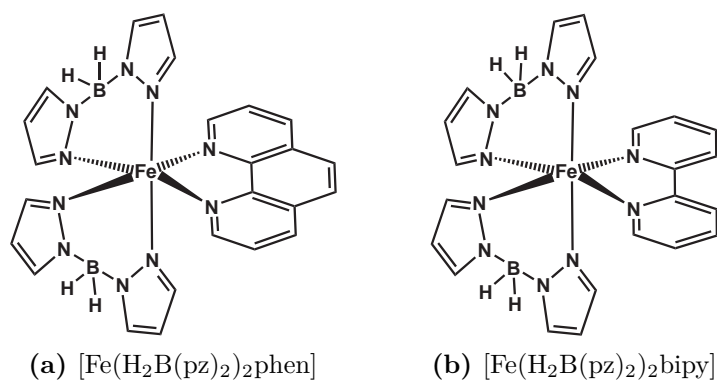


Figure 5.44: Bispyrazolylborate Iron(II)-Complexes

Whilst dissolved, the complex was very susceptible towards oxidation, so it was crucial to use repeatedly degassed solvents for the preparation or measurements in solution. In the solid state, the compounds were all insensitive to moisture or oxygen and could be stored under normal atmosphere indefinitely without decomposition.

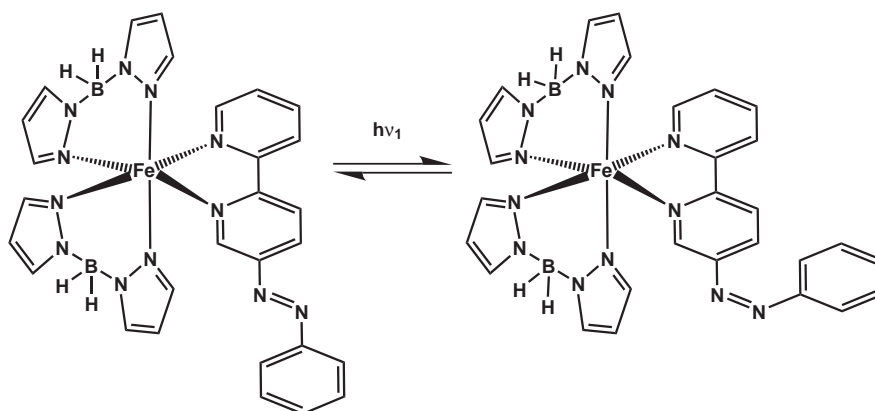


Figure 5.45: Switching of $[\text{Fe}(\text{H}_2\text{B}(\text{pz})_2)_2\text{monoazobipy}]$

The complexes with the switchable bipyridine-derivatives were prepared according to the procedure used above. The monosubstituted switch was attached to the bispyrazolyl-complex in this way. However the disubstituted switch, being virtually insoluble in all solvents was not successfully reacted with the bispyrazolylborate-iron.

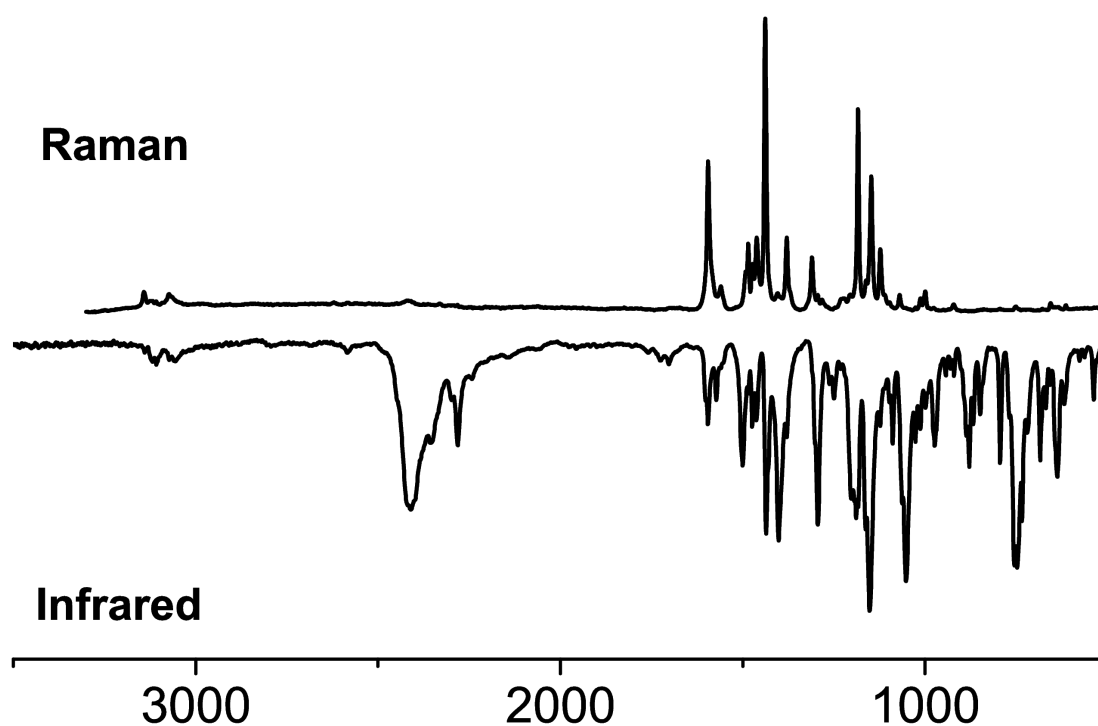


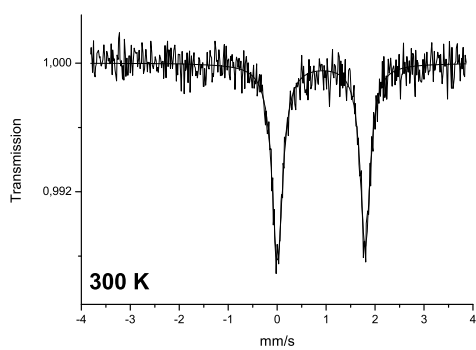
Figure 5.46: Vibrational Spectra of $[\text{Fe}(\text{H}_2\text{B}(\text{pz})_2)_2\text{monoazobipy}]$

The most distinctive difference between the infrared and raman spectrum (figure 5.46) of the complex is the absence of the boron-hydrogen vibrations at 2415 cm^{-1} and 2215 cm^{-1} , since these are virtually not raman-active.

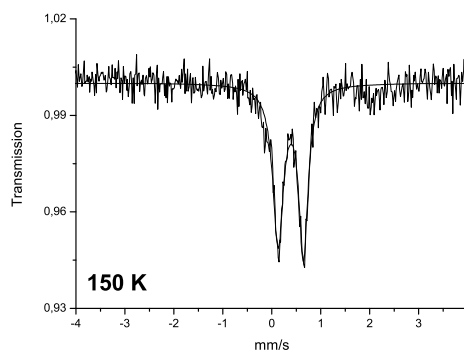
5.4 SCO of Azochelates

5.4.1 Mössbauer-spectra

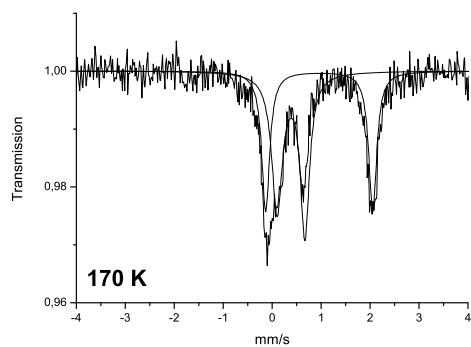
Mössbauer-spectra of the $[\text{Fe}(\text{H}_2\text{BPz})_2]$ -compounds are typical examples for iron(II)-spincrossover systems.



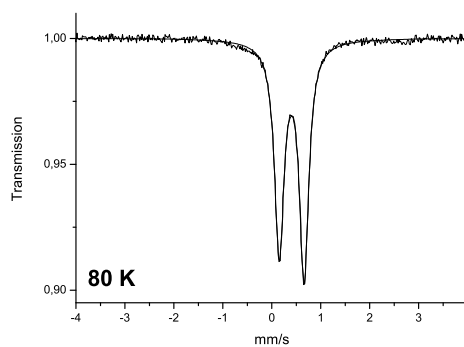
$$\delta_{IS}=1.01 \text{ mm/s}; \Delta_{EQ}=1.80 \text{ mm/s}$$



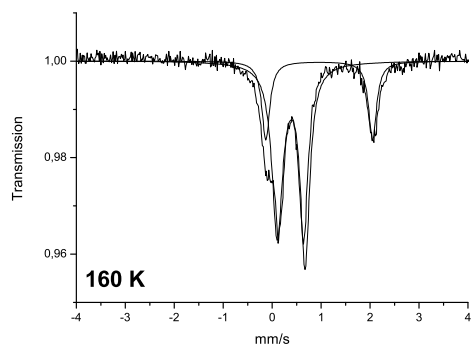
$$\delta_{IS}=0.39 \text{ mm/s}; \Delta_{EQ}=0.52 \text{ mm/s}$$



$$\begin{aligned} \delta_{IS}&=0.39 \text{ mm/s}; \Delta_{EQ}=0.59 \text{ mm/s} \\ \delta_{IS}&=0.96 \text{ mm/s}; \Delta_{EQ}=2.19 \text{ mm/s} \end{aligned}$$

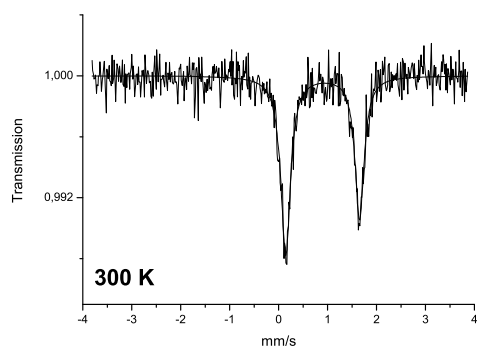


$$\delta_{IS}=0.41 \text{ mm/s}; \Delta_{EQ}=0.51 \text{ mm/s}$$

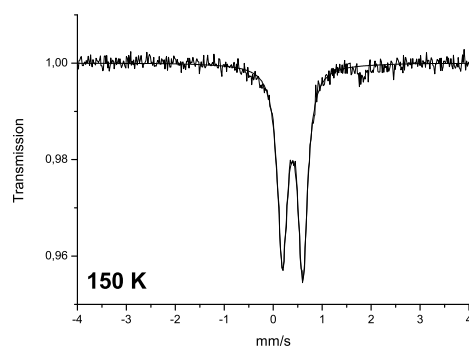


$$\begin{aligned} \delta_{IS}&=0.39 \text{ mm/s}; \Delta_{EQ}=0.57 \text{ mm/s} \\ \delta_{IS}&=0.96 \text{ mm/s}; \Delta_{EQ}=2.18 \text{ mm/s} \end{aligned}$$

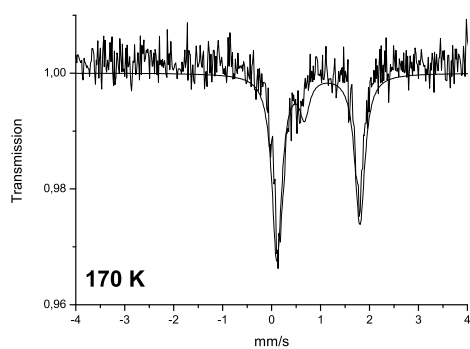
Figure 5.47: Mössbauer-spectra of $[\text{Fe}(\text{H}_2\text{BPz})_2\text{bipy}]$



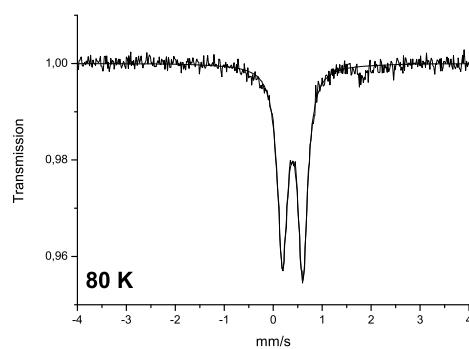
$$\delta_{IS}=1.01 \text{ mm/s}; \Delta_{EQ}=1.51 \text{ mm/s}$$



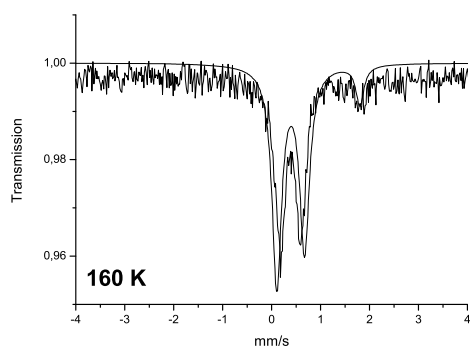
$$\delta_{IS}=0.40 \text{ mm/s}; \Delta_{EQ}=0.41 \text{ mm/s}$$



$$\begin{aligned} \delta_{IS}&=0.39 \text{ mm/s}; \Delta_{EQ}=0.56 \text{ mm/s} \\ \delta_{IS}&=0.96 \text{ mm/s}; \Delta_{EQ}=1.70 \text{ mm/s} \end{aligned}$$

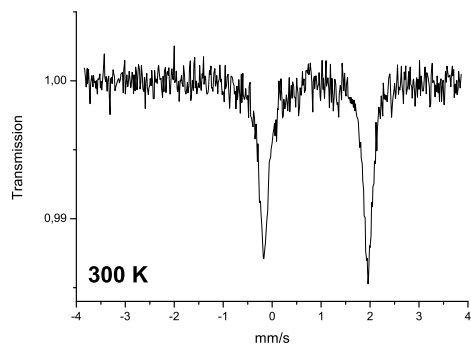


$$\delta_{IS}=0.41 \text{ mm/s}; \Delta_{EQ}=0.40 \text{ mm/s}$$

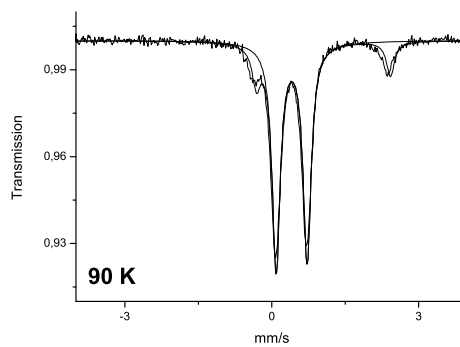


$$\begin{aligned} \delta_{IS}&=0.39 \text{ mm/s}; \Delta_{EQ}=0.57 \text{ mm/s} \\ \delta_{IS}&=0.95 \text{ mm/s}; \Delta_{EQ}=1.70 \text{ mm/s} \end{aligned}$$

Figure 5.48: Mößbauer-spectra of $[\text{Fe}(\text{H}_2\text{BPz})_2\text{phen}]$

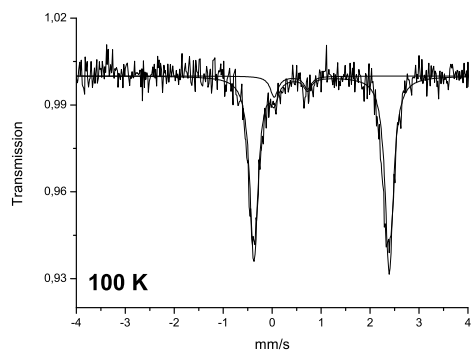


$$\delta_{IS}=1.01 \text{ mm/s}; \Delta_{EQ}=2.02 \text{ mm/s}$$



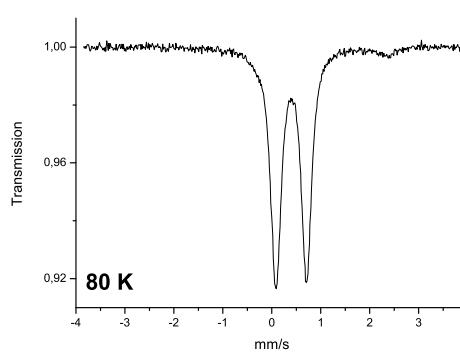
$$\delta_{IS}=0.50 \text{ mm/s}; \Delta_{EQ}=0.63 \text{ mm/s}$$

$$\delta_{IS}=1.15 \text{ mm/s}; \Delta_{EQ}=2.74 \text{ mm/s}$$

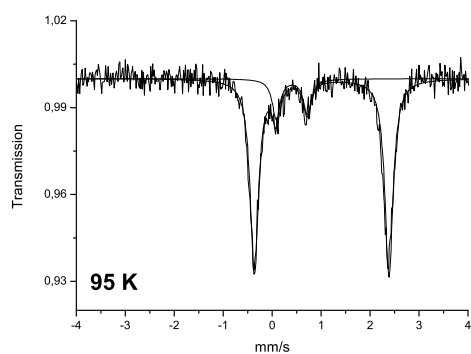


$$\delta_{IS}=0.50 \text{ mm/s}; \Delta_{EQ}=0.63 \text{ mm/s}$$

$$\delta_{IS}=1.15 \text{ mm/s}; \Delta_{EQ}=2.74 \text{ mm/s}$$



$$\delta_{IS}=0.53 \text{ mm/s}; \Delta_{EQ}=0.63 \text{ mm/s}$$



$$\delta_{IS}=0.50 \text{ mm/s}; \Delta_{EQ}=0.63 \text{ mm/s}$$

$$\delta_{IS}=1.11 \text{ mm/s}; \Delta_{EQ}=2.75 \text{ mm/s}$$

Figure 5.49: Mössbauer Spectra of $[\text{Fe}(\text{H}_2\text{bpz})_2(\text{monoazobipy})]$

The various gradients of the spin transition are in very good agreement with the

magnetic measurements in the next section. As usual for the iron(II) spin-crossover behaviour, the isomer shifts of the signals was more or less constant throughout the temperature range.

5.4.2 Magnetic Measurements

The measurements of the magnetic susceptibility nicely show different types of spin-transition as layed out in the introduction.

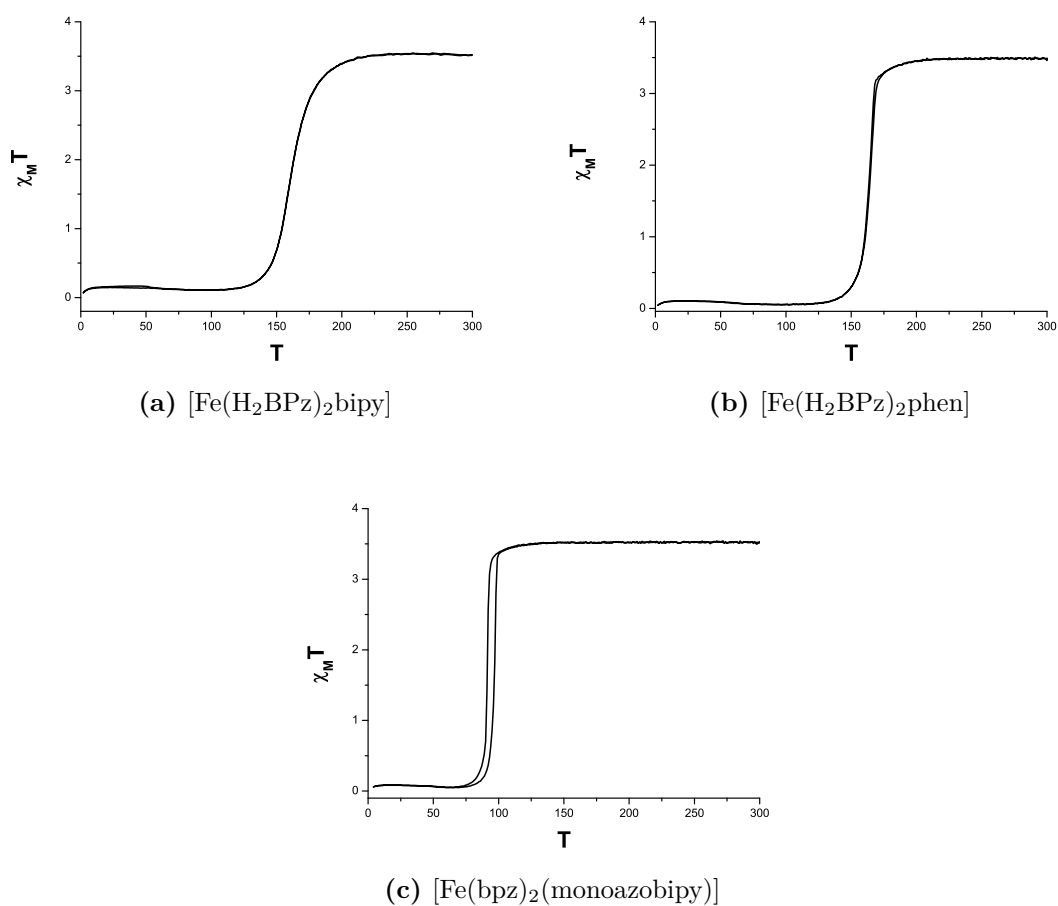


Figure 5.50: PPMS-Plots for the iron(II)-bispyrazolyborate-complexes

The $[\text{Fe}(\text{H}_2\text{BPz})_2\text{bipy}]$ exhibits a rather gradual transition to the lowspin-state, while the other two show a more abrupt transition in a region of only several Kelvin. The transition in the $[\text{Fe}(\text{H}_2\text{bpz})_2(\text{monoazobipy})]$ is particularly interesting, since it also shows a hysteresis loop about 6 K wide.

5.5 Photoinduced Switching

5.5.1 Ligand Switching

As done with the phenylazopyridines in the previous chapter, the two synthesized phenylazopyridines were dissolved in various solvents and their behaviour upon irradiation was followed with UV/Vis-spectroscopy. Albeit its extremely poor solubility, irradiation experiments were successful with the symmetric bipyridine, since the extinction-coefficients of azo-compounds are rather high, in which case already a very dilute sample of the substance yielded a satisfactory UV/Vis-spectrum.

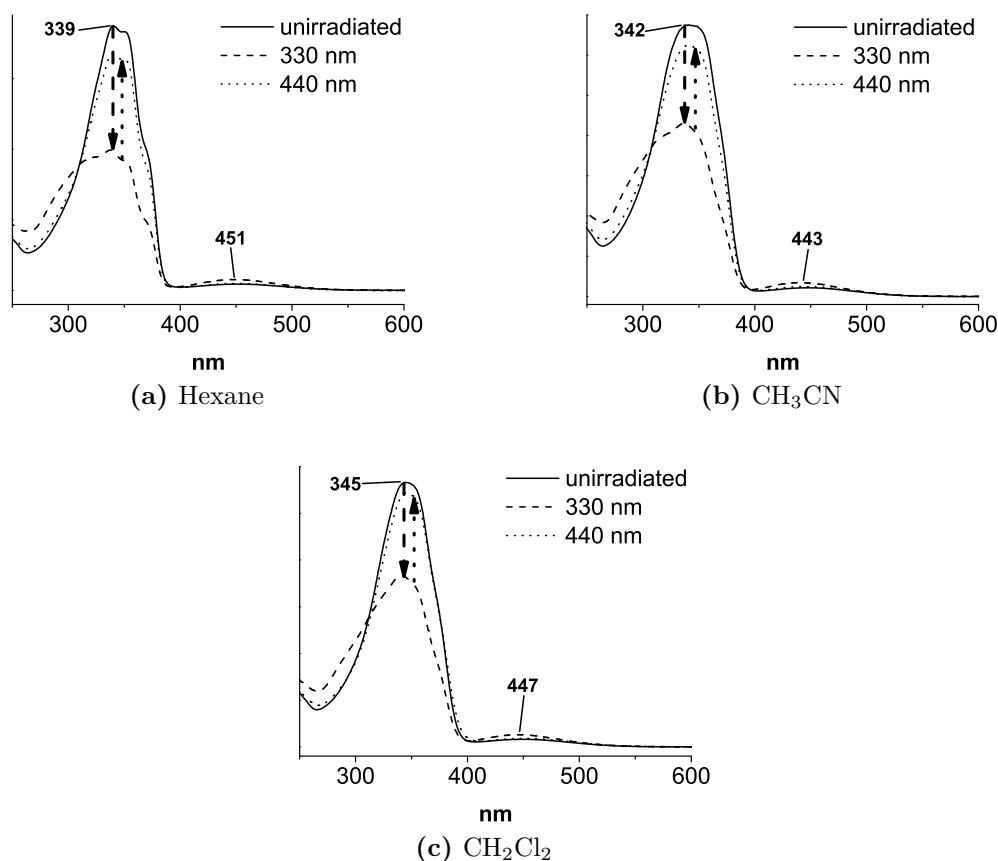


Figure 5.51: Irradiation of bisazobipyridine

The π - π^* -transition of the bisazobipyridine-ligand shows a slight solvent-dependency and is susceptible towards irradiation with light of either 365 nm or 330 nm. Since the transmittance of the 330 nm bandpass-filter was far higher than that of 365 nm,

the irradiations were done with 330 nm. As observed for most azopyridines, the optical spectra could not be completely transformed from the *trans*- to the *cis*-state. In addition to this, the increase in intensity in the n- π^* -transition is significantly smaller than in homoaromatic azobenzenes. In hexane, the decrease in intensity of the π - π^* -band was quantitatively the highest.

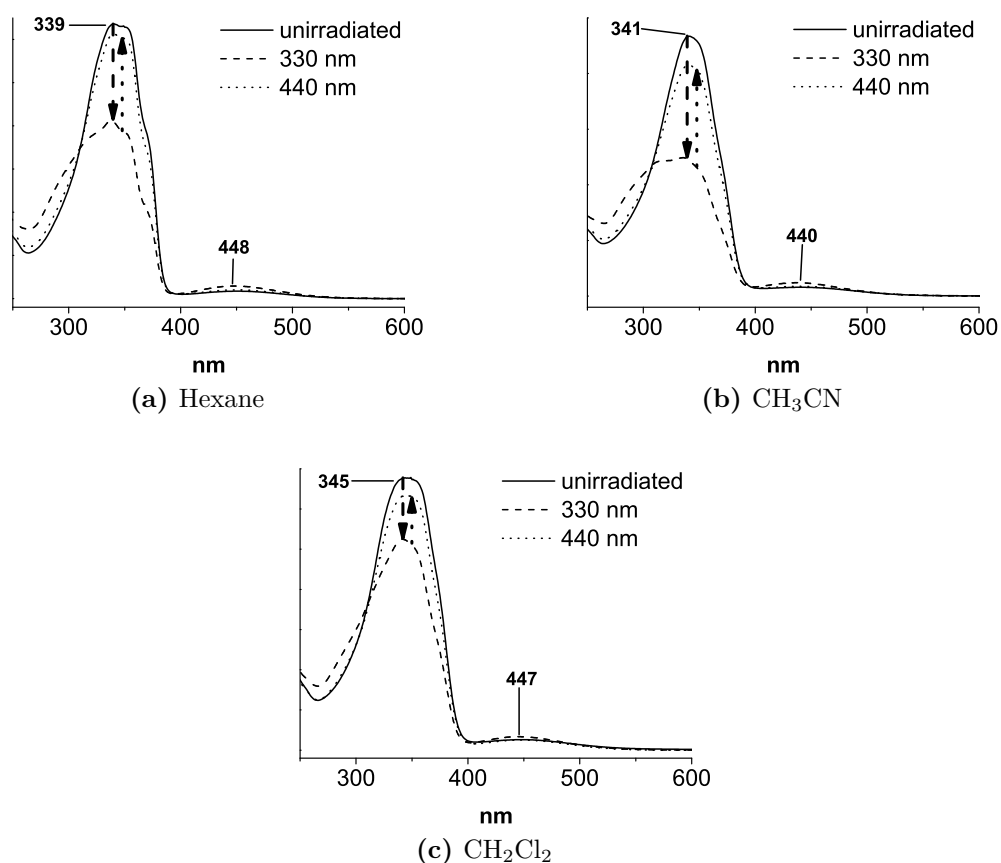


Figure 5.52: Monoazobipyridine

In contrast to the bisazobipyridine, the quantitative switching effect of the monoazobipyridine was at a maximum in acetonitril.

5.5.2 Complex Switching

UV/VIS

The complex $[\text{Fe}(\text{bpz})_2(\text{monoazobipy})]$ was dissolved in dichloromethane and dimethylsulfoxide and irradiated with 330 nm and 440 nm directly afterwards.

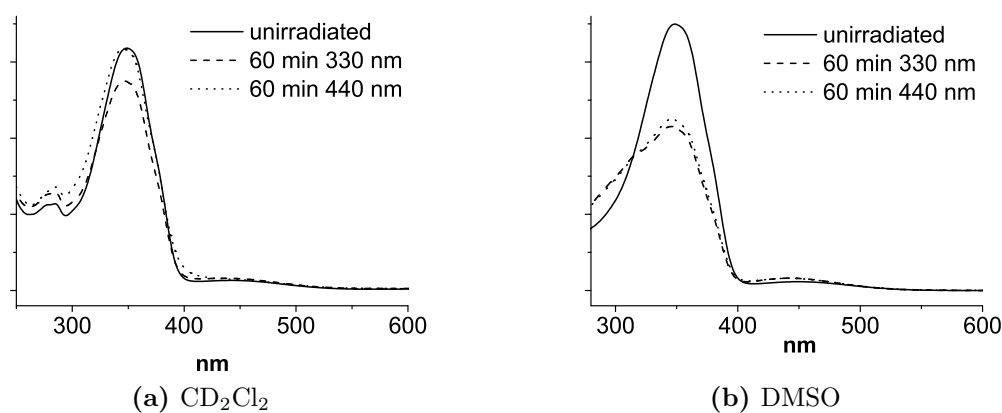


Figure 5.53: Irradiation of $[\text{Fe}(\text{H}_2\text{bpz})_2(\text{monoazobipy})]$

Interestingly, the backswitching in dimethylsulfoxide did not show any effect, but was virtually quantitative in dichloromethane. The subsequent Evans-measurements were therefore performed in dichloromethane as solvent.

Evans-Measurement

The Evans-irradiation experiment with the monoazobipy compound was carried out and evaluated as described in the previous chapter.

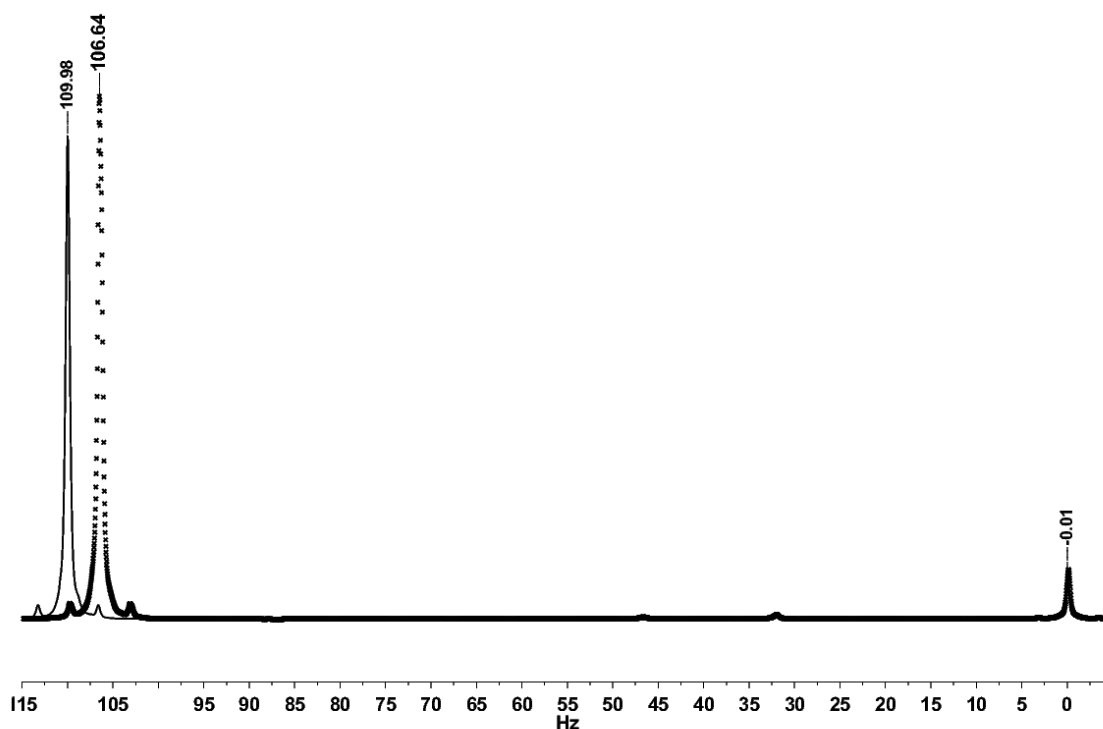


Figure 5.54: TMS-signal of the $[\text{Fe}(\text{H}_2\text{bpz})_2(\text{monoazobipy})]$ measurement in CD_2Cl_2

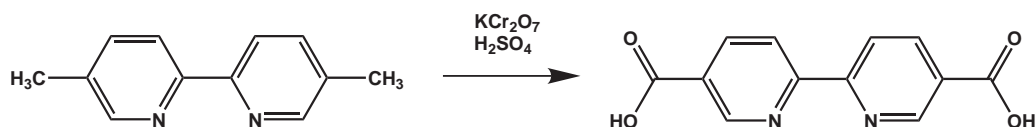
Sample	[mmol/L]	Δf [Hz]	χ_m	$\mu_{eff.}$
$[\text{Fe}(\text{H}_2\text{BPz}_2)_2\text{azobipy}]$ not irradiated	5.603	109.984	0.01173	5.31
$[\text{Fe}(\text{H}_2\text{BPz}_2)_2\text{azobipy}]$ 60 min 330 nm	5.603	106.625	0.01138	5.22

Table 5.5: $[\text{Fe}(\text{H}_2\text{bpz})_2(\text{monoazobipy})]$ in CD_2Cl_2

The measured effect was very small, but well within detectable limits. Due to the good solubility, the solution was far more concentrated than in the previous measurements with the salen-compounds, so the paramagnetic shift of the tetramethylsilane was much higher (see figure 5.54). The thermal reversibility of the switching could not be determined, since the solution changed its colour from dark green to red while resting in the NMR-instrument for 72 hours. This was not due to oxidative processes, but rather to decoordination of the azobipyridine ligand from the iron-center.

5.6 Syntheses

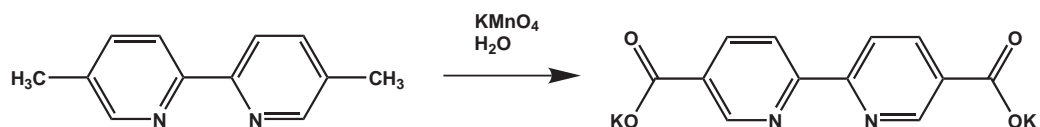
5.6.1 Synthesis of 2,2'-bipyridine-5,5'-dicarboxylate with



5 g of 5,5'-dimethyl-2,2'-bipyridine were added slowly to a cooled solution of 7.95 g of potassium dichromate in 30 mL of concentrated sulfuric acid. Stirring at 0°C was continued for one hour, then the mixture was slowly poured onto 500 mL of ice-water. The mixture was stirred until the ice had dissolved, and the white precipitate of 2,2'-bipyridine-5,5'-dicarboxylate was filtered off, washed several times with water and dried in vacuum. After drying, the product had a greenish colour due to the formation of Cr(III) during the oxidation.

Elemental analysis	C	H	N
Calculated	59.02	3.30	11.47
Found	55.56	3.55	10.87

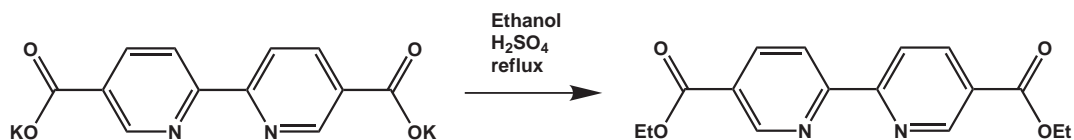
5.6.2 Synthesis of 2,2'-bipyridine-5,5'-dicarboxylate with KMnO_4



5 g of 5,5'-dimethyl-2,2'-bipyridine was suspended in a solution of 25 g potassium permanganate in 300 mL of water. The mixture was refluxed for two hours. At this point, the purple colour of the permanganate had completely vanished. The resulting precipitate of manganese dioxide was filtered off, resuspended in 100 mL of water and brought to reflux to redissolve any product. This procedure was repeated twice. The aqueous phases were united and brought to a pH-value of 5-6 with half-concentrated hydrochloric acid. The potassium salt of the diacid precipitated as a solid, was filtered off and dried in vacuum for several hours.

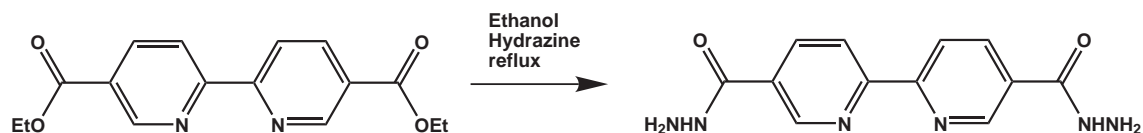
Elemental analysis	C	H	N
Calculated	59.02	3.30	11.47
Found	47.31	2.60	9.41

5.6.3 Synthesis of diethyl-2,2'-bipyridine-5,5'-dicarboxylate



10 g of 2,2'-bipyridine-5,5'-dicarboxylate were suspended in 250 mL of ethanol. To this suspension, 50 mL of concentrated sulfuric acid were added dropwise under vigorous stirring. After the addition was complete, the mixture was refluxed over night. The solution was now slightly yellow with no solid reactant visible any more. The solution was allowed to cool down to about 60°C and was then poured onto ice and shaken until all ice was molten. The diethylester precipitated as a colorless powder, was filtrated, washed with water and recrystallized from hot ethanol.

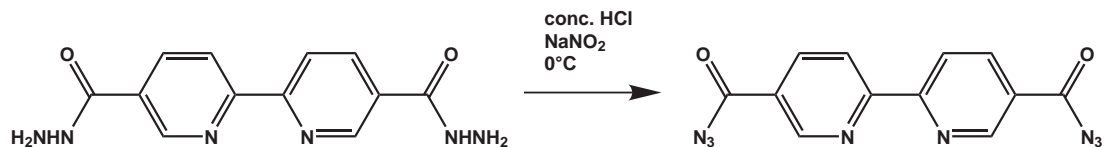
Elemental analysis	C	H	N
Calculated	63.99	5.37	9.33
Found	62.45	5.47	8.96

5.6.4 Synthesis of 2,2'-bipyridine-5,5'-dicarboxylic dihydrazide

8 g of diethyl-2,2'-bipyridine-5,5'-dicarboxylate were suspended in 50 mL of ethanol. To this, 50 mL of a 80% hydrazine-hydrate solution was added and brought to reflux. After six hours, the mixture was allowed to cool to room temperature and the dihydrazide was filtered. The product was washed with ethanol and dried in vacuum.

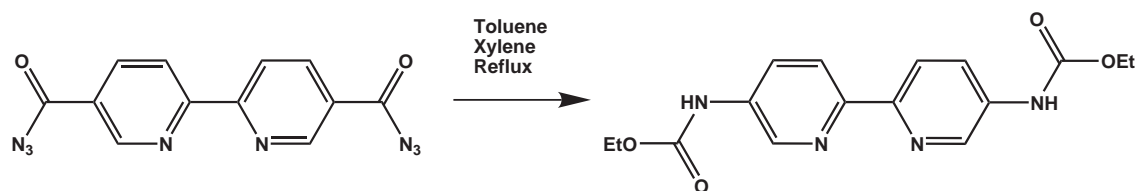
Elemental analysis	C	H	N
Calculated	38.40	3.22	14.93
Found	39.77	3.89	16.22

5.6.5 Synthesis of 2,2'-bipyridine-5,5'-dicarboxylic diazide



5.5 g of 2,2'-bipyridine-5,5'-dicarboxylic dihydrazide were suspended in 100 mL concentrated hydrochloric acid and cooled to 0°C. 2.76 g of sodium nitrite were dissolved in 20 mL of water and added dropwise to the dihydrazide-solution. The stirring was continued for two hours, when all of the dihydrazide had dissolved and the solution had turned yellow. The mixture was now diluted with 500 mL of water. The off-white precipitate was filtered, washed with ethanol twice and dried in vacuum.

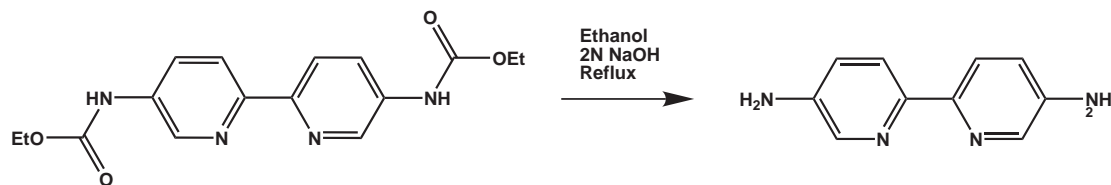
Elemental analysis	C	H	N
Calculated	37.31	2.35	18.13
Found	36.18	3.43	20.31

5.6.6 Synthesis of 5,5'-bis(ethoxycarbonylamino)-2,2'-bipyridine

4 g of 2,2'-bipyridine-5,5'-dicarboxylic diazide were suspended in a solution of 100 mL dry ethanol and 100 mL dry xylene and refluxed for 24 h. The solution was allowed to cool to room temperature, upon which the product precipitated as an off-white powder. The product was filtered and dried in vacuum.

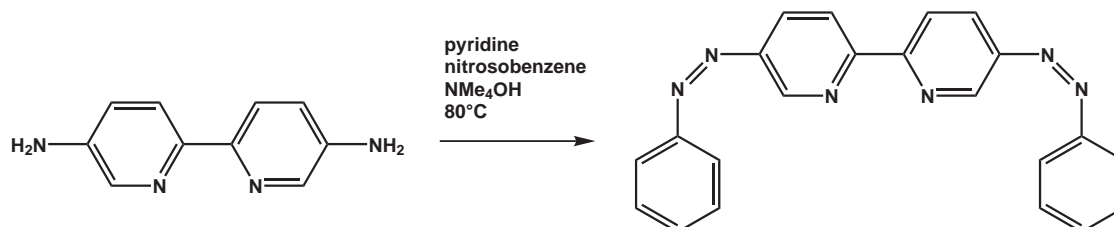
Elemental analysis	C	H	N
Calculated	58.17	5.49	16.96
Found	59.22	6.09	15.87

5.6.7 Synthesis of 5,5'-diamino-2,2'-bipyridine



2 g of 5,5'-bis(ethoxycarbonylamino)-2,2'-bipyridine were suspended in a mixture of 80 mL of ethanol and 80 mL of 2N aqueous sodium hydroxide solution. The mixture was refluxed for 24 h and allowed to cool to room temperature. The solution was brought to a pH of about 8 with dilute hydrochloric acid and the ethanol was distilled off. The residue was stored at 5°C over night, while the yellow dichydrochloride of the diaminobipyridine precipitated. The solution was filtered and the product was dried in high vacuum.

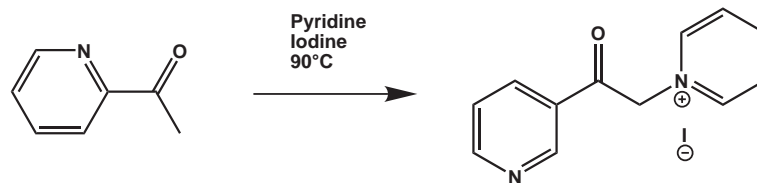
Elemental analysis	C	H	N
Calculated	64.50	5.41	30.09
Found	62.13	4.76	28.43

5.6.8 Synthesis of 5,5'-bis(phenyldiazenyl)-2,2'-bipyridine

1 g of 5,5'-diamino-2,2'-bipyridine dihydrochloride was suspended in 30 mL of pyridine and 10 mL of tetramethylammonium hydroxide. To this, a solution of 1.1 g of nitrosobenzene dissolved in 30 mL of pyridine was added. The solution was stirred at 80°C for 24 hours and then cooled to room temperature. The red precipitate was filtered off and washed several times with hot hexane and acetone. The product was then dried in vacuum.

Elemental analysis	C	H	N
Calculated	72.51	4.43	23.06
Found	69.87	4.31	21.28

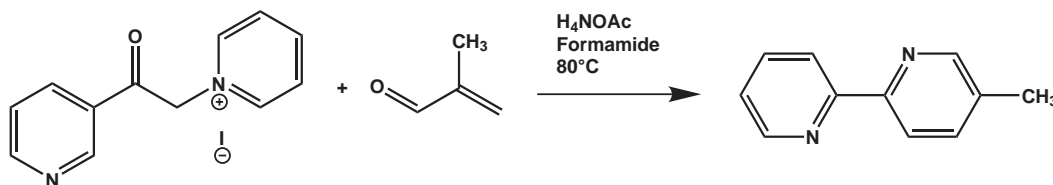
5.6.9 Synthesis of 1-(2-Pyridylacetyl)pyridinium iodide



A solution of 7.1g iodine and 2.8 mL of freshly distilled 2-acetylpyridine in 50 mL of pyridine were heated at 100°C over night. The solution was filtered and the residue was mixed with 5g charcoal powder in 300 mL of absolute ethanol and refluxed for one hour. The resulting suspension was filtered through a soxleth extraktion tube and extracted therein for three hours. The ethanol was evaporated under reduced pressure and the procedure was repeated once. After that, the ethanolic solution was reduced to about 50 mL and stored in a refrigerator overnight. The product was filtered and dried in high vacuum for several hours. The product underwent a colour change from yellow to beige when stored under normal atmosphere, so long-time storage under inert conditions is advised.

Elemental analysis	C	H	N
Calculated	44.19	3.40	8.59
Found	43.37	4.13	8.84

5.6.10 Synthesis of 5-Methyl-2,2'-bipyridine

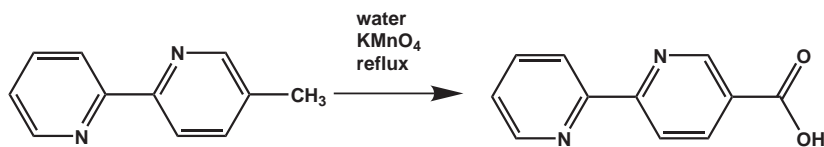


To a solution of 7.36g of 2-acetylpyridiniumiodide, dissolved in 175 mL formamide, 2.2 mL methacrolein and 11 g of ammonium acetate were added. The solution was heated at 80°C over night, allowed to cool to room temperature and extracted several times with diethyl ether. The ether extracts were washed with brine, dried over magnesium sulfate and the solvent was evaporated. The crude product was purified with column chromatography on silica gel with dichloromethane/methanol 95/5. The product was collected as a brown oil.

^1H NMR (400 MHz, $\text{DMSO}-d_6$) δ = 9.02 – 8.95 (m, 8H), 8.83 (ddd, J = 4.7, 1.6, 0.9 Hz, 4H), 8.70 (tt, J = 7.9, 1.4 Hz, 4H), 8.29 – 8.20 (m, 8H), 8.15 – 7.99 (m, 8H), 7.80 (ddd, J = 7.5, 4.8, 1.4 Hz, 4H), 6.47 (d, J = 7.3 Hz, 7H), 3.27 (s, 1H), 2.46 (dt, J = 3.7, 1.9 Hz, 2H).

^{13}C NMR (110 MHz, $\text{DMSO}-d_6$) δ = 194.77 (s), 153.77 (s), 152.87 (s), 149.64 (d, J = 4.2 Hz), 141.46 (s), 132.44 (s), 131.03 (s), 125.36 (s).

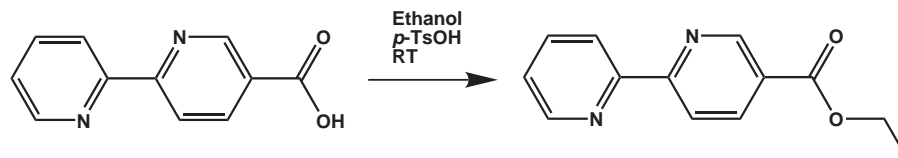
5.6.11 Synthesis of 2,2'-bipyridinyl-5-carboxylic acid



5 g of 5-Methyl-2,2'-bipyridine were dissolved in 250 mL of water. To this solution, 20 g of potassium permanganate were added and the mixture was heated at 80°C over night. At this point, the colour had changed from purple to dark brown. The solution was filtered through a paper filter to remove the manganese dioxide. The residue was redispersed in 200 mL water and brought to reflux and then filtered again. The combined aqueous phases were reduced to about 50 mL and then brought to a pH-value of 3-4 using 2M hydrochloric acid. The resulting precipitate was filtered and dried in high vacuum to yield the potassium salt of 2,2'-bipyridinyl-5-carboxylic acid as a white solid.

Elemental analysis	C	H	N
Calculated	44.99	2.99	8.74
Found	44.29	1.89	10.27

5.6.12 Synthesis of Ethyl-2,2'-bipyridinyl-5-carboxylate



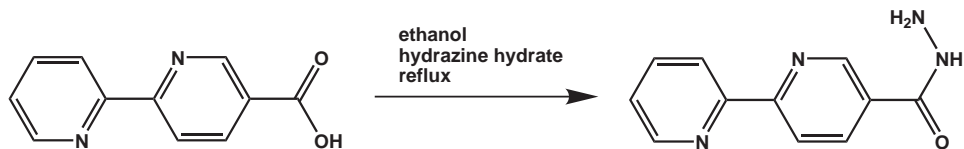
88g *p*-toluenesulfonic acid were dissolved in 250 mL of ethanol. To this solution, 10 g of 2,2'-bipyridinyl-5-carboxylic acid were added. The solution was stirred over night at 50°C. The solution was allowed to cool to room temperature and reduced to about one quarter of its original volume. The solution was made slightly alkaline (pH 9-10) through the slow addition of a saturated sodium carbonate solution. The solution was extracted with copious amounts of ethyl acetate. The combined organic extracts were washed with brine, dried over magnesium sulfate and evaporated to dryness. The resulting pale white solid was used without further purification.

Elemental analysis	C	H	N
Calculated	68.41	5.30	12.27
Found	66.15	5.55	11.81

^1H NMR (400 MHz, CDCl_3) δ = 9.27 (s, 1H), 8.76 (s, 1H), 8.59 – 8.48 (m, 2H), 8.42 (d, J = 8.1 Hz, 1H), 7.93 (t, J = 7.8 Hz, 1H), 7.42 (s, 1H), 4.42 (q, J = 7.2 Hz, 2H), 1.41 (t, J = 7.1 Hz, 3H).

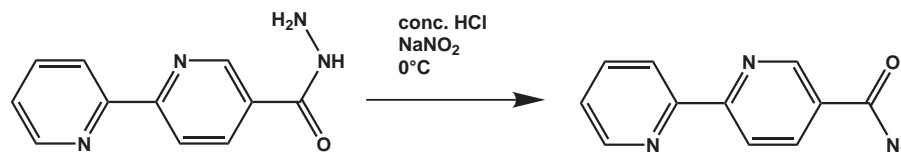
^{13}C NMR (110 MHz, CDCl_3) δ = 165.12 (s), 150.54 (s), 148.46 (s), 138.31 (s), 126.41 (s), 124.80 (s), 122.51 (s), 120.97 (s), 61.54 (s), 14.29 (s).

5.6.13 Synthesis of 2,2'-bipyridine-5-carboxylic hydrazide



5 g of Ethyl-2,2'-bipyridinyl-5-carboxylate were dissolved in 40 mL of ethanol. 40 mL of aqueous hydrazine hydrate solution was added dropwise. After complete addition of the hydrazine, the solution was refluxed for 6 hours.

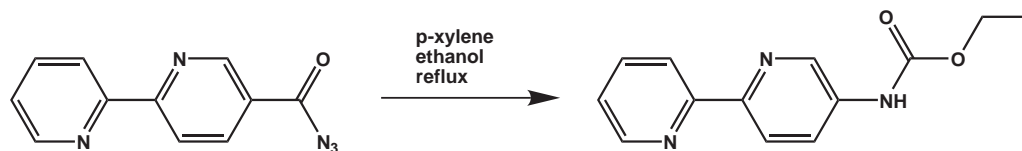
Elemental analysis	C	H	N
Calculated	63.99	5.37	9.33
Found	62.45	5.47	8.96

5.6.14 Synthesis of 2,2'-bipyridine-5-carboxylic azide

4.1 g of 2,2'-bipyridine-5-carboxylic hydrazide were suspended in 75 mL of concentrated hydrochloric acid and cooled to about 0°C. To this a solution of 1.41 g sodium nitrite in the minimum amount water was added dropwise, not letting the temperature rising above 10°C. After addition of the sodium nitrite, stirring at 0°C was continued for one hour. The cooling was removed and the reaction was stirred over night at room temperature. The mixture was filtered and the product was dried in high vacuum.

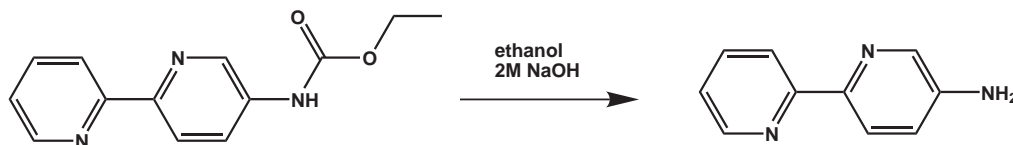
Elemental analysis	C	H	N
Calculated	63.99	5.37	9.33
Found	62.45	5.47	8.96

5.6.15 Synthesis of 5-ethoxycarbonylamino-2,2'-bipyridine



4.8 g of 2,2'-bipyridine-5-carboxylic azide were dispersed in a mixture of 150 mL dry ethanol and 150 mL dry xylene. The mixture was refluxed over night and the cooled to room temperature. Most of the solvent was distilled of, and the remaining solution was filtered.

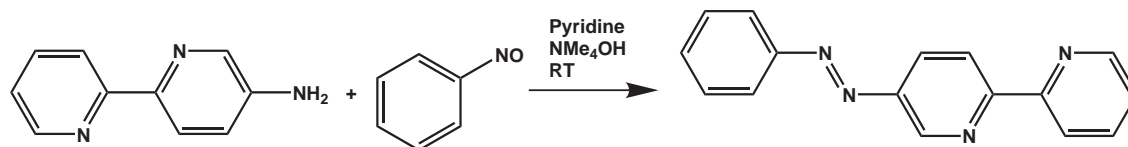
Elemental analysis	C	H	N
Calculated	63.99	5.37	9.33
Found	62.45	5.47	8.96

5.6.16 Synthesis of 5-amino-2,2'-bipyridine

1.5 g of 5-ethoxycarbonylamino-2,2'-bipyridine were suspended in a mixture of 50 mL of ethanol and 50 mL of 2N aqueous sodium hydroxide. The mixture was refluxed for 24 hours and then reduced to about a third of its initial volume. The solution was made slightly acidic with dilute hydrochloric acid and stored in the refrigerator over night. The precipitate was filtered and dried in vacuum.

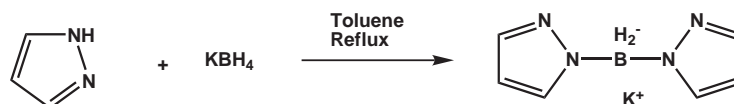
Elemental analysis	C	H	N
Calculated	63.99	5.37	9.33
Found	62.45	5.47	8.96

5.6.17 Synthesis of 5-phenyldiazenyl-2,2'-bipyridine



To a solution of 850 mg of 5-amino-2,2'-bipyridine and 10 mL tetramethylammonium hydroxide in 20 mL of pyridine a solution of 700 mg of nitrosobenzene in 15 mL pyridine was added dropwise. The solution was heated at 80 °C over night and then allowed to cool to room temperature. The volume of the solution was reduced to half and then the mixture was filtered. The orange precipitate was dispersed in 100 mL of water, stirred at room temperature for 10 min, filtered again and dried several hours in high vacuum.

Elemental analysis	C	H	N
Calculated	73.83	4.65	21.52
Found	73.48	4.60	21.52

5.6.18 Synthesis of Potassium Dihydrobis(pyrazolyl)borate

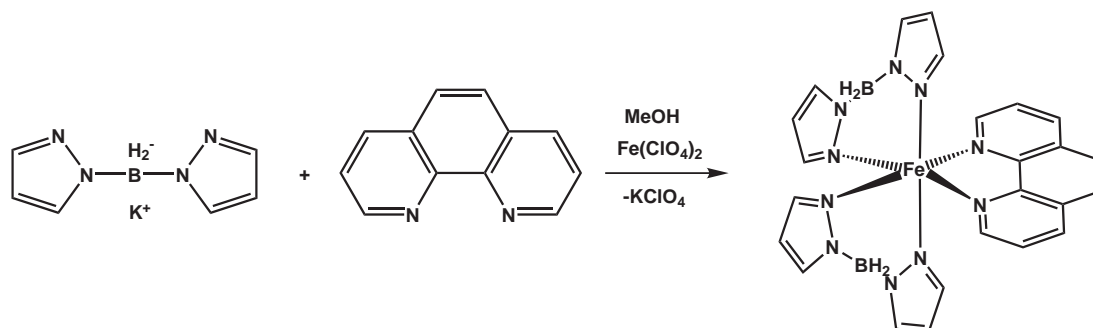
5.4 g of potassium tetrahydroborate and 27.2 g of pyrazole were suspended in 100 mL of dry toluene and refluxed for 24 h. The clear, slight yellow solution was filtered hot through a glass frit to remove any unreacted substrates or impurities and slowly allowed to cool down to room temperature. The precipitate was filtered off and washed twice with dichloromethane and diethylether and dried in vacuum.

Elemental analysis	C	H	N
Calculated	38.73	4.33	30.11
Found	39.52	3.97	29.73

^1H NMR (400 MHz, CD_3CN) δ = 7.47 (dd, J = 2.0, 0.7 Hz, 2H), 7.36 (dd, J = 1.7, 0.6 Hz, 2H), 6.03 – 6.02 (m, 2H). ^{13}C NMR (110 MHz, CD_3CN) δ = 138.61 (s),

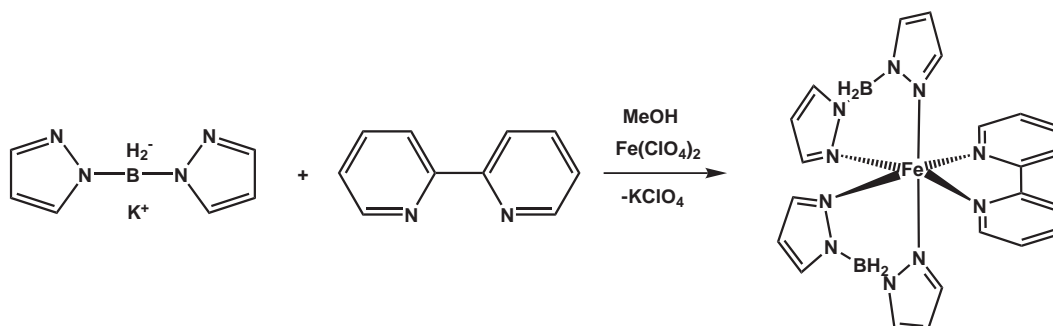
134.01 (s), 102.87 (s).

5.6.19 Synthesis of $[\text{Fe}(\text{H}_2\text{B}(\text{pz})_2)_2\text{phen}]$



744 mg of potassium dihydro(bispyrazolyl)borate and 726 mg of iron(II)-perchlorate hexahydrate were dissolved in 10 mL of dry and degassed methanol each. The two solutions were mixed, stirred at room temperature for 15 minutes and immediately filtered. The precipitated potassium perchlorate was washed twice with 5 mL methanol. To the colourless iron(II)-bispyrazolyborate-solution, 360 mg 1,10-phenanthroline in 10 mL of methanol were added dropwise. The purple precipitate was filtered off, washed with methanol and dried in vacuum.

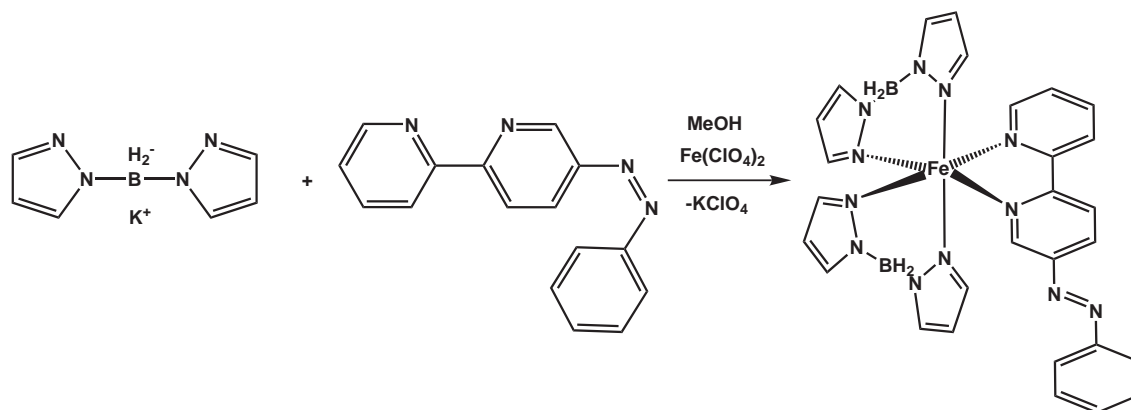
Elemental analysis	C	H	N
Calculated	54.39	4.56	26.43
Found	54.13	4.53	26.59

5.6.20 Synthesis of $[\text{Fe}(\text{H}_2\text{B}(\text{pz})_2)_2\text{bipy}]$ 

744 mg of potassium dihydro(bispyrazolyl)borate and 726 mg of iron(II)-perchlorate hexahydrate were dissolved in 10 mL of dry and degassed methanol each. The two solutions were mixed, stirred at room temperature for 15 minutes and immediately filtered. The precipitated potassium perchlorate was washed twice with 5 mL methanol. To the colourless iron(II)-bispyrazolyborate-solution, 312 mg 2,2'-bipyridine in 10 mL of methanol were added dropwise. The purple precipitate was filtered off, washed with methanol and dried in vacuum.

Elemental analysis	C	H	N
Calculated	52.22	4.78	27.68
Found	51.80	4.79	28.07

5.6.21 Synthesis of $[\text{Fe}(\text{H}_2\text{B}(\text{pz})_2)_2\text{monoazobipy}]$



744 mg of potassium dihydro(bispyrazolyl)borate and 726 mg of iron(II)-perchlorate hexahydrate were dissolved in 10 mL of dry and degassed methanol each. The two solutions were mixed, stirred at room temperature for 15 minutes and immediately filtered. The precipitated potassium perchlorate was washed twice with 5 mL methanol. To the colourless iron(II)-bispyrazolyborate-solution, 521 mg 5-phenyldiazenyl-2,2'-bipyridine in 10 mL of methanol were added dropwise. The greenish precipitate was filtered off, washed with methanol and dried in vacuum.

Elemental analysis	C	H	N
Calculated	55.12	4.63	27.55
Found	54.89	4.87	27.21

6 Thin Films of SCO Compounds

6.1 Assignment

When creating devices that are switchable on a molecular level, in addition to the bistability of the compounds of interest, these compounds have to be somehow deposited in a well-ordered fashion, e.g. as thin-layered films or as nanoparticles. But this drastic change of the chemical environment also influences the electronic properties of the suitable candidates, since especially the spin-transition of spin-crossover compounds in the bulk is critically influenced by cooperative interactions in the crystal lattice. These cooperative effects are heavily reduced, or even completely eliminated when monomolecular layers of spin-crossover compounds are formed. The electronic properties are even further influenced by the new interaction with the surface, on which the films or nanoparticles are deposited.

The goal of understanding is hereby to characterize these influences on spin crossover materials, when they are deposited as thin films or nanoparticles, especially the influence of thickness/particle size and the various deposition methods at hand. Several publications deal with thin films of spin crossover compounds, either via spin-coating^[93] or the step-wise formation of thin layers^[94].

6.2 Deposition

The literature-known complexes $[\text{Fe}(\text{H}_2\text{BPz})_2\text{bipy}]$ and $[\text{Fe}(\text{H}_2\text{BPz})_2\text{phen}]$ were found to be very promising candidates to form ordered layers, since it is possible to sublime them at comparatively mild conditions.

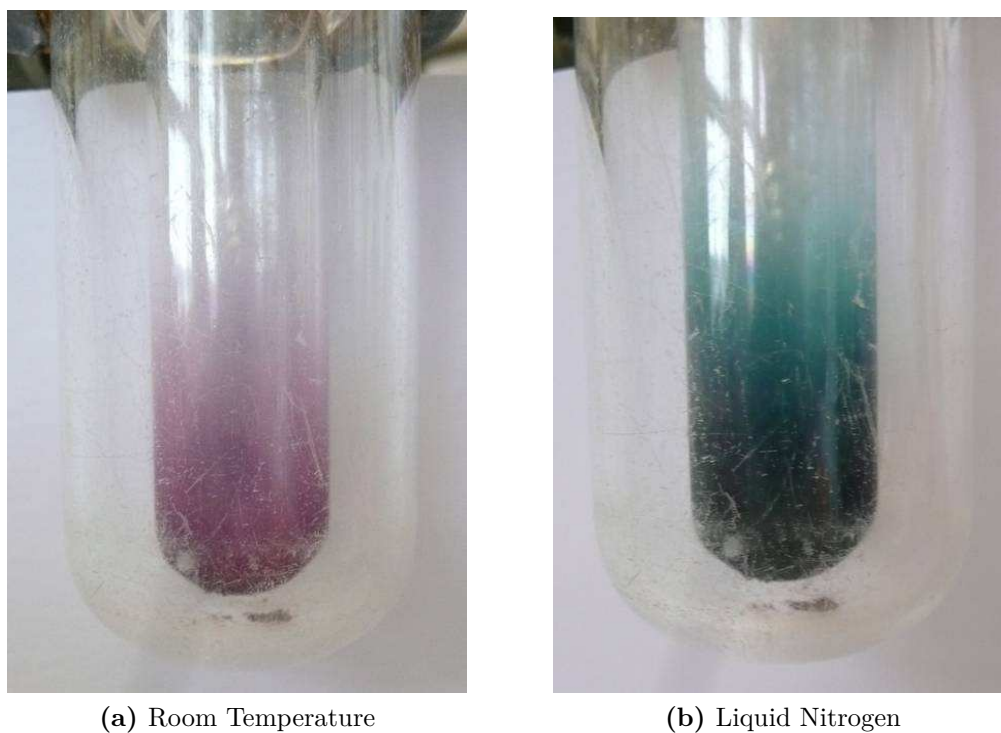


Figure 6.1: Sublimation of $[\text{Fe}(\text{H}_2\text{BPz})_2\text{phen}]$

As seen in figure 6.1, when being sublimated onto a liquid-nitrogen cooled sublimation finger, the compound keeps its thermochromic behaviour, which is typical for spin-crossover complexes. Elemental analysis proved the compound to be sublimable without decomposition. The sublimations were carried out using a standard oil-bath at 150°C and the vacuum of a standard schlenk-line with attached rotary-valve vacuum pump (about 10^{-2} mbar).

The next step was to prepare defined samples for the spectroscopic measurements. The sample was sublimated onto a quartz carrier.

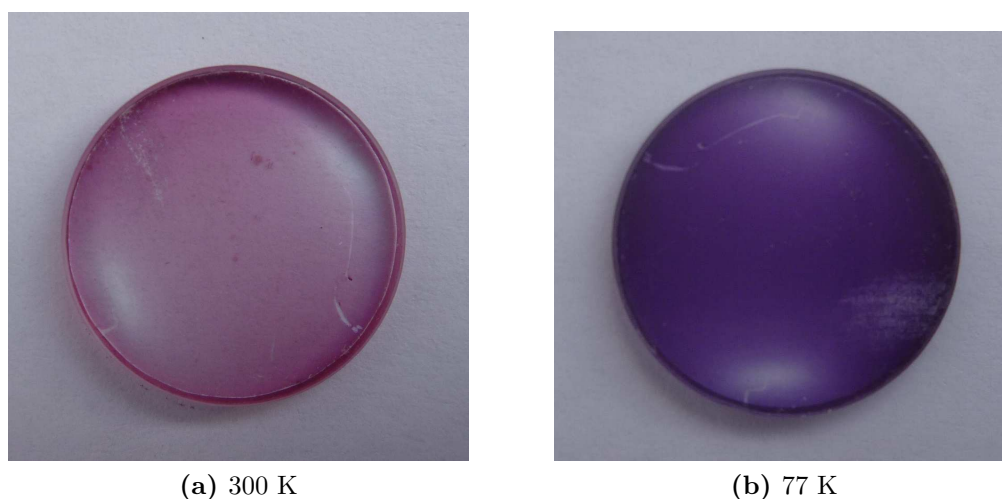


Figure 6.2: Film of $[\text{Fe}(\text{H}_2\text{BPz})_2\text{bipy}]$ on quartz carrier

In contrast to the bipyridine-complex, the phenanthroline complex shows as strong thermochromism and changes its colour from purple to deep-green.

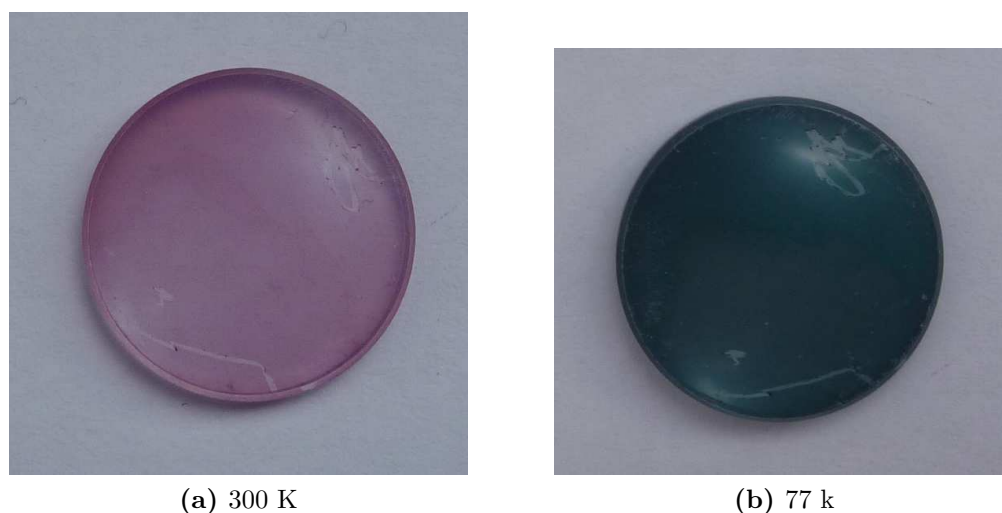


Figure 6.3: Film of $[\text{Fe}(\text{H}_2\text{BPz})_2\text{phen}]$ on quartz carrier

By varying the time of the sublimation-procedure, the thickness of the deposited films can be readily controlled.

6.3 Optical Spectroscopy

The optical properties of the spin-transition was investigated with temperature-dependent UV/Vis-measurements. For this purpose thin-layered films were deposited

on quartz-carriers and cooled down using a nitrogen-cryostat.

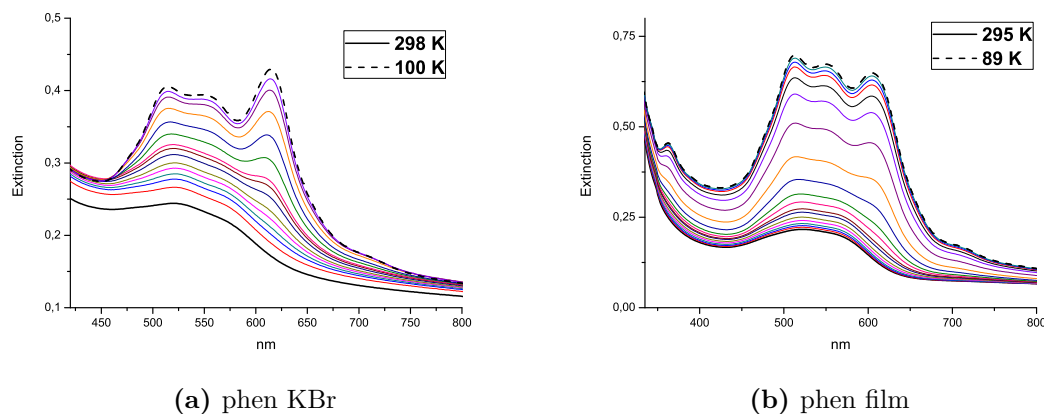


Figure 6.4: Spin-transition in bpz phen

In both cases, the spectra of the KBr-pellet and the thin films differ in the temperature-dependent behaviour. However, the main feature of all measurements is the temperature-dependent increase of the metal-to-ligand charge-transfer band at 615 nm (phen) and 635 nm (bipy) when lowering the temperature.

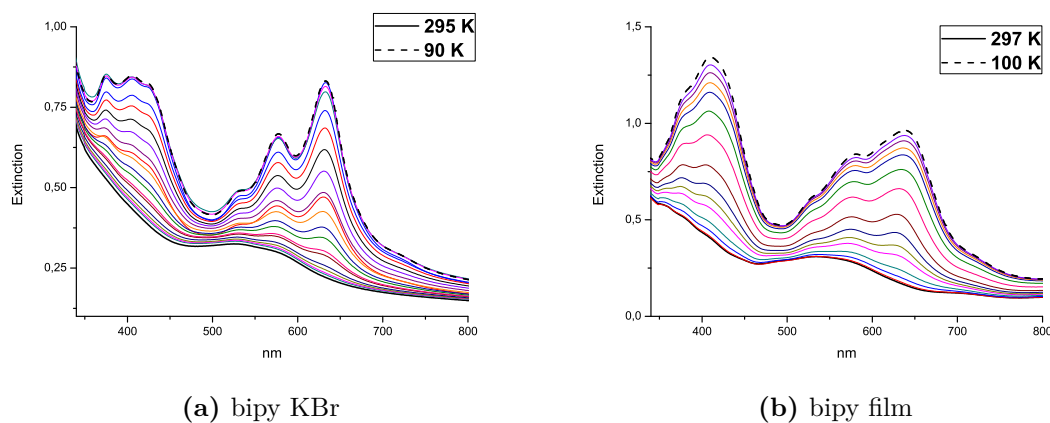


Figure 6.5: Spin-transition in bpz bipy

The ability of the deposited films to perform LIESST was also investigated. The quartz-carriers were brought into the continuous-flow cryostat by CryoVac and cooled to a temperature of 10 K. Then the films were irradiated with a LED emitting 525 nm. The resulting spectra are depicted in figure 6.6.

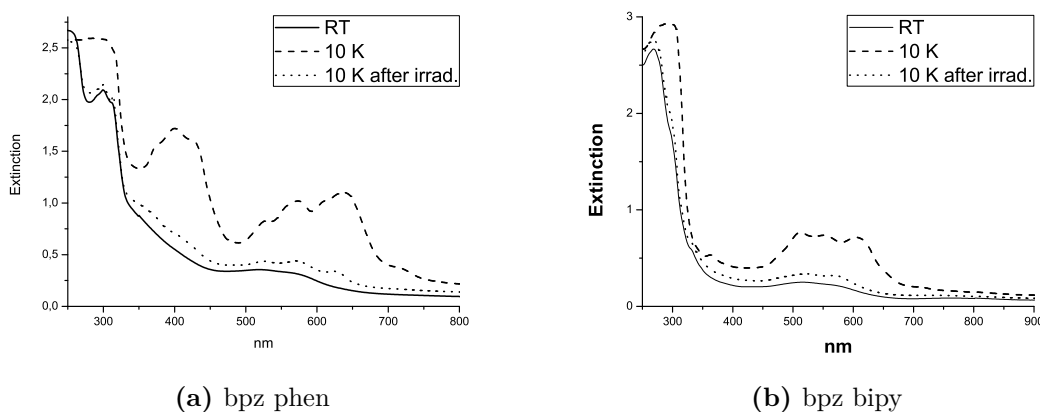


Figure 6.6: LIESST of [Fe(HBPz)]-complexes

Evaluation of the MLCT-band at 615 nm (phen) and 635 nm (bipy) gave a light-induced switching to the high-spin state at 10 K of over 80 %. This is the first example of LIESST in a thin-layered film deposited by vacuum sublimation.

The UV/Vis-spectra measured on thin films as well as in KBr-pellets of the monoazobipy complex were of no further use for this study, since the electronic transitions influenced by the spin-transition all were completely masked by the very intense absorption of the $\pi - \pi^*$ and the $n - \pi^*$ transitions of the coordinated azo-ligand. The raman-spectra of the thin films exhibits a strong fluorescence and is only of little experimental value. The temperature-dependent behaviour of several bands in the spectrum of the bulk-substance was already described by Moliner^[95] and could be reproduced.

7 Scientific Methods

7.1 Synthetic Procedures

All syntheses dealing with air- and moisture-sensitive compounds were carried out using standard schlenk techniques. Nitrogen 5.0 and Argon 4.6 were used as inert gases. Manipulation and storage of the compounds was carried out in an argon glove-box (Labmaster 130, M.Braun). All chemicals were bought from ABCR, Acros and Sigma-Aldrich. All solvents were of *pro analysis* grade and dried by the following methods:

- Ethanol and toluene were distilled over sodium.
- Methanol was distilled over magnesiummethanolate.
- Diethylether and tetrahydrofuran were distilled over lithiumaluminiumhydride.
- Benzene, n-hexane, dichloromethane, acetonitrile, pyridine, and chloroform were distilled over calciumhydride.
- Acetone was distilled over Calciumsulfate (*Drierite*)

All solvents were distilled under an atmosphere of argon prior to use.

7.2 Spectroscopic Methods

Elemental Analysis

All elemental analysis for carbon, nitrogen, sulphur and hydrogen were carried out on an Euro Vector Euro EA 3000. Halogene contents were titrated against silver nitrate

after incineration.

Infrared

The mid-range infrared spectra have been recorded on a Genesis Typ 1 spectrometer by Mattson as kaliumbromide-pellets (prepared with a pressure of 10t/cm²). FIR spectra were recorded on an IFS v66/S Spectrometer by Bruker in a thin layer of apizon-grease on polyethylene-foil.

Raman

Ramanspectra were measured on a Bruker IFS 66/CS fourier-transform raman spectrometer in the range of 3000 cm⁻¹ with a resolution of 2 cm⁻¹. A 350 mW Nd:YAG-laser with excitation wavelength of 1064nm was used.

Resonance-Raman

The resonance-raman spectra were recorded on a Dilor XY raman spectrometer, equipped with a helium cryostat, triple monochromator and CCD-detector.

UV/Vis

UV-measurements were recorded on a Cary 5000 UV/Vis spectrometer with a spectral resolution of 1nm.

Mößbauer-spectroscopy

Mößbauer-spectra were recorded on a self-constructed spectrometer using a linear transmission geometry. The drive consists of a MR-260A drive-system and a MVT-1000 velocity-transducer, both by Wissenschaftliche Elektronik GmbH, Starnberg. The source is rhodium-embedded ⁵⁷Cobalt with an activity of 25 mCurie. As cryostat, the continuous-flow cryostat CF506 equipped with temperature controller ITC502

by Oxford Instruments, was used. All Mößbauer-parameters are calculated with respect to a 25 μm thick foil of α -iron. The data points were fitted with the software environment for fitting EFFI.

NMR

All NMR-spectra were recorded on a Bruker Avance pulse-fourier-transform spectrometer with a proton frequency of 400.13 MHz and a ^{13}C frequency of 110.62 MHz. All measurements were performed at 300K.

Magnetic Measurements

The magnetic measurements were carried out on a Quantum Design PPMS-9T, equipped with a helium-cooled 9 Tesla magnet at a field strength of 1 Tesla.

Mass Spectrometry

A MAT 8230 mass spectrometer from Finnigan was used to measure the mass spectra with an electron-energy of 70 eV for the electron-ionisation and isobutane as ion-source in the chemical ionisation.

Irradiation Experiments

The sample solutions were irradiated with a UV-spotlight UV-P 250C by Panacol-Elosol GmbH. Bandpassfilters in the desired wavelength were purchased from Laser Components Ltd.

7.3 Quantum-chemical Calculations

The calculations were performed with the built-in routines of the Gaussian09W and the ORCA software package. Gaussian is installed on a vector array composed of six NEC-SX9 nodes, each one having 16 vector processors with a peak performance of 100 GFLOPS and 512GB local memory, ORCA on a linux-based cluster network

of inhomogenous composition. Singlepoint calculations were done using the program package ORCA by Neese et al., installed on a linux-based cluster network. Full optimizations, frequency calculations and singlepoints were carried out using a total of 8 cores and 10GB of main memory. All structures were pre-optimized on a standard desktop computer with the hybridfunctional b3lyp, using the LANL2DZ basisset. The basissets and functionals used for full optimization, frequency calculation and singlepoints are mentioned in the respective sections. The GaussView program delivered all depictions of optimized geometries and molecular orbitals and their respective energies.

8 Summary and Outlook

Several new compounds (figure 8.1) have been synthesized and characterized for their possible use as molecular switches. It was shown that a coordinated switching function is not desirable, for its desactivation of the isomerisation process.

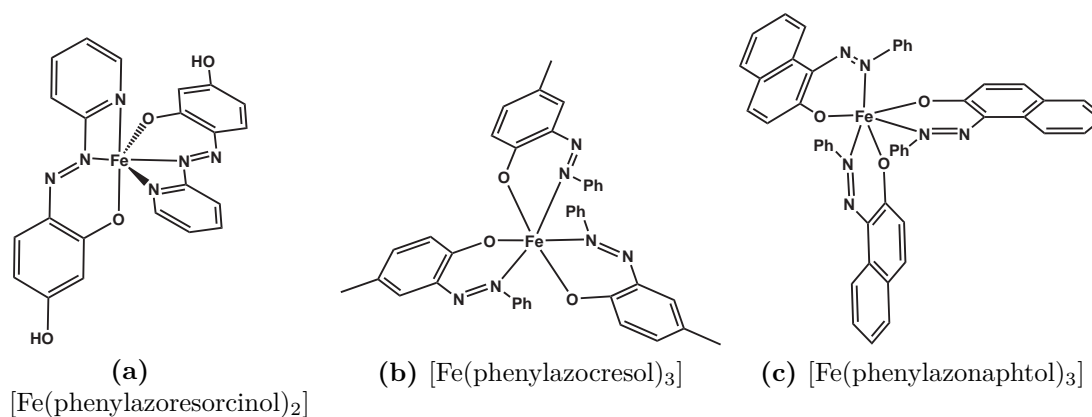


Figure 8.1: Complexes with coordinated azo-functions

In addition to the unfavorable coordination of the azo-group, the investigated systems all showed no spin-crossover behaviour, so even if the isomerisation of the azo-ligand would have been successful, a change of the spin-state would be highly unlikely.

As consequence of these fruitless attempts to create switchable single molecules, a coordination setup was designed to avoid the coordination of the azo-group. Several complexes with the five-coordinate salen-unit and photoswitchable ligands which were coordinated via a pyridine-nitrogen were synthesized and characterized (figure 8.2).

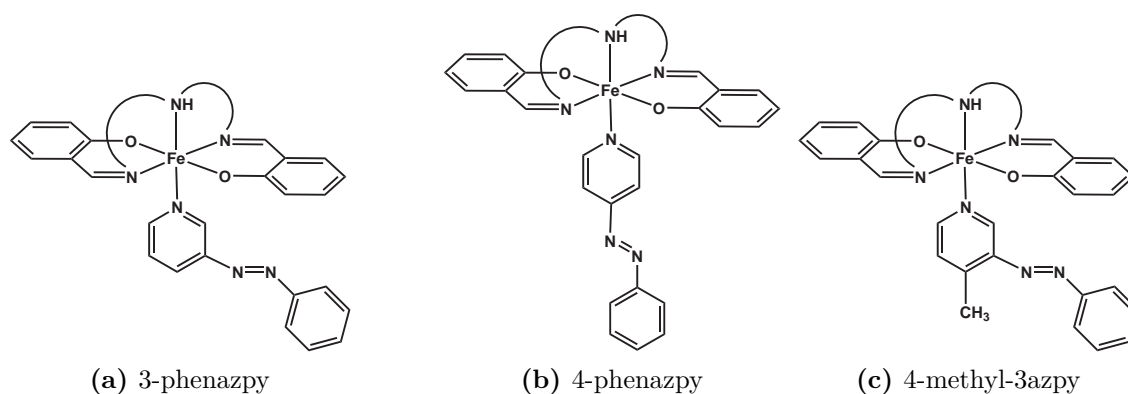


Figure 8.2: Salten-type compounds

These compounds showed a well defined optical switchability as well as a temperature-dependent gradual and incomplete spin-transition from high-spin to low-spin, but the magnetic measurements in solution strongly suggest that the coordination of the pyridine-ligands is rather unstable towards prolonged irradiation with ultraviolet light. To further optimise the presented switching-concept, other ligands than pyridine derivatives have to be evaluated, e.g. pyrazol and imidazol-ligands with switchable azo-functions.

Two new switchable chelating azo-ligands with a bipyridine-core were synthesized, characterized and proven to be reversibly switchable with different wavelengths.

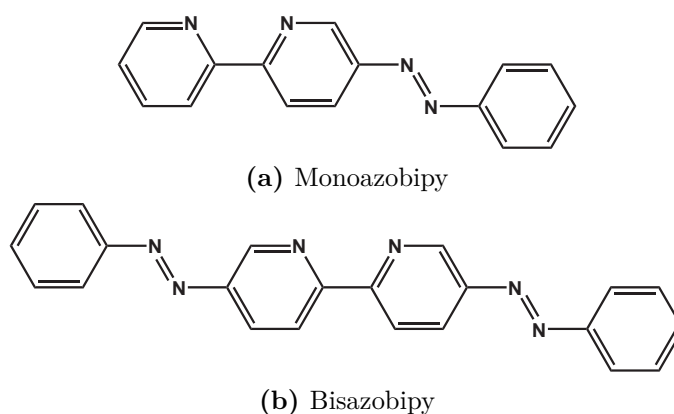


Figure 8.3: New Azoswitches

A novel photoswitchable iron(II) spin-crossover complex was prepared with one of the aforementioned azobipyridines and characterized.

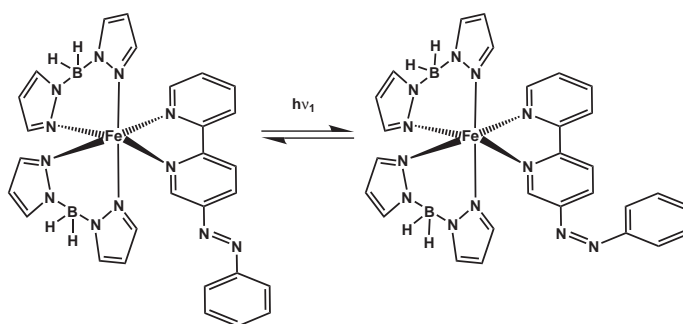


Figure 8.4: Switchable azobipyridine-complex

The literature-known predecessors without the switchability but similar spin-transition behaviour were also synthesized. All compounds showed to be sublimable at mild conditions to form thin-layered films on any desired substrate which kept all their spin-crossover properties, including the ability to perform LIESST-switching.

The influence on the spin-state of the metal and thus the performance of the presented complexes as molecular switches is still in need of improvement. Ligand systems that exert a stronger influence on the coordination center have to be synthesized (e.g. figure 8.5).

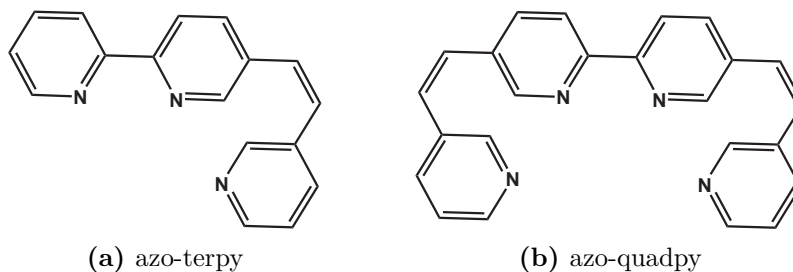


Figure 8.5: Improved azochelates with switchable coordination

Not only disturbing the aromatic system of the ligand, but rather changing the coordination number itself should improve the magnetic switching by orders of magnitude. In the field of surface modification, the newly synthesized family of spin-crossover complexes opens up a vast field of possible applications.

Bibliography

- [1] Tasaki, A. *Journal of Applied Physics* **1970**, *41*, 1000.
- [2] Cambi, L.; Szegoe, L. *Berichte der Deutschen Chemischen Gesellschaft* **1931**, *64*, 2591.
- [3] Stoufer, R. C.; Hadley, W. B.; Busch, D. H. *Journal of the American Chemical Society* **1961**, *83*, 3732.
- [4] Madeja, K.; Konig, E. *Journal of Inorganic and Nuclear Chemistry* **1963**, *25*, 377.
- [5] Konig, E.; Madeja, K. *Chemical Communications* **1966**, 61.
- [6] Gutlich, P.; Goodwin, H. A. *Spin Crossover in Transition Metal Compounds I* **2004**, *233*, 1.
- [7] Gutlich, P.; Hauser, A.; Spiering, H. *Angewandte Chemie-International Edition in English* **1994**, *33*, 2024.
- [8] Zarembowitch, J.; Roux, C.; Boillot, M. L.; Claude, R.; Itie, J. P.; Polian, A.; Bolte, M. *Molecular Crystals and Liquid Crystals Science and Technology Section a-Molecular Crystals and Liquid Crystals* **1993**, *234*, 247.
- [9] Ksenofontov, V.; Gaspar, A. B.; Gutlich, P. *Spin Crossover in Transition Metal Compounds Iii* **2004**, *235*, 23.
- [10] Niel, V.; Munoz, M. C.; Gaspar, A. B.; Galet, A.; Levchenko, G.; Real, J. A. *Chemistry-a European Journal* **2002**, *8*, 2446.
- [11] Qi, Y.; Muller, E. W.; Spiering, H.; Gutlich, P. *Chemical Physics Letters* **1983**, *101*, 503.
- [12] Bousseksou, A.; Negre, N.; Goiran, M.; Salmon, L.; Tuchagues, J. P.; Boillot, M. L.; Boukheddaden, K.; Varret, F. *European Physical Journal B* **2000**, *13*,

- 451.
- [13] Baadji, N.; Piacenza, M.; Tugsuz, T.; Della Sala, F.; Maruccio, G.; Sanvito, S. *Nature Materials* **2009**, *8*, 813.
- [14] D'Avino, G.; Grisanti, L.; Guasch, J.; Ratera, I.; Veciana, J.; Painelli, A. *Journal of the American Chemical Society* **2008**, *130*, 12064.
- [15] Mahfoud, T.; Molnar, G.; Bonhommeau, S.; Cobo, S.; Salmon, L.; Demont, P.; Tokoro, H.; Ohkoshi, S. I.; Boukheddaden, K.; Bousseksou, A. *Journal of the American Chemical Society* **2009**, *131*, 15049.
- [16] Moessbauer, R. L. *Zeitschrift fuer Physik* **1958**, *151*, 124.
- [17] Szabo, A.; Ostlund, N. S. *Modern quantum chemistry : introduction to advanced electronic structure theory*; Dover Publications: Mineola, N.Y., 1996.
- [18] Hohenberg, P.; Kohn, W. *Physical Review B* **1964**, *136*, B864.
- [19] Kohn, W.; Sham, L. J. *Physical Review* **1965**, *140*, 1133.
- [20] Ye, S. F.; Neese, F. *Inorganic Chemistry* **2010**, *49*, 772.
- [21] Schwemer, J.; Pepe, I. M.; Paulsen, R.; Cugnoli, C. *Journal of Comparative Physiology* **1984**, *154*, 549.
- [22] Decurtins, S.; Gutlich, P.; Hasselbach, K. M.; Hauser, A.; Spiering, H. *Inorganic Chemistry* **1985**, *24*, 2174.
- [23] Decurtins, S.; Gutlich, P.; Kohler, C. P.; Spiering, H. *Journal of the Chemical Society-Chemical Communications* **1985**, 430.
- [24] Juhasz, G.; Hayami, S.; Sato, O.; Maeda, Y. *Chemical Physics Letters* **2002**, *364*, 164.
- [25] Collison, D.; Garner, C. D.; McGrath, C. M.; Mosselmans, J. F. W.; Roper, M. D.; Seddon, J. M. W.; Sinn, E.; Young, N. A. *Journal of the Chemical Society-Dalton Transactions* **1997**, 4371.
- [26] Vanko, G.; Renz, F.; Molnar, G.; Neisius, T.; Karpati, S. *Angewandte Chemie-International Edition* **2007**, *46*, 5306.
- [27] Gutlich, P.; Ensling, J.; Tuzcek, F. *Hyperfine Interactions* **1994**, *84*, 447.
- [28] Gutlich, P. *Molecular Crystals and Liquid Crystals Science and Technology Section a-Molecular Crystals and Liquid Crystals* **1997**, *305*, 17.

- [29] Roux, C.; Zarembowitch, J.; Gallois, B.; Granier, T.; Claude, R. *Inorganic Chemistry* **1994**, *33*, 2273.
- [30] Sour, A.; Boillot, M. L.; Riviere, E.; Lesot, P. *European Journal of Inorganic Chemistry* **1999**, 2117.
- [31] Boillot, M. L.; Chantraine, S.; Zarembowitch, J.; Lallemand, J. Y.; Prunet, J. *New Journal of Chemistry* **1999**, *23*, 179.
- [32] Boillot, M. L.; Sour, A.; Delhaes, P.; Mingotaud, C.; Soyer, H. *Coordination Chemistry Reviews* **1999**, *192*, 47.
- [33] Cembran, A.; Bernardi, F.; Garavelli, M.; Gagliardi, L.; Orlandi, G. *Journal of the American Chemical Society* **2004**, *126*, 3234.
- [34] Bandara, H. M. D.; Friss, T. R.; Enriquez, M. M.; Isley, W.; Incarvito, C.; Frank, H. A.; Gascon, J.; Burdette, S. C. *Journal of Organic Chemistry* **2010**, *75*, 4817.
- [35] Schultz, T.; Quenneville, J.; Levine, B.; Toniolo, A.; Martinez, T. J.; Lochbrunner, S.; Schmitt, M.; Shaffer, J. P.; Zgierski, M. Z.; Stolow, A. *Journal of the American Chemical Society* **2003**, *125*, 8098.
- [36] Ignatin, A. A.; Barachevskii, V. A.; Strokach, Y. P.; Alfimov, M. V.; Guglielmetti, R. *Zhurnal Nauchnoi I Prikladnoi Fotografii* **2003**, *48*, 27.
- [37] Morgunov, R. B.; Mushenok, F. B.; Aldoshin, S. M.; Sanina, N. A.; Yur'eva, E. A.; Shilov, G. V.; Tkachev, V. V. *New Journal of Chemistry* **2009**, *33*, 1374.
- [38] Toman, P.; Bartkowiak, W.; Nespurek, S.; Sworakowski, J.; Zalesny, R. *Chemical Physics* **2005**, *316*, 267.
- [39] Kajimoto, S.; Mori, A.; Fukumura, H. *Photochemical and Photobiological Sciences* **2010**, *9*, 208.
- [40] Seal, P.; Chakrabarti, S. *Journal of Physical Chemistry A* **2010**, *114*, 673.
- [41] Bossi, M. L.; Rodriguez, J. B.; Aramendia, P. F. *Journal of Photochemistry and Photobiology a-Chemistry* **2006**, *179*, 35.
- [42] Renth, F.; Foca, M.; Petter, A.; Temps, F. *Chemical Physics Letters* **2006**, *428*, 62.
- [43] Siewertsen, R.; Renth, F.; Temps, F.; Sonnichsen, F. *Physical Chemistry Chemical Physics* **2009**, *11*, 5952.

- [44] Tosić, O.; Altenhoner, K.; Mattay, J. *Photochemical and Photobiological Sciences* **2010**, *9*, 128.
- [45] Guerchais, V.; Ordronneau, L.; Le Bozec, H. *Coordination Chemistry Reviews* **2010**, *254*, 2533.
- [46] Xia, C. J.; Fang, C. F.; Zhao, P.; Liu, H. C. *European Physical Journal D* **2010**, *59*, 375.
- [47] Morimoto, M.; Irie, M. *Journal of the American Chemical Society* **2010**, *132*, 14172.
- [48] Takahashi, M.; Turek, P.; Nakazawa, Y.; Tamura, M.; Nozawa, K.; Shiomi, D.; Ishikawa, M.; Kinoshita, M. *Physical Review Letters* **1991**, *67*, 746.
- [49] Nakazawa, Y.; Tamura, M.; Shirakawa, N.; Shiomi, D.; Takahashi, M.; Kinoshita, M.; Ishikawa, M. *Physical Review B* **1992**, *46*, 8906.
- [50] Banister, A. J.; Bricklebank, N.; Lavender, I.; Rawson, J. M.; Gregory, C. I.; Tanner, B. K.; Clegg, W.; Elsegood, M. R. J.; Palacio, F. *Angewandte Chemie-International Edition in English* **1996**, *35*, 2533.
- [51] Rawson, J. M.; Alberola, A.; Whalley, A. *Journal of Materials Chemistry* **2006**, *16*, 2560.
- [52] Gatteschi, D.; Bogani, L.; Cornia, A.; Mannini, M.; Sorace, L.; Sessoli, R. *Solid State Sciences* **2008**, *10*, 1701.
- [53] Gatteschi, D. *Advanced Materials* **1994**, *6*, 635.
- [54] Moore, G. E. *Electronics Magazine* **1965**, *38*.
- [55] Raymo, F. M. *Advanced Materials* **2002**, *14*, 401.
- [56] Fabbrizzi, L.; Licchelli, M.; Pallavicini, P. *Accounts of Chemical Research* **1999**, *32*, 846.
- [57] Willner, I.; Katz, E. *Angewandte Chemie-International Edition* **2000**, *39*, 1180.
- [58] Yersin, H. *Transition Metal and Rare Earth Compounds Iii* **2004**, *241*, 1.
- [59] Lindstro.F; Womble, A. E. *Talanta* **1973**, *20*, 589.
- [60] Bornholdt, C.; Ph.D. thesis; 2008.
- [61] Matsumoto, N.; Ohta, S.; Yoshimura, C.; Ohyoshi, A.; Kohata, S.; Okawa, H.; Maeda, Y. *Journal of the Chemical Society-Dalton Transactions* **1985**, 2575.

- [62] Evans, D. F. *Journal of the Chemical Society* **1959**, 2003.
- [63] Bain, G. A.; Berry, J. F. *Journal of Chemical Education* **2008**, *85*, 532.
- [64] Neese, F.; Schwabe, T.; Grimme, S. *Journal of Chemical Physics* **2007**, *126*.
- [65] Case, F. H. *Journal of Organic Chemistry* **1951**, *16*, 941.
- [66] Tzalis, D.; Tor, Y.; Failla, S.; Siegel, J. S. *Tetrahedron Letters* **1995**, *36*, 3489.
- [67] Dietrich-Buchecker, C.; Jimenez, M. C.; Sauvage, J. P. *Tetrahedron Letters* **1999**, *40*, 3395.
- [68] Bencini, A.; Lippolis, V. *Coordination Chemistry Reviews* **2010**, *254*, 2096.
- [69] Janiak, C.; Deblon, S.; Wu, H. P.; Kolm, M. J.; Klufers, P.; Piotrowski, H.; Mayer, P. *European Journal of Inorganic Chemistry* **1999**, 1507.
- [70] Semmelhack, M. F.; Helquist, P.; Jones, L. D.; Keller, L.; Mendelson, L.; Ryono, L. S.; Smith, J. G.; Stauffer, R. D. *Journal of the American Chemical Society* **1981**, *103*, 6460.
- [71] Yang, X. J.; Wu, B.; Janiak, C.; Sun, W. H.; Hu, H. M. *Zeitschrift Fur Anorganische Und Allgemeine Chemie* **2004**, *630*, 1564.
- [72] Albrecht, M.; Janser, I.; Lutzen, A.; Hapke, M.; Frohlich, R.; Weis, P. *Chemistry-a European Journal* **2005**, *11*, 5742.
- [73] Venanzi, L. M. *Journal of the Chemical Society* **1958**, 719.
- [74] Hapke, M.; Staats, H.; Wallmann, I.; Lutzen, A. *Synthesis-Stuttgart* **2007**, 2711.
- [75] Ukai, T.; Kawazura, H.; Ishii, Y.; Bonnet, J. J.; Ibers, J. A. *Journal of Organometallic Chemistry* **1974**, *65*, 253.
- [76] Bailey, T. R. *Tetrahedron Letters* **1986**, *27*, 4407.
- [77] Grammenudi, S.; Vogtle, F. *Angewandte Chemie-International Edition in English* **1986**, *25*, 1122.
- [78] Newkome, G. R.; Gross, J.; Patri, A. K. *Journal of Organic Chemistry* **1997**, *62*, 3013.
- [79] Whittle, C. P. *Journal of Heterocyclic Chemistry* **1977**, *14*, 191.
- [80] Curtius, T. *Journal für Praktische Chemie* **1894**, *50*, 275.
- [81] Katritzky, A. R.; Scriven, E. F. V.; Majumder, S.; Akhmedova, R. G.; Vakulenko, A. V.; Akhmedov, N. G.; Murugan, R.; Abboud, K. A. *Organic and Biomolecular*

- Chemistry* **2005**, *3*, 538.
- [82] Bakke, J. M. *Pure and Applied Chemistry* **2003**, *75*, 1403.
- [83] Fletcher, D. A.; Gowenlock, B. G.; Orrell, K. G. *Journal of the Chemical Society-Perkin Transactions 2* **1997**, 2201.
- [84] Kirpal, A.; Reiter, E. *Chemische Berichte* **1925**, *58*, 699.
- [85] Bartlett, E. H.; Eaborn, C.; Walton, D. R. M. *Journal of the Chemical Society C-Organic* **1970**, 1717.
- [86] Kalbandkeri, R. G.; Padma, D. K.; Vasudevamurthy, A. R. *Zeitschrift Fur Anorganische Und Allgemeine Chemie* **1979**, *450*, 103.
- [87] Cai, D.; Larsen, R. D.; Reider, P. J. *Tetrahedron Letters* **2002**, *43*, 4285.
- [88] Cai, D. W.; Hughes, D. L.; Verhoeven, T. R. *Tetrahedron Letters* **1996**, *37*, 2537.
- [89] Chung, C. W. Y.; Toy, P. H. *Journal of Combinatorial Chemistry* **2007**, *9*, 115.
- [90] Barclay, J. E.; Leigh, G. J.; Houlton, A.; Silver, J. *Journal of the Chemical Society-Dalton Transactions* **1988**, 2865.
- [91] Barclay, J. E.; Hills, A.; Hughes, D. L.; Leigh, G. J. *Journal of the Chemical Society-Dalton Transactions* **1988**, 2871.
- [92] Real, J. A.; Munoz, M. C.; Faus, J.; Solans, X. *Inorganic Chemistry* **1997**, *36*, 3008.
- [93] Naik, A. D.; Garcia, Y. *Journal of Physics: Conference Series* **2010**, *217*, 012032.
- [94] Cobo, S.; Molnar, G.; Real, J. A.; Bousseksou, A. *Angewandte Chemie-International Edition* **2006**, *45*, 5786.
- [95] Moliner, N.; Salmon, L.; Capes, L.; Munoz, M. C.; Letard, J. F.; Bousseksou, A.; Tuchagues, J. P.; McGarvey, J. J.; Dennis, A. C.; Castro, M.; Burriel, R.; Real, J. A. *Journal of Physical Chemistry B* **2002**, *106*, 4276.

Danksagung

Mein besonderer Dank gilt Prof. Dr. Felix Tuczek für die Möglichkeit, dieses interessante und abwechslungsreiche Thema zu bearbeiten.

Des Weiteren danke ich:

- Dr. Gerhard Peters für die vielen NMR-Spektren und vor allem für die Geduld bei den zahlreichen Evans-Messungen.
- Frau Cornelissen, Frau Pehlke und Frau Karbstein für die vielen Spektren, Elementar- und Halogenanalysen.
- Henning Lühmann für die PPMS-Messungen.

Meinen Eltern, ohne deren ständige Unterstützung, Ermutigung und Bestätigung diese Arbeit nicht möglich gewesen wäre

Herrn Dr. René-Hermann Römer, der mir während meiner gesamten Zeit in Kiel ein wahrer Freund gewesen ist.

Julia für die letzten acht Jahre, was musstest du alles ertragen von mir!

Eidesstattliche Erklärung

Hiermit erkläre ich an Eides statt, dass ich die vorliegende Arbeit nur unter Verwendung der angegebenen Hilfsmittel und unter Einhaltung der Regeln guter wissenschaftlicher Praxis der Deutschen Forschungsgemeinschaft erstellt habe. Ich habe keine vorangegangenen Promotionsversuche unternommen, und diese Arbeit wurde an keiner anderen Stelle im Rahmen eines Promotionsverfahrens eingereicht.

KIEL, DEN

Dipl.-Chem. Alexander Bannwarth

Lebenslauf

Persönliche Daten

Alexander Bannwarth
Holtenauer Strasse 342
24106 Kiel

geb. am 20. Oktober 1980
in Bad Säckingen
Staatsangehörigkeit: Deutsch

Schulbildung

1987-1991: Grundschule am Heidenstein Schwörstadt
1991-2000: Georg-Büchner Gymnasium Rheinfelden

Wehrdienst

September 2000 bis August 2001: 5. StFmBtl 10 in Sigmaringen

Hochschulausbildung

Oktober 2001: Beginn Studium des Studiums der Chemie an der
Christian-Albrechts-Universität zu Kiel

Juli 2003: Diplomchemiker-Vorprüfung

Oktober 2005: Diplomchemiker-Hauptprüfung

Januar 2006 bis Oktober 2006: Diplomarbeit bei Prof. Dr. F. Tucek
am Institut für Anorganische Chemie der Universität Kiel mit dem
Thema: Photoschaltbare Spin-Crossover Komplexe auf der Basis von
Azopyridin-Liganden.

seit November 2006: Promotion bei Prof. Dr. F. Tucek am Institut
für Anorganische Chemie der Universität Kiel.